



IntechOpen





---

# Reliability and Ecological Aspects of Photovoltaic Modules

Edited by Abdülkerim Gök

Published in London, United Kingdom

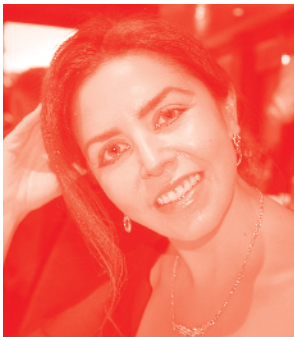
---



IntechOpen







Supporting open minds since 2005



Reliability and Ecological Aspects of Photovoltaic Modules

<http://dx.doi.org/10.5772/intechopen.82211>

Edited by Abdülkerim Gök

#### Contributors

Titu-Marius I. Băjenescu, Rütü Eke, Mahmoud Zendehele, Narges Yaghoobi, Niaz Mohammadreza Yaghoobinia, Hervé Joël Tchognia Nkuissi, Francisco Konan, Bouchaib Hartiti, Jean-Marie Ndjaka, Leonimer Melo, Dario Toginho, Alex Archela, Mohamad Kharseh, Holger Wallbaum, Laurentiu Fara, Dan Craciunescu, Claudia Barolo, Nicole Mariotti, Matteo Bonomo

#### The Editor(s) and the Author(s)

The rights of the editor(s) and the author(s) have been asserted in accordance with the Copyright Designs and Patents Act 1988. All rights to the book as a whole are reserved by INTECHOPEN LIMITED. The book as a whole (compilation) cannot be reproduced, distributed or used for commercial or non-commercial purposes without INTECHOPEN LIMITED's written permission. Enquiries concerning the use of the book should be directed to INTECHOPEN LIMITED rights and permissions department ([permissions@intechopen.com](mailto:permissions@intechopen.com)).

Violations are liable to prosecution under the governing Copyright Law.



Individual chapters of this publication are distributed under the terms of the Creative Commons Attribution - NonCommercial 4.0 International which permits use, distribution and reproduction of the individual chapters for non-commercial purposes, provided the original author(s) and source publication are appropriately acknowledged. More details and guidelines concerning content reuse and adaptation can be found at <http://www.intechopen.com/copyright-policy.html>

#### Notice

Statements and opinions expressed in the chapters are those of the individual contributors and not necessarily those of the editors or publisher. No responsibility is accepted for the accuracy of information contained in the published chapters. The publisher assumes no responsibility for any damage or injury to persons or property arising out of the use of any materials, instructions, methods or ideas contained in the book.

First published in London, United Kingdom, 2018 by IntechOpen

IntechOpen is the global imprint of INTECHOPEN LIMITED, registered in England and Wales

registration number 11011648, 5th floor, Lower Thames Street, London

EC R 4AF, United Kingdom

Printed in Croatia

British Library Cataloguing-in-Publication Data

A catalogue record for this book is available from the British Library

Additional hard and PDF copies can be obtained from [orders@intechopen.com](mailto:orders@intechopen.com)

Reliability and Ecological Aspects of Photovoltaic Modules

Edited by Abdülkerim Gök

p. cm

Print ISBN 978-1-78548-282-5

Online ISBN 978-1-78548-283-2

eBook (PDF) ISBN 978-1-78548-284-9

An electronic version of this book is freely available thanks to the support of libraries working with Knowledge Unlatched. KU is a collaborative initiative designed to make high quality books Open Access for the public good. More information about the initiative and links to the Open Access version can be found at [www.knowledgeunlatched.org](http://www.knowledgeunlatched.org)

# We are IntechOpen, the world's leading publisher of Open Access books Built by scientists, for scientists

4,500+

Open access books available

118,000+

International authors and editors

130M+

Downloads

151

Countries delivered to

Our authors are among the  
**Top 1%**

most cited scientists

12.2%

Contributors from top 500 universities



**WEB OF SCIENCE™**

Selection of our books indexed in the Book Citation Index  
in Web of Science® Core Collection (BKCI)

Interested in publishing with us?  
Contact [book.department@intechopen.com](mailto:book.department@intechopen.com)

Numbers displayed above are based on latest data collected.  
For more information visit [www.intechopen.com](http://www.intechopen.com)





# Meet the editor



Dr. Abdülkerim Gök is a research associate in the Department of Materials Science and Engineering at Gebze Technical University, Turkey. After completing his BS in Materials Science and Engineering at Anadolu University, Turkey in 2008, he received his MSc in Chemical Engineering from Columbia University, New York, USA, in 2010, and his PhD in Materials Science and Engineering from Case Western Reserve University, Cleveland, Ohio, USA, in 2013. His research interests include performance, lifetime, and degradation science of photovoltaic (PV) modules, the effect of environmental stressors on PV module materials, predictive and diagnostic degradation pathway models, and reproducible statistical methods.















---

---



„...., †

,..... ‡ ^  
„...., †

€, f

>

%a.... ‡ ^

„...., „  
„...., † €, f

€Šf

> , €

$f$

” ...

$f$  † $f$

” %

” ^ ” ...Š“œ

>

€> ,

$f$

†

€

€ , , ‘

€ , € ,

Š“œ

’

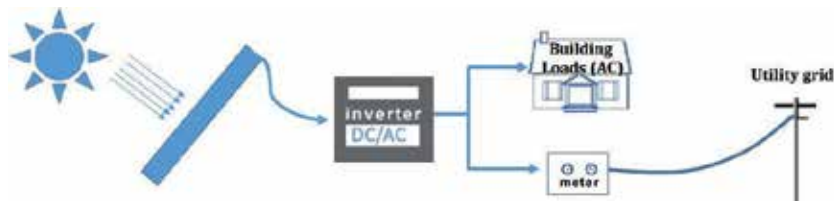
Š†œ

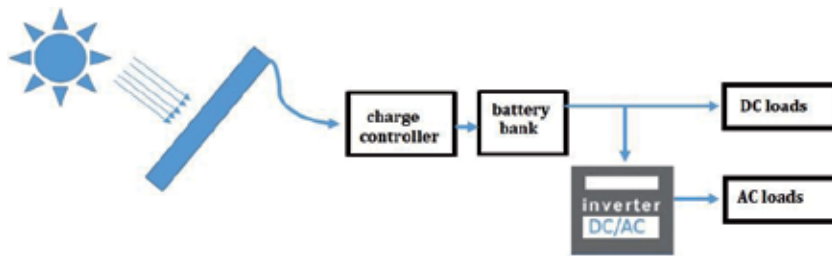
”

€

’

€•‘ , ”





•	–€–	€ ~
TM	š– ff	€€ ‡
> <	– f	– >
•	— ^	€ >
• œ	š– f €	€€ f
TM	€ –‡ €	‡€
“	– ^ ~	€

>€ , > f  
< < œ „ ... † ( ‡^ , > €‡ €% Œ € )  
<  
<  
<  
<  
< %  
,  
,  
€

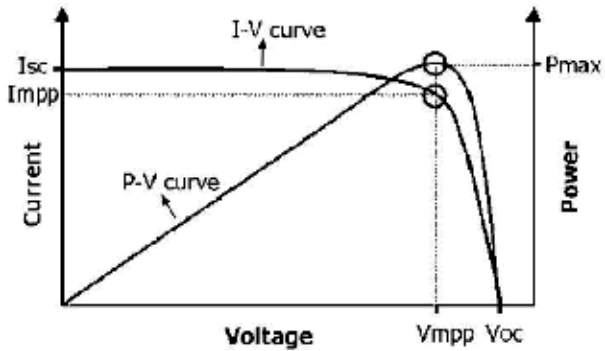
“

”

<<

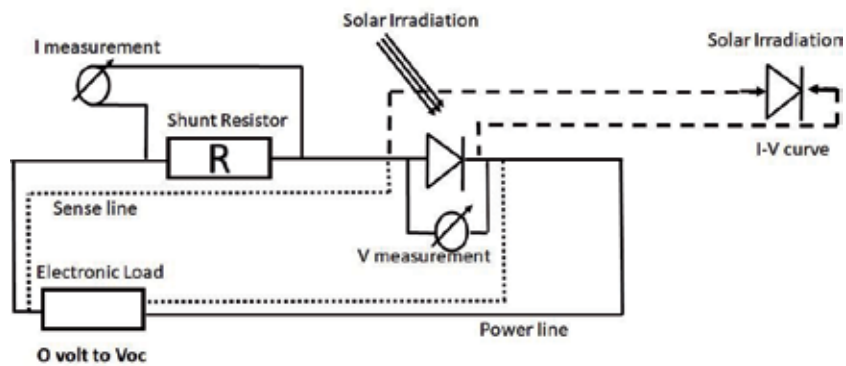
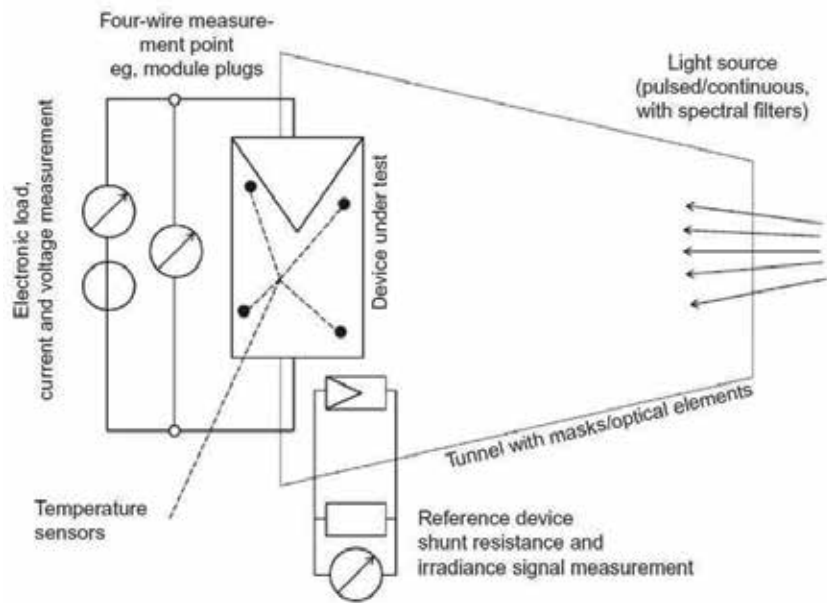
< “







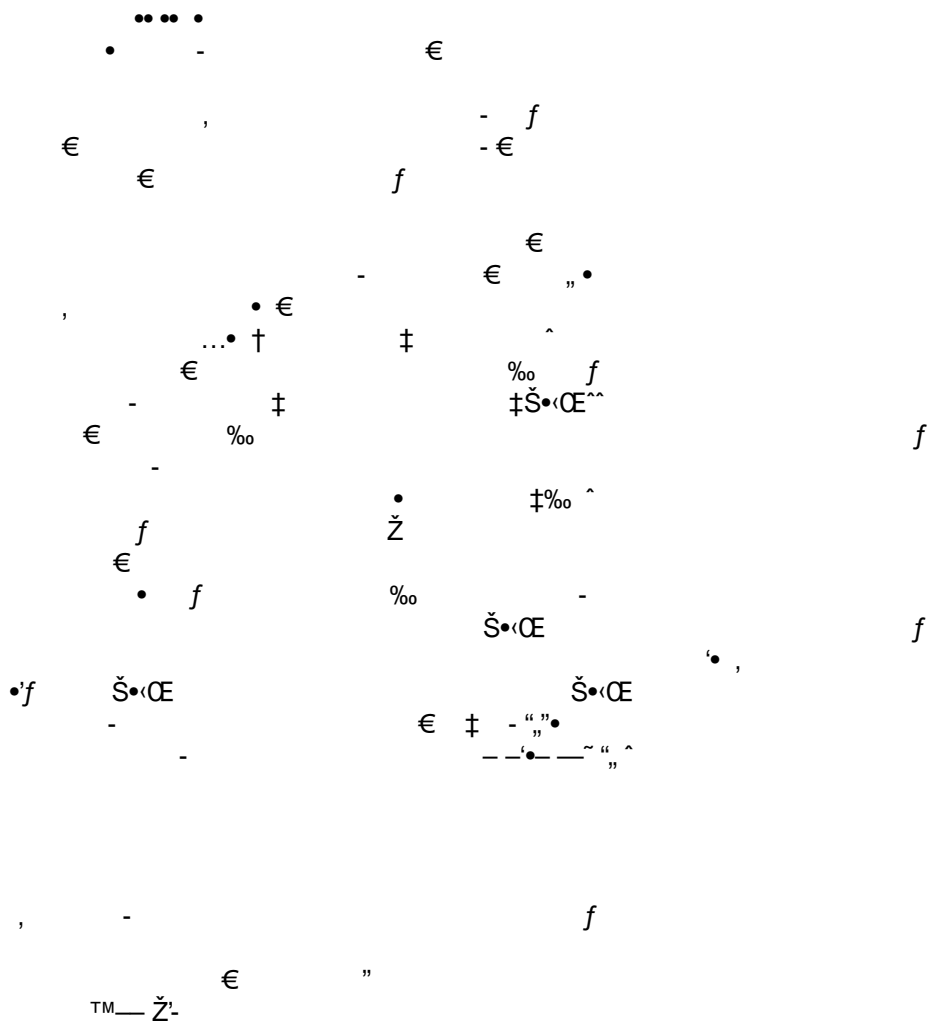




• ••••

• • • • •

••€•



..  
 f„€...† .. €  
 • - , ‡ €...† • - „  
 • , „ , • • •...† • €•,  
 • € • ,

^ %Š‡  
 ... - € ‹ • - Œ €Ž • Œ Œ‡ Œ' , -€Ž • €  
 ‡ -  
 “ .. ”

IntechOpen

• • • • •  
 • • • • • € €  
 • • € • •

. . . . .  
 € - . . , f , , , , , † ‡ , ^ † % % % Š †  
 f f f , œ • Ž , “  
 , ' ^  
 . . . . .  
 , f , , , , , † ‡ , Š † f ž ž , f œ , f ' f - † ,  
 ž . . — . ~ ™ . š  
 ) . . . . . ) . . . . .  
 . . . . . ,  
 ‹ œ • † - . . . . , f , , % % % ž †  
 „ - ž f , ž ž , ž %  
 % - ) . . . . . ) • j .  
 ) . . ~ . , f ž  
 . . . . . ž • ø • ž  
 - ^ ) ) ~ ^ ž % . . . , f ž ž ž † ž †  
 „ - ž f ^ , f † f % , ^ , ^ %  
 ‘ . . š —  
 ~ . . ) . . . . . • ~ . . . . .  
 ) . . . . . £ £ † - . . . .  
 f † † š † f f † œ ™ , f % ^ f ^ f % f ž % ^ ž  
 † □ . — j ¥ š •  
 - š š • š . ^ • . ¥  
 . . . . .  
 | . . ' ž § ) . . . . . ) . . . . .  
 , f , , , , , † ž , Š † f f f , œ • • , f ,  
 - š . . . . .  
 . . . . . ) . . . . .  
 - . . ™ . . . † “ . . , f f ž  
 ž ž ž † f % - % , , † ,  
 ž ) . ž . ~ ) . . .  
 • ) . . . . . • | ) § . . .  
 ™ . . † - . . . . . , f - ž % ž ž †  
 „ - ž ^ - ž % , ^ ž % † †  
 „ - ) . . . . . ) • j .  
 ) . . . . . ) . . . . .  
 . . . . . † - œ • .  
 . . . . . • ø •  
 ž • - ^ ) ) ~ ž . . . , f ž ž ž % • ž †  
 „ - ž ^ ž , f † f % , ^ , ^  
 f - ™ † ž ž ^ ) . . . . .  
 ) . . . . . ~ . . . . .

¢ ¨),  
 • • • † †œœi • • •  
 • œ • • • œ † ž' • • • † •  
 , f „  
 — ¢ Š • • •  
 • • • • •  
 • • • • •  
 • • • • • ~ — • •  
 TM • • • • •  
 , f ž... † ž f ^ ž † Š † f f † œ<sup>TM</sup>  
 • • • , f , ff—  
 , — • □ › — •  
 ¢ • • □ • • □—  
 • • • • • • •  
 • • • • •  
 • • © • © • • • • •  
 † › • • • ž , — • •  
 › • • • • • — • TM • • •  
 —œ • • • , f ^ , %<sub>00</sub> , f †...  
 • □ ... , f † • • „—ž^ „—  
 ž Š • • Š › • • • • •  
 • • • • • © •  
 • • • † › • ž •  
 ~ › • • • › • • • • •  
 † § • • TM • • † “•  
 • • • • • , f — ž%<sub>00</sub> ž ž †  
 „—ž^ ^—ž, %<sub>00</sub> , ^ž' %<sub>00</sub> †  
 %<sub>00</sub> — ¢ TM • • • • •  
 • • • • • • •  
 ~ • • † © † — £ • • • • • , ff—  
 ‘ Š • • “ •  
 Šš • • • “— • • •  
 TM • • • • • • • • •  
 • • • • •  
 • • • — • — • •  
 , ff †... †, † † ^ ‘ , Š †  
 f ‘œ , „ „  
 † ¢ • • • a “ •  
 “ Š • • —Š › • • •  
 › • • • ~ • • •  
 , f †... † † † ž † — , Š † † f f † œ<sup>TM</sup>  
 • , ff' f † †  
 — TM › • • ~š • • • • •  
 • • • • • › • •

••

>





# Comparing Different PV Module Types and Brands Under Working Conditions in the United Kingdom

Mohamad Kharseh and Holger Wallbaum

## Abstract

The present work demonstrates the performance evaluation and economic analysis of different PV module types and brands at the working conditions of Padiham (53.5 N, 2.3 W) in the UK. The total area of PV plant was assumed to be 100 square meters. The simulations were carried out for modules installed on the roof and on the south-facing façade of a residential building. The comparison study is carried out to define the most suitable module type and brands for the considered place in the current study. The energy and economic performance of the grid-connected PV system are analyzed under the meteorological conditions of Padiham. The modules were characterized by evaluating their annual electrical energy generation and different figures of merit of the grid-connected PV systems such as the investment, annual profit, net present value, levelized cost of electricity, and the payback time. The simulations show that in this specific setup, monocrystalline modules have the best energy performance, while thin-film modules have the best economic performance.

**Keywords:** PV system, simulations, different PV brands, potential

## 1. Introduction

Today, most of the global energy comes from using fossil energy carrier. There is mounting evidence that global warming and, consequently, climate changes are anthropogenic and attributed to fossil-fuel consumption. The strong fossil-fuel dependence of our current energy system has resulted in daily fossil-fuel consumption of 98.2 million barrels of oil equivalent (Mbbbl) in 2017 [1]. It is worth to mention that fossil fuel represents 75% of total global energy consumption, while renewable energy resources represent only 25% [2]. Consequently, about 36.8 billion tons of carbon dioxide emissions are emitted into the atmosphere annually for global energy production [3]. Observations provide evidence that atmospheric CO<sub>2</sub> levels caused by human activities have increased by 25% over the last century, which leads to rising global temperature [4].

In helping to face those challenges and achieving the EU targets for 2020 and 2050, in addition to improving the performance of the existing energy conversion systems, utilizing the available local renewable energy resources is needed as well. Although the current efficiency of such systems is still relatively low and the

capital cost is still high, the abundance of solar energy that strikes our planet makes the use of solar panel economically viable [5, 6]. It is worth mentioning that the growing demand for renewable energy sources in recent years led to advancing the manufacturing of solar cells. The fast decrease in system prices combined with the increases in the performance make it economically feasible, and, consequently, increased amounts installed globally [7]. Regarding the worldwide installed capacity, solar photovoltaic is now the third largest renewable energy source with annual capacity additions reaching 93.7 GW and 94.3 GW in 2017 and 2018, respectively [2, 8]. By the end of 2018, the total accumulated capacity is 480 GW [8]. Because they have no moving parts, PVs are stable over time, with typical durability of 25 years, and low maintenance is required during their operation [9].

Indeed, many different PV module types and brands are available in the market. The performance of each type and brand varies from one to another and strongly depends on the meteorological and working conditions. Current work, therefore, presents a comparison between different module types and brands under the meteorological conditions of Padiham (53.5 N, 2.3 W) in the UK.

## 2. Photovoltaic system overview

Photovoltaic (PV) system is a technology that converts solar energy into electricity. Because no moving parts, such systems are reliable, and low maintenance is required during the operation. In addition to the fact that PV systems do not emit any greenhouse gases during operation, manufacturing such systems results in very low emissions. In average, less than 2 years is needed for a PV module to generate the same amount of energy that has been used to fabricate the module depending on the type of module [10].

Recently, the PV module has been integrated to building external envelope. Such a system is the so-called building-integrated photovoltaics (BIPV). The most advantage of BIPV is that such a system generates the electricity at the place where it is demanded, as well as PV modules can replace some parts of the building envelope components. This can result in reducing the initial costs of BIPV due to lowering the costs of conventional envelope materials. PV modules can be integrated into different parts of the envelope such as roof (flat or slope), façade, and shading devices for windows.

The electric output of a PV system depends on different factors such as:

The availability of and accessibility to solar radiation, which in turn is influenced by the climate, the inclination, and orientation of the modules

The PV technology is related to facts such as efficiency and its decline with time and the cell temperature

The over shading in some areas of the modules

## 3. Objective

This work aim is to evaluate the performance of a photovoltaic (PV) system installed on the roof or integrated to the south-facing façade of residential apartments in Padiham (53.5 N, 2.3 E), UK. Moreover, the work presents a comparison

Brands	Type		
	Monocrystalline	Polycrystalline	Thin film
	Motech XS72D3-320	Hanwha Solar One 310	Stion STO-150
	Panasonic N330	JA Solar 48-225/4BB	Solar Frontier SF170-S
	Silevo 310	Trina 315	Stion STN-125
	Sunpreme 360	SunTech 320	SolTech Energy 80
	Solar World SW350 XL	Jinko Solar JKM270	
	Silevo 220	Motech IM72C3-310	
	Optimus 60 OPT280	Canadian Solar CS6X-320P	
	LG Solar 320	Solar World SW260	
	Jinko Solar JKM275M	Yingli Solar YL305P	
	Solar World SW325 XL	PEAK BLK 255	
	JA Solar 72-315/SI	Gintech 240	
	Hyundai HiS-S265MG	Hyundai HiS-S250MG	
	Mitsubishi PV-MLE265HD2	Kyocera KD220GH-4FB2	

Table 1.  
 Considered PV module types and brands [11].

between the energy and economic performance of the most common PV module types, which are:

1. Polycrystalline module
2. Monocrystalline module
3. Thin-film module

Of course, a tremendous number of companies are making different brands of PV modules. Therefore, in order to identify the suitable module type and brand, performances of different module type and brands are compared under the meteorological conditions of Padiham, UK. The present work considers only the brands that were mentioned in the report prepared by the Fraunhofer Institute for Solar Energy Systems, ISE [11] (see Table 1). The electricity generation profiles of the installed PV system will be identified. Annual electricity generation profile, energy efficiency, and different figures of merit of economic performance of different module types and brands will be illustrated at the working conditions of the considered city.

#### 4. Determination of available solar energy

The first and most important step before designing a photovoltaic system is the determination of the available solar energy (ASE) on an inclined surface in the considered site. ASE can be either measured or simulated. Solar radiation simulations have advantages over measurements and are more reliable over the years [12]. Unlike measured solar radiation, simulated solar radiation can account for universal climate variations over many years, without having the burden of having to process decades of field data. Also, the actual measurements of the ASE are

January	February	March	April	May	June	July	August	September	October	November	December
0.32	0.34	0.37	0.39	0.41	0.39	0.41	0.41	0.38	0.34	0.30	0.30

Table 2.  
Clearness index in Padiham, UK [18].

Input Data									
Latitude	55.871254	N	degree	Month	Clearness K <sub>T</sub>	PV Specification			
Longitude	12.826451	e	degree	Jan	0.33	fill factor	0.77		
Standard Longitude	15	degrees		Feb	0.39	derating factor	0.90		
Slop angle $\beta$	50.0	degrees		Mar	0.44	short circuit current	9.09	A	
Surface azimuth	180.0	degrees		Apr	0.48	open circuit voltage	45.73	V	
Avilable area	100	m <sup>2</sup>		May	0.3	voltage temp. coefficient	340.00	%/C	
Inflation rate	0.7%	%		Jun	0.48	NOCT (nominal operating cell temperature)	45.00	C	
Real interest rate	3.4%			Jul	0.49				
Electrical price escalation rate	1.0%			Aug	0.49	nomional capacity	320.00	W	
Electricity price	0.207	S/kWh		Sep	0.45	module price	480.00	\$	
				Oct	0.38	Area	1.64	m <sup>2</sup>	
				Nov	0.39	module degradation rate	1.0%	%	
				Dec	0.35				

Figure 1.  
Input data interface of the developed excel-based model to simulate the PV system.

costly due to the high price of the required instruments. Therefore, simulation is a common method to calculate the available solar energy at a particular location. In this work, a computational model was built to estimate the available solar energy, with the resolution of 1 hour, per square meter of surface considering different slopes and azimuth angles. The model can be used to determine the optimal azimuth and slope angles of the PV modules. The optimum angles are defined as the angles that result in maximum annual electricity generation. More details about the model can be found in Ref [13].

It should be noted that the model was built based on well-known theoretical relations for calculating available solar energy. These relations have been tested by a number of studies [14, 15]; the reader is recommended to consult Section 2 in Refs. [16, 17]. It is also worth noting that in the current study, the cloudy day approach was taken in the calculation of the available solar energy. The clearness index of the city of Padiham, which was taken from [18], is tabulated in Table 2. The specifications of the considered PV module, which appeared in Figure 1 as input data, were collected from the technical brochure of each module, which was provided by the factory of each considered module. Some of the specifications of the PV module are certain wattage, voltage, and amperage which are called electrical characteristics of the module. These characteristics of the module are defined under specific conditions which are called standard test conditions (STC). STC, which is the universal standard, is a set of laboratory test conditions including irradiance of 1000 W/m<sup>2</sup>, air mass of AM1.5, and cell temperature of 25°C [16].

## 5. Simulation PV system

Because an electric grid is available in Padiham, a grid-connected system will be considered in the current work. In such a system, the electric grid acts as a virtual storage system, which in turn can reduce the net costs of PV systems. However, these systems require an inverter to convert the DC (direct current) voltage into AC voltage. Also, to reduce the initial cost of the system, grid-connected PV systems

have another advantage. Indeed, the electricity consumption of a building is not constant over the day and varies depending on the occupancy of the building, user behavior, and used equipment. On another side, the electricity output of the PV system varies during the day with the position of the sun in the sky.

Consequently, there might be periods when the output of the PV system exceeds the electricity demand of the building or vice versa. Therefore, in a grid-connected system, the electricity demand of the building is met by a combination of solar energy and grid electricity. In other words, when the output of the PV system exceeds the demand of the building, the system will export the exceeded energy to the grid and vice versa. Namely, when the output of the PV system is not enough to cover the demand of the building, the system will import electricity from the grid.

In current work, an Excel-based model has been built to simulate hour-by-hour energy and economic performance of a grid-connected PV system for different slope angle. As mentioned above the model can be used to determine the optimal inclination angle so that the annual generation of PV module can be maximized. The model can also simulate a PV system installed on south-facing façade or a vertical wall of any azimuth angle. Furthermore, the model was built using well-known theoretical relations for calculating the electricity generation of the PV system. For more details, the reader is recommended to consult Refs. [19, 20]. In order to be able to simulate the energy and economic performance of the PV system, assumptions had to be made. In the current study, the assumptions are based on realistic current conditions in the UK and data collected from literature review (see Table 3)<sup>1</sup> [21–33].

## 5.1 Component and installation costs

The price PV module was taken based on the price given by different suppliers. According to the component price collected from literature review, the replacement of the inverter (which takes place every 8th year) and the installation cost were assumed to be 322 \$/kW and 0.018 \$/W, respectively [2325].

## 5.2 Operation and maintenance costs

Operation and maintenance (O&M) represent expenses on equipment and services that occur after the system is installed. Fortunately, solar panels have 25 years

Factor	Value	Factor	Value
Inflation rate	0.1%	Labor cost	18 \$/kW
Real interest rate	0.6%	Operation	10 \$/kW y
Elect. price	20.1 /kWh	Inverter lifetime	8 y
Feed-in tariff	6.7 /kWh	Wire efficiency	98%
Elect. price escalation	1%/y	Lifetime of the project	25 y
Degradation rate	1%/y	Inverter price	322 \$/kW
Cell temperature	$T_c$ $T_a$ 1:25 NOCT 20 $G_s$		

Table 3.  
 Assumptions made in the present work.

<sup>1</sup>  $T_c$  is the cell temperature,  $T_a$  is the ambient air temperature, NOCT is the nominal operating temperature, and  $G_s$  is the available solar radiation ( $W/m^2$ ).

of warranty. Product warranties usually cover major maintenance. Therefore, O&M costs during the first 25 years (which was assumed to be the project economic life) will be only for surface cleaning of PV modules and supervising. In 2013 in the USA, the cost of supervision and twice a year cleaning of the panels was reported to be 8.3 \$/kW per year [22]. Therefore, in current work, the annual O&M cost of the project will be assumed 10 \$/kW y.

## 6. Results and discussions

The developed model was used to simulate the performance of grid-connected PV system. As mentioned above, different brands of PV modules were tested in the present work, see Table 1.

### 6.1 Thin-film module type

Among the brands of the thin film mentioned in the report prepared by the Fraunhofer Institute for Solar Energy Systems, ISE [11], only the price of four brands was collected so far.

The electrical output of the PV module per square meter of different brands of thin-film PV module installed on the roof is shown in Figure 2. As shown, the annual electrical output per square meter of selected modules varies from a minimum of 127 to a maximum of 151 kWh/m<sup>2</sup>y. The optimal slope angle of the module was found to be 49° facing the south. From an energy viewpoint, the results illustrated in Figure 2 show that Stion STO-150 thin film is the best among the considered thin-film module brands.

Energy performance of PV modules strongly depends on the module temperature variations. Therefore, as expected, simulations show that the efficiency of the PV modules during colder months is higher than those during the warmer months. Figure 3 shows that the efficiency of the thin-film PV module ranged from 9.6% (SolTech Energy 80 in August) to 12% (Stion STO-150 in January).

In order to compare the different brands from the economic point of view, the levelized cost of electricity and the accumulative cash flow were determined for each brand. As shown in Figure 4, the levelized cost of electricity varies from a

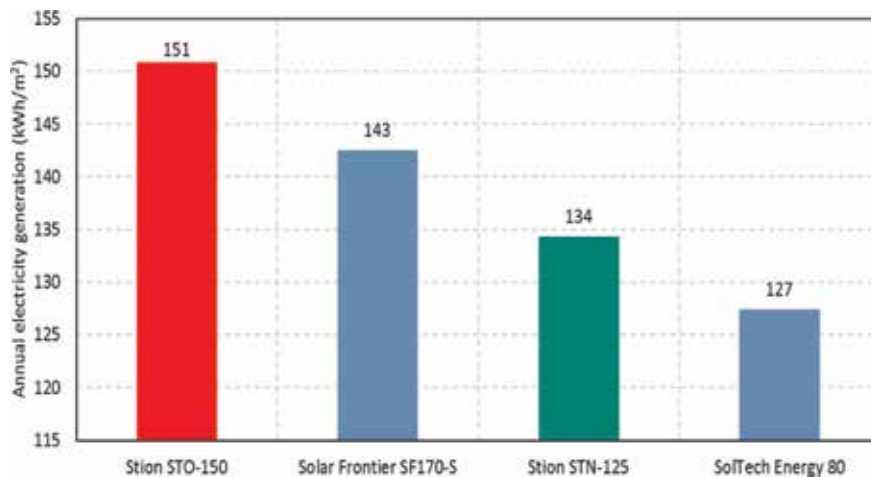


Figure 2. Electricity output per square meter of thin-film PV module installed on the roof. The optimal slope angle of the module was found to be 49 facing the south.

minimum of 7.5 (Stion STN-125) to a maximum of 15.3 /kWh (SolTech Energy 80). Thus, from the levelized cost of electricity viewpoint, Stion STN-125 is the best among the considered brands.

Figure 3 shows the accumulative cash flow of Stion STO-150 (of the best energy performance) and Stion STN-125 (of the best economic performance). Apparently, the installation cost of Stion STO-150 is 39% more than the initial cost of Stion STN-125 for the same available area of PV cells (which is in our case 100<sup>2</sup>m<sup>2</sup>).

In other words, by using Stion STO-150, the annual electricity is increased by 12%, and the initial cost of such a system is increased by 39% in comparing to Stion STN-125 (see Figure 3). Hence, the preference of the decision-maker should be considered in order to select the most suitable PV brand, namely, either the brand of the best energy performance or the brand of the best economic performance.

Repeating the simulation for the module installed on the south-facing façade leads to the same conclusion. Explicitly, from an energy viewpoint, the Stion STO-150 thin film is the best brand among the considered brands. While from the economic viewpoint, Stion STN-125 thin film is the best brand among the considered brands.

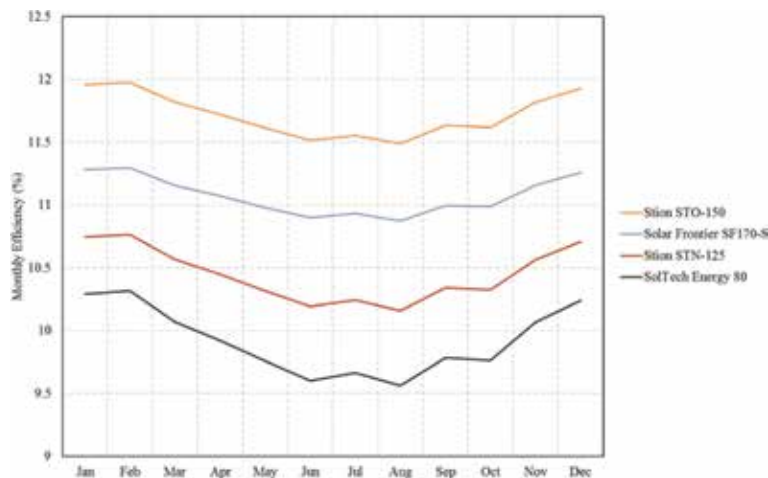


Figure 3. Monthly average efficiency of different brands of thin-film module at working conditions of Padiham, UK.

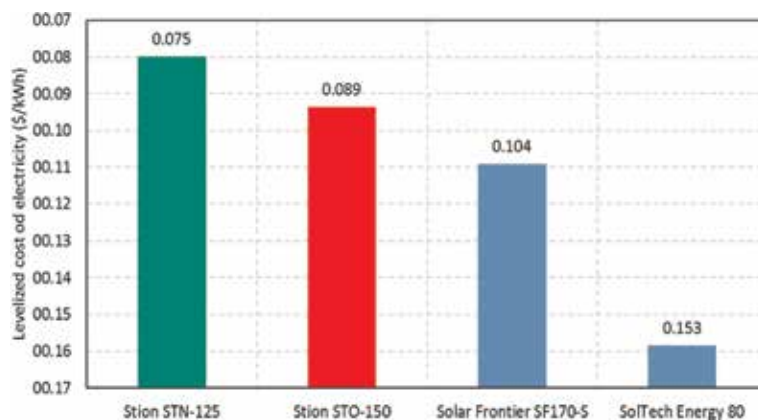


Figure 4. The levelized cost of electricity of different brands of thin-film module at working conditions of Padiham, UK.



Table 5 shows the comparison between two different thin-film PV module brands that are installed on the roof of the building and installed on the southern façade. As shown, modules that are installed on the roof can generate up to 31% more annual electricity as compared with the same modules installed on the façade. This can be attributed to the fact that a module on the roof receives more solar energy than a module installed on the façade. On the other hand, the greater solar radiation on the roof makes the temperature of modules that are installed on the roof slightly higher. Consequently, the average annual efficiency of the system installed on the façade will be slightly higher. However, the abundant amount of the solar energy on the roof, as compared with the façade, overcomes the improvement in the efficiency. So, as it was expected, installing a PV system on the roof is better than on the southern wall.

## 6.2 Polycrystalline module type

In this section, a comparison between 13 different brands of the polycrystalline PV module is presented. Recall that the selected brands were chosen based on the report prepared by Fraunhofer Institute for Solar Energy Systems, ISE [5].

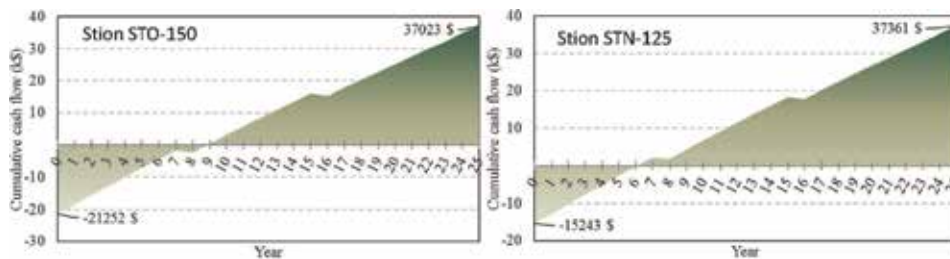


Figure 5. Accumulative cash flow of Stion STO-150 (on the left) and Stion STN-125 (on the right) at the current conditions in the UK.

Brand	Annual elect. (kWh/m <sup>2</sup> )	Annual efficiency (%)	LCOE ( /kWh)	Initial cost (\$/100 m <sup>2</sup> )	Payback time (year)
Stion STO-150	151	11.7	8.9	21,252	9
Stion STN-125	134	10.4	7.5	15,243	6
Difference	12%	13%	19%	39%	50%

Table 4. Comparing two thin-film modules of best energy and best economic performance.

	Annual elect. (kWh/m <sup>2</sup> )			Avg. annual efficiency (%)			LCOE ( /kWh)		
	Roof	Facade	Difference (%)	Roof	Facade	Difference (%)	Roof	Facade	Difference (%)
Stion STO-150	151	115	31	11.7	11.8	1	8.9	11.6	23
Stion STN-125	134	103	30	10.4	10.6	2	7.5	9.8	23

Table 5. Comparison between installing modules on the roof and on the south-façade

The annual electrical output per square meter of different brands of polycrystalline that are installed on the roof is illustrated in Figure 6. As shown, the annual electrical output per square meter of selected modules varies from a minimum of 162 to a maximum of 215 kWh/m<sup>2</sup> y. The optimal slope angle of the module was found to be 48° facing south.

As expected, simulations show that the efficiency of the polycrystalline PV modules during colder months is higher than those during the warmer months. The PV module voltage reduction causes efficiency reduction due to increasing the operating temperature of the module. Figure 7 shows that the efficiency of polycrystalline PV module ranged from 11.7% (Kyocera KD220GH-4FB2 in August) to 17.6% (Hanwha Solar One 310 in February).

Hence, from the energy viewpoint, Hanwha Solar One 310 module seems to be the best among the considered polycrystalline module brands.

In order to compare the different brands from the economic point of view, the levelized cost of electricity and the accumulative cash flow were determined for

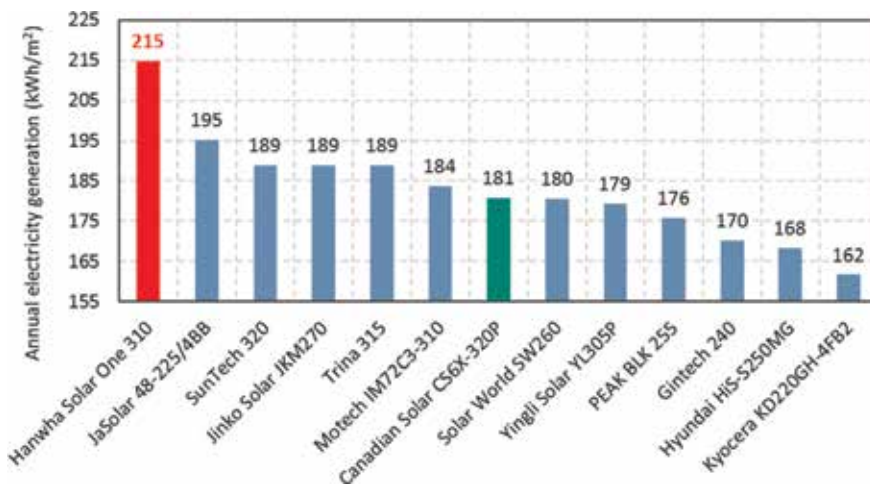


Figure 6.  
 Electrical output per square meter of polycrystalline PV module installed on the roof. The optimal slope angle of the module was found to be 48 facing south.

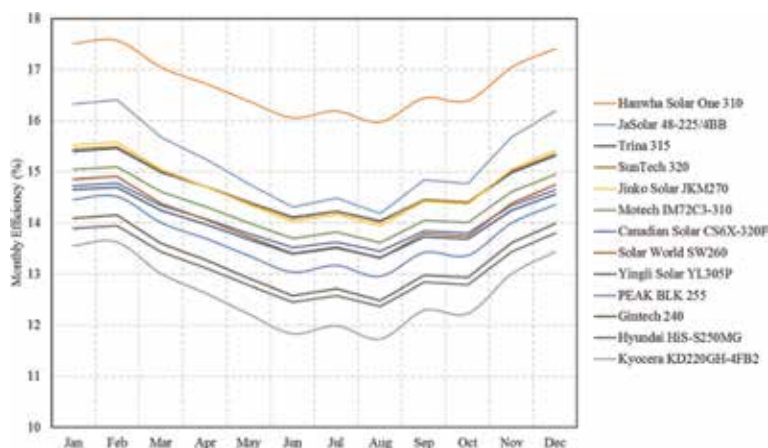
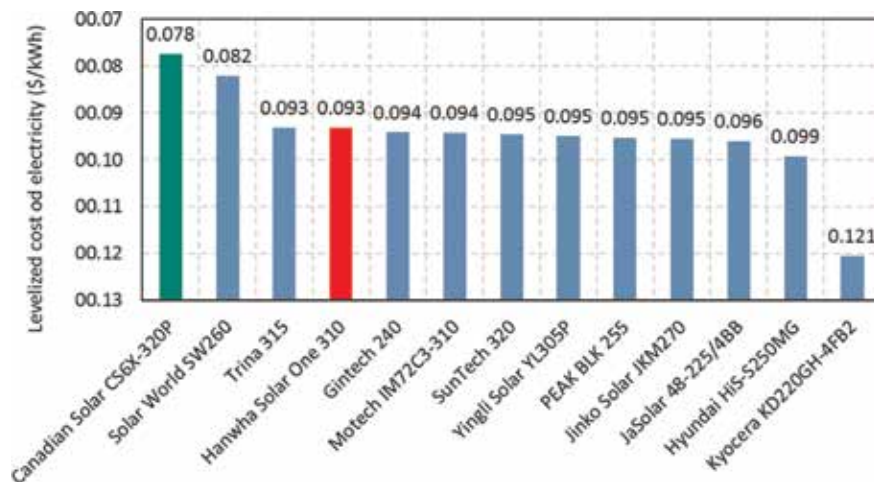


Figure 7.  
 Monthly average efficiency of different brands of the polycrystalline module at working conditions of Padiham, UK.

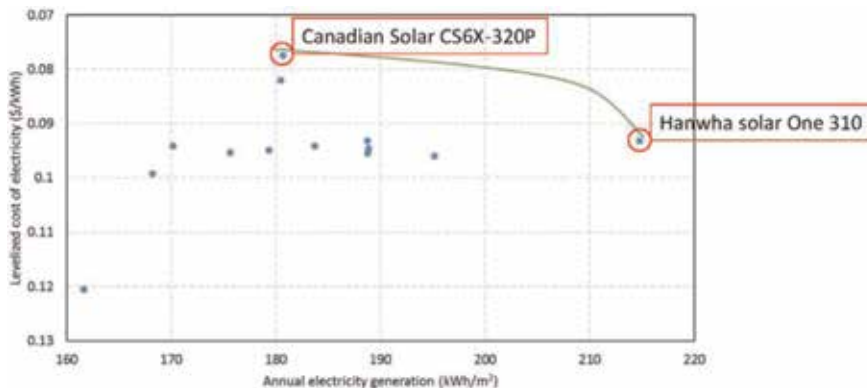
each brand taking into account the assumptions shown in Table 3. As shown in Figure 8, the levelized cost of electricity varies from a minimum of 7.8 (Canadian Solar CS6X-320P) to a maximum of 12.1/kWh (Kyocera KD220GH-4FB2).

Figure 9 shows the levelized cost of electricity versus the annual electricity generation per square meter of different polycrystalline brands. One can say that the annual electricity generation and levelized cost of electricity are somehow contradicting. As shown the Hanwha Solar One 310 seems to be the best from annual electricity generation viewpoint, while Canadian Solar CS6X-320P seems to be the best from levelized cost of electricity viewpoint.

Figure 10 shows the accumulative cash flow of Hanwha Solar One 310 (of the best energy performance) and Canadian Solar CS6X-320P (of the best economic performance). Apparently, the installation cost of Hanwha Solar One 310 is 61% more than the initial cost of Canadian Solar CS6X-320P for the same available area of PV cells (which is in our case assumed 100 m<sup>2</sup>). In another word, by using Hanwha Solar One 310, the annual electricity is increased by 19%, and the initial cost of such system is increased by 61% in comparison to Canadian Solar



The levelized cost of electricity of different brands of the polycrystalline module at working conditions of Padiham, UK.



The levelized cost of electricity versus annual electricity generation per square meter of different brands of the polycrystalline module at working conditions of Padiham, UK.

CS6X-320P (see Table 6). Hence, the preference of the decision-maker should be considered in order to select a suitable PV brand.

In order to investigate the potential of installing polycrystalline PV modules on the south-facing façade, the analyses were repeated for the modules installed on south-facing façade. The simulations show that a similar conclusion can be drawn with regard to modules installed on the roof. Namely, in the case of installing PV cell on the south-facing façade, among the considered brands (Table 1), the best polycrystalline brand from energy viewpoint is Hanwha Solar One 310, while Canadian Solar CS6X-320P seems to be the best brand from the economic view-point. Table 7 shows the comparison between the two different polycrystalline PV module brands installed on the roof of the building and installed on the south-facing façade. As shown, modules which are installed on the roof can generate 30% more electricity per year. This is due to the fact that the roof module receives more solar energy compared to the façade. Still, the temperature of modules installed on

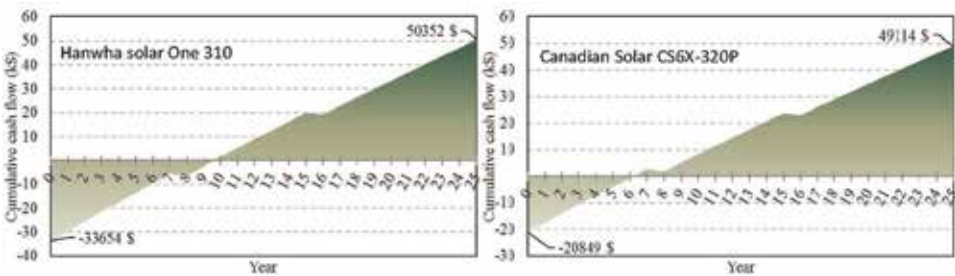


Figure 10.  
Accumulative cash flow of Hanwha solar one 310 (on the left) and Canadian solar CS6X-320P (on the right) at the current conditions in the UK.

	Annual electricity (kWh/m <sup>2</sup> )	Avg. annual efficiency (%)	LCOE ( /kWh)	Initial cost (\$/100 m <sup>2</sup> )	Payback time (year)
Hanwha Solar One 310	215	16.7	9.3	33,654	9.8
Canadian Solar CS6X-320P	181	14.0	7.8	20,849	6.2
difference	19%	19%	19%	61%	58%

Table 6.  
Comparing two polycrystalline modules of best energy and economic performance.

	Annual elect. (kWh/m <sup>2</sup> )			Avg. annual efficiency (%)			LCOE ( /kWh)		
	Roof	Facade	Difference (%)	Roof	Facade	Difference (%)	Roof	Facade	Difference (%)
Hanwha Solar One 310	215	166	30	16.7	17	2	9.3	12.1	23
Canadian Solar CS6X-320P	181	140	29	14.0	14.3	2	7.8	10.0	22

Table 7.  
Comparison between installing modules on the roof and on the south-facing façade

the roof will be slightly higher; the average annual efficiency of the system installed on façade will be slightly higher (Table 7). However, the improvement in efficiency due to the temperature effect on the façade system can be neglected as compared to the increased electricity output of the rooftop system.

### 6.3 Monocrystalline module type

In this section a comparison between 13 different brands of monocrystalline mentioned in the report prepared by Fraunhofer Institute for Solar Energy Systems, ISE, is shown [5].

Figure 11 illustrates the annual electrical output per square meter of different brands of monocrystalline installed on the roof. As shown, the annual electrical output per square meter of the selected modules varies from a minimum of 175 to a maximum of 226 kWh/m<sup>2</sup> y. The optimal slope angle of the module was found to be 48° facing the south. Thus, from the energy viewpoint, Motech XS72D3-320 module seems to be the best among the considered monocrystalline module brands.

As expected, simulations show that the efficiency of the monocrystalline PV modules during colder months is higher than those during the warmer months. The PV module voltage reduction causes efficiency reduction due to increasing the operating temperature of the module. Figure 12 shows that the efficiency of monocrystalline PV module ranged from 12.9% (Mitsubishi PV-MLE265HD2 in August) to 18.6% (Motech XS72D3-320 in February).

In order to compare the different brands from the economic point of view, the levelized cost of electricity was calculated for each brand. The economic analyses were carried out taking into account the assumptions shown in Table 3. Results illustrations in Figure 13 shows that the levelized cost of electricity varies from a minimum of 7.5 (Solar World SW325 XL) to a maximum of 12.2 /kWh (Panasonic N330).

Figure 14 shows the levelized cost of electricity versus the annual electricity generation per square meter of different monocrystalline brands. As shown, the annual electricity generation and levelized cost of electricity are somehow contradicting. Apparently, among the considered monocrystalline brands, Motech

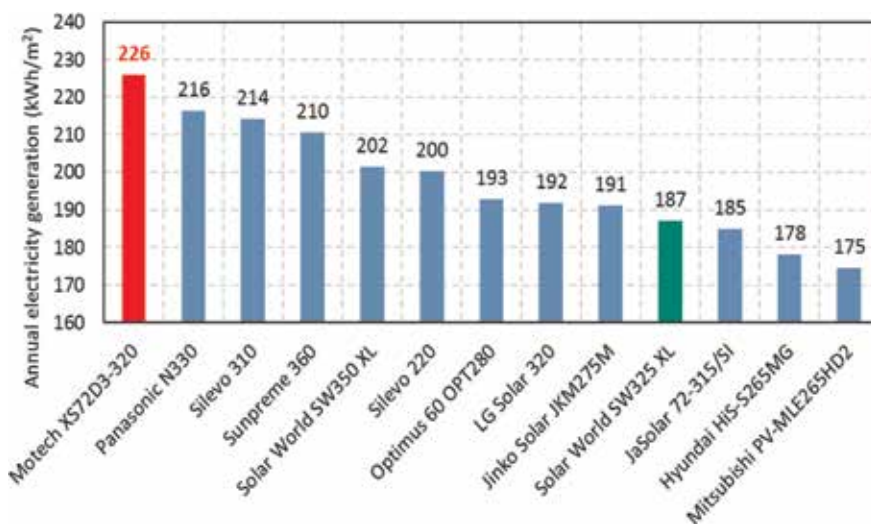


Figure 11. Electrical output per square meter of monocrystalline PV module installed on the roof. The optimal slope angle of the module was found to be 48° facing the south.



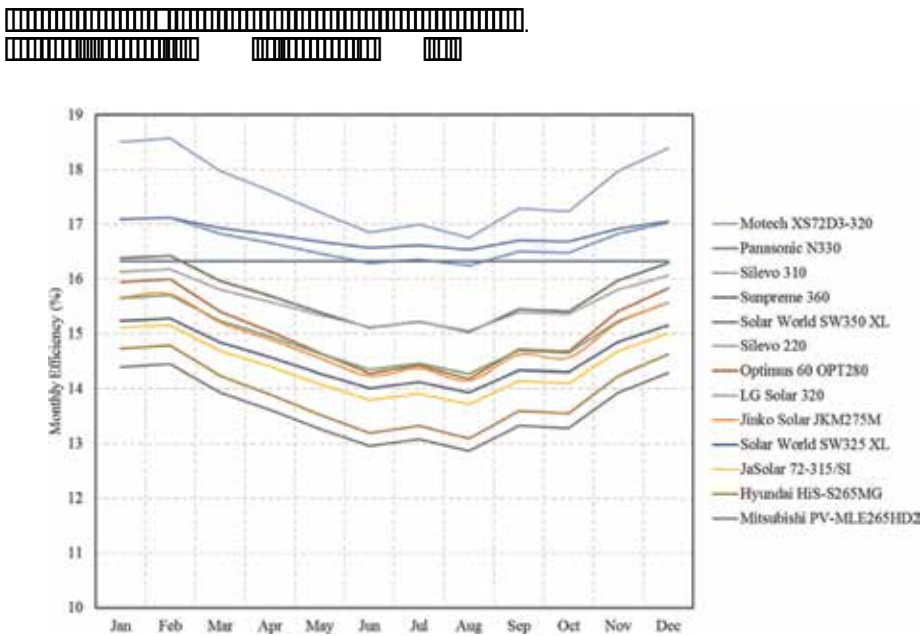


Figure 12.

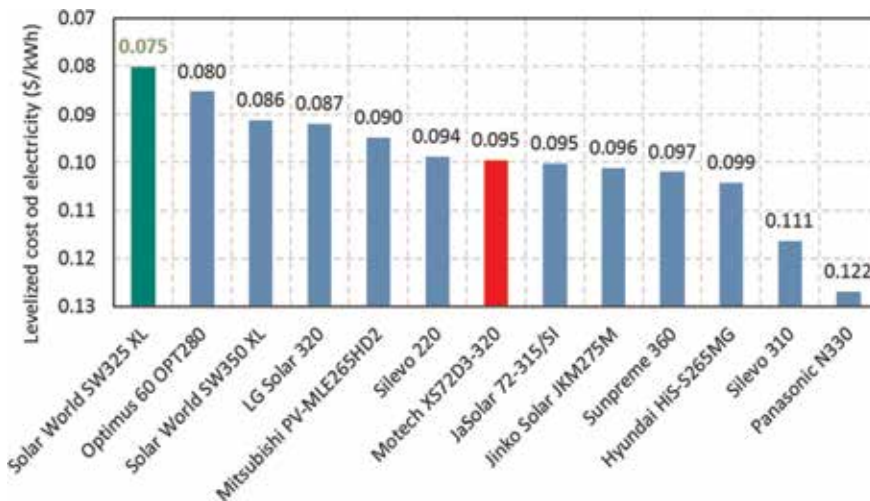
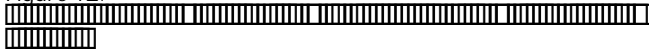
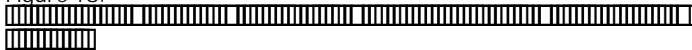


Figure 13.



XS72D3-320 and Solar World SW325 XL are the best from annual electricity generation and levelized cost of electricity, respectively.

Figure 15 shows the accumulative cash flow of Motech XS72D3-320 (of the best energy performance) and Solar World SW325 XL (of the best economic performance). Obviously, the installation cost of Motech XS72D3-320 is 71% more than the initial cost of Solar World SW325 XL for the same available area of PV cells (which is in our case assumed to be 100 m<sup>2</sup>).

In another word, as shown in Table 8, comparing to Solar World SW325 XL, using Motech XS72D3-320 results in increasing the annual electricity by 21% (positive), while the initial cost of such system is 71% higher (negative). Hence, the preference of the decision-maker should be considered in order to choose the most suitable PV brand.

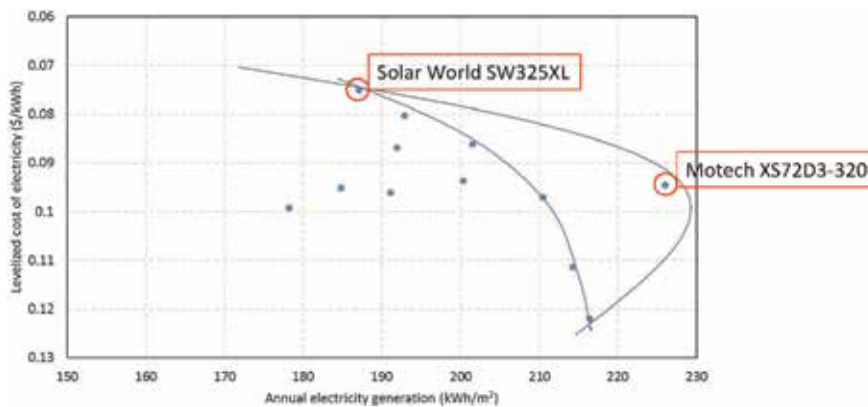


Figure 14. The levelized cost of electricity versus annual electricity generation per square meter of different brands of the monocrystalline module at working conditions of Padiham.

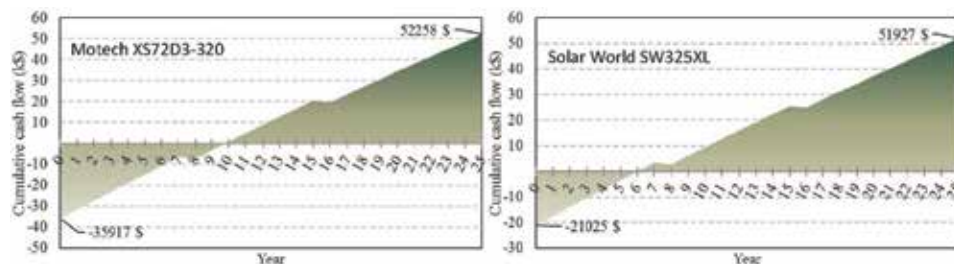


Figure 15. Accumulative cash flow of Motech XS72D3-320 (on the left) and solar world SW325 XL (on the right) at the current conditions in the UK.

	Annual elect. (kWh/m <sup>2</sup> )	Annual efficiency (%)	LCOE ( $\text{\$/kWh}$ )	Initial cost ( $\text{\$/100 m}^2$ )	Payback time (year)
Motech XS72D3-320	226	17.5	9.5	35,917	9.9
Solar World SW325 XL	187	14.5	7.5	21,025	6
Difference	21%	21%	27%	71%	65%

Table 8. Comparing two monocrystalline modules of best energy and economic performance.

In order to investigate the potential of installing a PV system on the south-facing façade, the analyses were repeated for the module installed on the southern façade. The simulations which show the same conclusions from the module's installation on the roof can be drawn. Namely, in the case of installing PV cell on the south-facing façade, among the considered brands (see table 1), the best monocrystalline brand from energy viewpoint is Motech XS72D3-320, while Solar World SW325 XL seems to be the best brand from the economic viewpoint. Table 9 shows the comparison between the two different monocrystalline PV module brands installed on the roof of the building or installed on the southern façade. Because the rooftop modules receive more solar radiation than those installed on the façade, the rooftop system generates 2930% more electricity per year. More solar energy leads to higher



module temperature, and consequently, the average annual efficiency of the system installed on the façade will be slightly higher. However, the difference in efficiency can be neglected as compared to the improved electricity output of the rooftop system.

6.4 Monocrystalline vs. polycrystalline vs. thin film

Figure 16 illustrates the results of the above simulations. The brands of the best energy performance and of the best economic performance for each module type have been specified. From the energy viewpoint, Motech XS72D3-320, Hanwha

	Annual elect. (kWh/m <sup>2</sup> )			Avg. annual efficiency (%)			LCOE ( /kWh)		
	Roof	Facade	Difference (%)	Roof	Facade	Difference (%)	Roof	Facade	Difference (%)
Motech XS72D3-320	226	175	29	17.5	17.9	2	9.5	12.2	22
Solar World SW325 XL	187	144	30	14.5	14.8	2	7.5	9.7	23

Table 9.



PV Type	Monocrystalline		Polycrystalline		Thin film	
Brand	Motech XS72D3-320	Solar World SW325XL	Hanwha Solar One 310	Canadian Solar CS6X-320P	Stion STO-150	Stion STN-125
Energy performance						
Economic performance						

Figure 16.

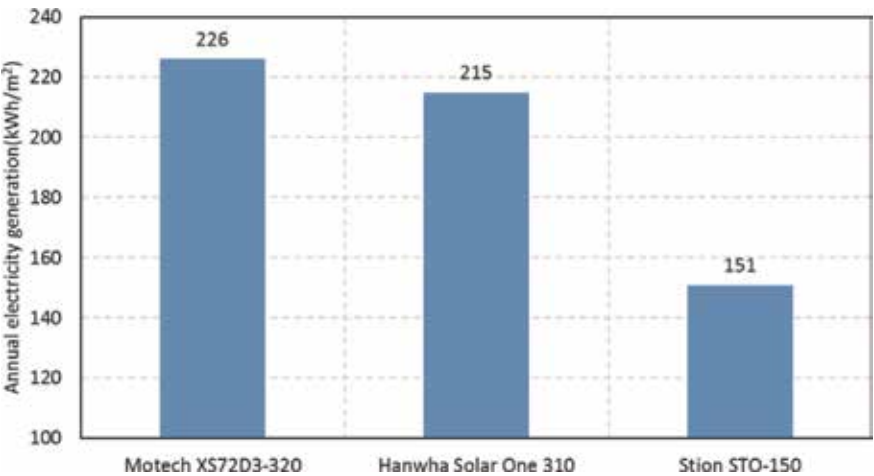
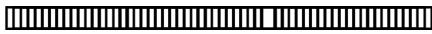


Figure 17.







Solar One 310, and Stion STO-150 represent the best brands for monocrystalline, polycrystalline, and thin film, respectively. While from the economic viewpoint, Solar World SW325XL, Canadian Solar CS6X-320P, and Stion STN-125 represent the best brand for monocrystalline, polycrystalline, and thin film, respectively. Hence, we do see a typical trade-off phenomenon between the environmental/energetic and the economic performance.

Figure 17 shows the comparison between electricity generation of Motech XS72D3-320, Hanwha Solar One 310, and Stion STO-150, which represent the best brands from an energy viewpoint for monocrystalline, polycrystalline, and thin film, respectively. As shown:

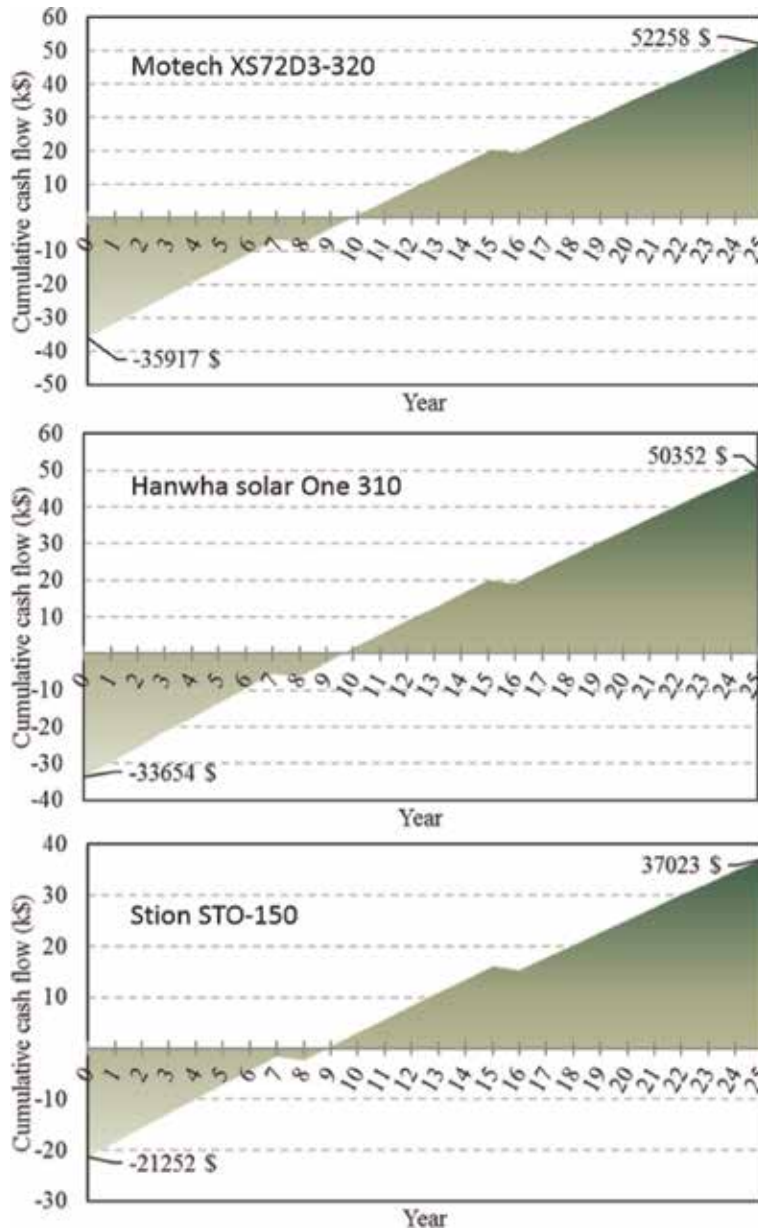


Figure 18.  
Economic comparison between different modules of the best energy output.

- Monocrystalline can give 5% more annual electricity than polycrystalline.
- Monocrystalline can give 50% more annual electricity than thin-film module.
- The polycrystalline module can give 42% more annual electricity than thin-film module.

From the economic viewpoint, it seems that the thin-film module has the best economic performance (see Figure 18).

Figure 19 shows the comparison between the accumulative cash flow of Solar World SW325XL, Canadian Solar CS6X-320P, and Stion STN-125, which represent

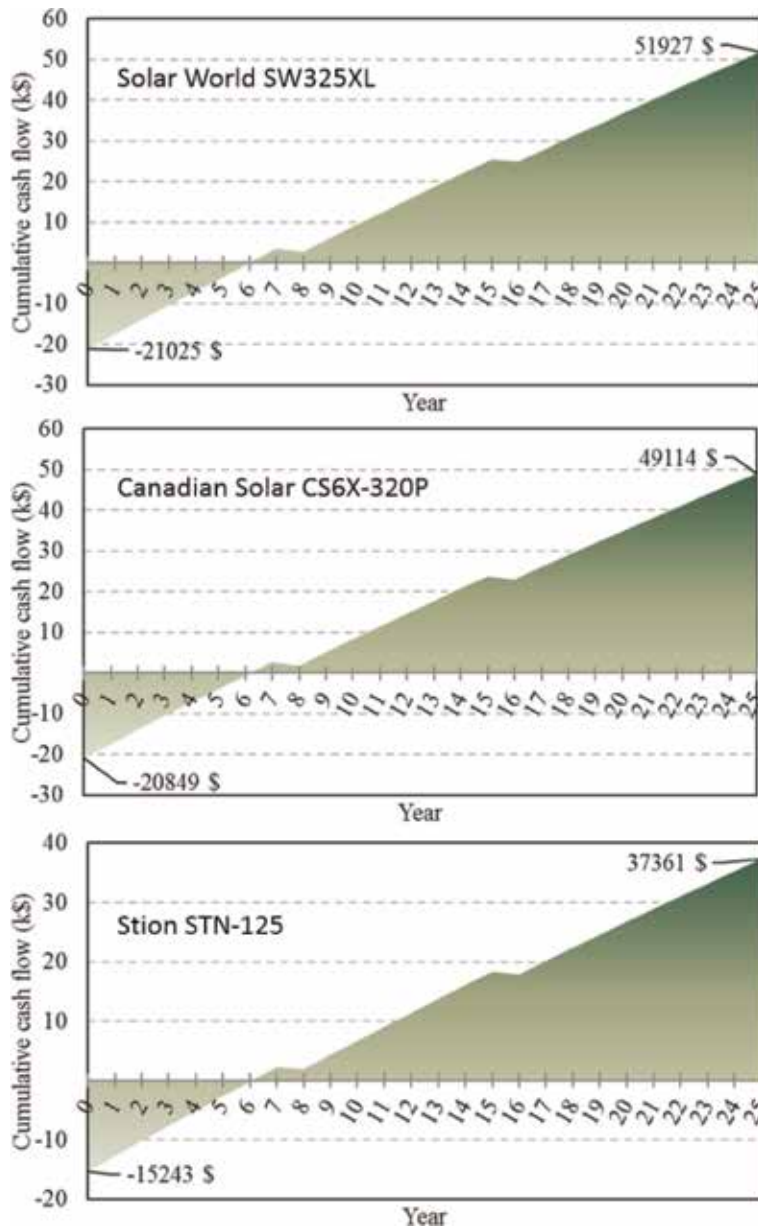


Figure 19.  
 Economic comparison between different modules of the best economic performance.

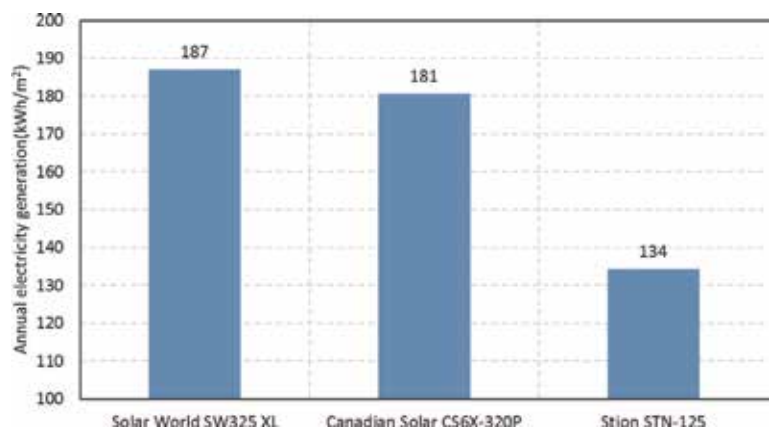


Figure 20.  
Energy comparison between different modules of the best economic performance.

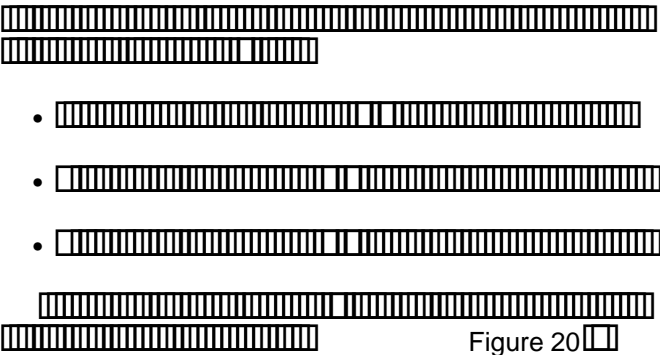
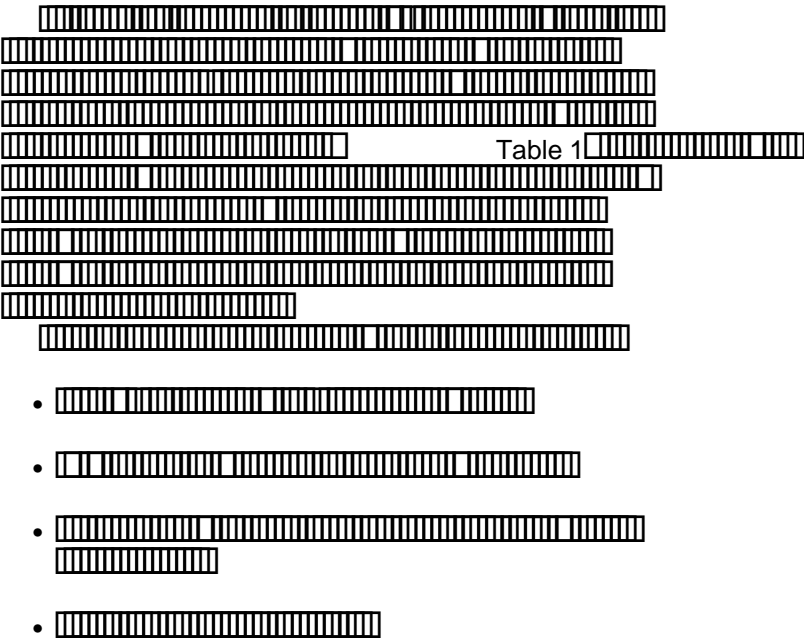


Figure 20

7. Conclusion



- 1.54 \$/W thin-film-based system
- 1.84 \$/W monocrystalline-based system
- The payback time of the systems varies from 6 to 10 years.

Another important conclusion that can be drawn from the results achieved in this work is that the energy and economic performance of a PV module are contradicting. In other words, for each module type, the brand that shows the best energy performance is not the same brand of the best economic performance. Therefore, the preference of the decision-maker should be considered as an essential factor before choosing the PV type and brand.

Comparing the results from different module types and brands show that:

- Motech XS72D3-320 which is a monocrystalline module shows the best energy performance compared to other monocrystalline brands, while Solar World SW325XL shows the best economic performance.
- Regarding polycrystalline module type, among the considered brands, Hanwha Solar One 310 and Canadian Solar CS6X-320P show the best energy and economic performance, respectively.
- Among the selected thin-film module brands, Stion STO-150 shows the best energy performance, while Stion STN-125 shows the best economic performance.

Finally, simulations indicate that monocrystalline module type shows the best energy performance, while thin-film module type shows the best economic performance at the current conditions in the UK.

## Acknowledgements


The authors are grateful to EC DREEAM (H2020-EeB-2015, GA 680511) project that is funded by the EC and supported by Chalmers Area of Advance Energy.

## Author details

Mohamad Kharseh\* and Holger Wallbaum  
Chalmers University of Technology, Gothenburg, Sweden

\*Address all correspondence to: [mohamad.kharseh@chalmers.se](mailto:mohamad.kharseh@chalmers.se)

## IntechOpen

© 2020 The Author(s). Licensee IntechOpen. Distributed under the terms of the Creative Commons Attribution - NonCommercial 4.0 License (<https://creativecommons.org/licenses/by-nc/4.0/>), which permits use, distribution and reproduction for non-commercial purposes, provided the original is properly cited. 

## References

- [1] Coyne D. World Oil 2018–2050: World Energy Annual Report (Part 2) [Internet]. 2018. Available from: <http://peakoilbarrel.com/world-oil-2018-2050-world-energy-annual-report-part-2/> [Accessed: 07-05-2019]
- [2] IEA. Global Energy & CO2 Status Report: The Latest Trends in Energy and Emissions in 2018. International Energy agency 2019. Available from: [www.iea.org/geco/renewables/](http://www.iea.org/geco/renewables/)
- [3] Jackson R, Le Quéré C, Andrew R, Canadell J, Peters G, Roy J, et al. Warning signs for stabilizing global CO2 emissions. *Environmental Research Letters*. 2017;12:110202
- [4] Moomaw W, Yamba F, Kamimoto M, Maurice L, Nyboer J, Urama K, et al. Introduction. In: IPCC Special Report on Renewable Energy Sources and Climate Change Mitigation. Cambridge, United Kingdom and New York, NY, USA: Cambridge University Press; 2011
- [5] Bilgili M. Hourly simulation and performance of solar electric-vapor compression refrigeration system. *Solar Energy*. 2011;85:2720-2731. DOI: 10.1016/j.solener.2011.08.013
- [6] Wrobel J, Sanabria Walter P, Schmitz G. Performance of a solar assisted air conditioning system at different locations. *Solar Energy*. 2013; 92:69-83. DOI: 10.1016/j.solener.2013.02.030
- [7] Nyholm E, Goop J, Odenberger M, Johnsson F. Solar photovoltaic-battery systems in Swedish households: Self-consumption and self-sufficiency. *Applied Energy*. 2016;183: 148-159. DOI: 10.1016/j.apenergy.2016.08.172
- [8] IRENA. Renewable Capacity Statistics 2019. International Renewable Energy Agency 2019. ISBN 978-92-9260-123-2
- [9] Taylor M, Daniel K, Ilaas A, So E. Renewable Power Generation Costs in 2014 [Internet]. 2015. Available from: [www.irena.org/documentdownloads/publications/irena\\_re\\_power\\_costs\\_2014\\_report.pdf](http://www.irena.org/documentdownloads/publications/irena_re_power_costs_2014_report.pdf) [Accessed: 08-06-2016]
- [10] Helen EH. Humphries. Evaluation of PV Systems in Gärdsten [thesis]. Göteborg: Chalmers University of Technology; 2013
- [11] Fraunhofer I. Photovoltaics Report [Internet]. 2016. Available from: <http://ecee.colorado.edu/ecen5009/Resources/Photovoltaics/Fraunhofer2016.pdf> [Accessed: 15-12-2016]
- [12] Al-Khawaja MJ. Determination and selecting the optimum thickness of insulation for buildings in hot countries by accounting for solar radiation. *Applied Thermal Engineering*. 2004;24: 2601-2610. DOI: 10.1016/j.applthermaleng.2004.03.019
- [13] Kharseh M, Wallbaum H. How adding a battery to a grid-connected photovoltaic system can increase its economic performance: A comparison of different scenarios. *Energies*. 2019; 12:19. DOI: 10.3390/en12010030
- [14] El Chaar L, Lamont LA. Global solar radiation: Multiple on-site assessments in Abu Dhabi, UAE. *Renewable Energy*. 2010;35:1596-1601. DOI: 10.1016/j.renene.2009.10.007
- [15] Basunia MA, Yoshiob H, Abec T. Simulation of solar radiation incident on horizontal and inclined surfaces. *Journal of Engineering Research*. 2012;27:27-35. DOI: 10.24200/tjer.vol9iss2pp27-35
- [16] Duffie JA, Beckman WA. Solar engineering of thermal processes. 4th ed. New Jersey: Wiley; 2006. p. 910. DOI: 10.1002/9781118671603

- [17] Yoon K, Yun G, Jeon J, Kim KS. Evaluation of hourly solar radiation on inclined surfaces at Seoul by photogrammetrical method. *Solar Energy*. 2014;100:203-216. DOI: 10.1016/j.solener.2013.11.011
- [18] Tukiainen M. Gaisma: World Sunrise, sunset, dawn and dusk times [Internet]. 2016. Available from: [www.gaisma.com/](http://www.gaisma.com/) [Accessed: 10-06-2016]
- [19] Al-Sabounchi AM, Yalyali SA, Al-Thani HA. Design and performance evaluation of a photovoltaic grid-connected system in hot weather conditions. *Renewable Energy*. 2013;53:71-78. DOI: 10.1016/j.renene.2012.10.039
- [20] Torres-Ramírez M, Nofuentes G, Silva JP, Silvestre S, Muñoz JV. Study on analytical modelling approaches to the performance of thin film PV modules in sunny inland climates. *Energy*. 2014;73:731-740. DOI: 10.1016/j.energy.2014.06.077
- [21] Dalenbäck J. Personam communication with Jan-Olof Dalenbäck, Professor in Building Services Engineering/Project manager CIT Energy Management AB. Jan-Olof. Dalenback@chalmers.se. 2017
- [22] Paudel AM, Sarper H. Economic analysis of a grid-connected commercial photovoltaic system at Colorado State University-Pueblo. *Energy*. 2013;52:289-296. DOI: 10.1016/j.energy.2013.01.052
- [23] Harder E, Gibson JM. The costs and benefits of large-scale solar photovoltaic power production in Abu Dhabi, United Arab Emirates. *Renewable Energy*. Shenzhen, Guangdong: JA Energy Co; 2011;36:789-796. DOI: 10.1016/j.renene.2010.08.006
- [24] Khalid A, Junaidi H. Study of economic viability of photovoltaic electric power for Quetta—Pakistan. *Renewable Energy*. 2013;50:253-258. DOI: 10.1016/j.renene.2012.06.040
- [25] Chandel M, Agrawal GD, Mathur S, Mathur A. Techno-economic analysis of solar photovoltaic power plant for garment zone of Jaipur city. *Case Studies in Thermal Engineering*. 2014;2:1-7. DOI: 10.1016/j.csite.2013.10.002
- [26] Kaplanis S, Kaplani E. Energy performance and degradation over 20 years performance of BP c-Si PV modules. *Simulation Modelling Practice and Theory*. 2011;19:1201-1211. DOI: 10.1016/j.simpat.2010.07.009
- [27] CIA. World Factsbook [Internet]. 2016. Available from: [www.cia.gov/library/publications/the-world-factbook/](http://www.cia.gov/library/publications/the-world-factbook/) [Accessed: 15-06-2016]
- [28] Skoczek A, Sample T, Dunlop ED. The results of performance measurements of field-aged crystalline silicon photovoltaic modules. *Progress in Photovoltaics: Research and Applications*. 2009;17:227-240. DOI: 10.1002/pip.874
- [29] Sánchez-Friera P, Piliouline M, Pelaez J, Carretero J, Sidrach de Cardona M. Analysis of degradation mechanisms of crystalline silicon PV modules after 12 years of operation in southern Europe. *Progress in Photovoltaics: Research and Applications*. 2011;19:658-666. DOI: 10.1002/pip.1083
- [30] Flowers ME, Smith MK, Parsekian AW, Boyuk DS, McGrath JK, Yates L. Climate impacts on the cost of solar energy. *Energy Policy*. 2016;94:264-273. DOI: 10.1016/j.enpol.2016.04.018
- [31] Eurostat Statistics Explained. Electricity Prices for Household Consumers [Internet]. 2016. Available from: [http://ec.europa.eu/eurostat/statistics-explained/index.php/File:Electricity\\_prices\\_for\\_household\\_consumers\\_second\\_half\\_2014\\_\(%C2%B9\)\\_\(EUR\\_per\\_kWh\)\\_YB15.png](http://ec.europa.eu/eurostat/statistics-explained/index.php/File:Electricity_prices_for_household_consumers_second_half_2014_(%C2%B9)_(EUR_per_kWh)_YB15.png) [Accessed: 15-04-2016]

[32]The Global Economy. Sweden: Real Interest Rate [Internet]. 2016. Available from: [http://www.theglobaleconomy.com/Sweden/Real\\_interest\\_rate/](http://www.theglobaleconomy.com/Sweden/Real_interest_rate/) [Accessed: 10-04-2016]

[33]Tom J, Alice L. Personal communication with JA Energy Co., Limited. Shenzhen, Guangdong: JA Energy Co; 2016

# Analysis of the Solar Tracking System for a Mobile Robot Prototype

Dario Guilherme Togninho, Alex Archela  
and Leonimer Flávio de Melo

## Abstract

Methods to detect the position of the sun and orientate a solar panel to its position are used in order to optimize the power generated. Two possible approaches are using light depending resistor (LDR) sensors, or using a GPS and equations that model the geometry between the Earth and the Sun. The main objective of this work is the proposal of a prototype system to optimize the harvesting of solar energy on photovoltaic panels. In this chapter, a mobile robot powered by a solar panel orientated by a LDR matrix and a GPS device was developed. The LDRs were used as the representation of vectors normal to a surface, where its sum resulted in the most lighted point. The GPS, in turn, provided location, date and time data, which were used in the calculations of the Sun azimuth and zenith, used to orientate the panel. The obtained results show that an orientated photovoltaic panel has a better performance when compared to a static panel. Possibilities and opportunities of research tend to grow for the next years with many possible works to be done in the future, both in mobile robotics and in other systems powered by photovoltaic panels.

**Keywords:** photovoltaics, embedded, robotics, tracking, optimization

## 1. Introduction

The use of photovoltaic energy is one of the most promising alternative energy resources. Given the high fossil fuel consumption and economic and environmental impact of other sources, solar energy has become one of the most viable alternatives, given its low impact and the fact that it is renewable.

The sun provides both thermal and light energies, and in order to convert its light energy to electrical energy, photovoltaic cells are used. The cells of the panel used in this work are made of silicon. According to [1], the efficiency of large-area commercial cells is about 24%, and the upper limit of the silicon solar cell efficiency is 29%. In order to optimize the energy generated by a photovoltaic panel, instead of using it in a fixed position, methods of tracking the position of the sun and adjusting the panel accordingly are used, so the sun rays are perpendicular to the photosensitive surface [2].



The works of [3, 4] show systems that use light-dependent resistor (LDR) as a way to obtain the sun position [5]. On the other hand, the work of [6] shows an approach that allows the control of a photovoltaic cell based on its temperature, and the work of [7] shows a different design to the motors that control the position of photovoltaic panels, in order to decrease the energy used by the drivers [8].

In this chapter a method that uses both GPS and a LDR matrix is described, with the solar panel attached to a mobile robot, using ARM microcontroller device (STM32F407). Also there is a comparison of both approaches, in order to find the most efficient position for the panel and the possible applications both in the field of mobile robots and in others.

## 2. Solar tracking approaches

Similar to the work of [9], in this paper a solar panel powers a mobile robot, but the main difference is that the panel on the robot of [9] has two motors to move it in the x-axis and y-axis [10]. The robot used in this work has a panel that moves in the  $\theta$ -axis (spherical coordinates), and the adjustment of the panel position consists in operating this  $\theta$ -axis motor and adjusting the position of the robot [11, 12].

### 2.1 LDR approach

The LDR matrix consists of a Styrofoam half-sphere with 20 LDRs attached on its surface, each one representing a coordinate of the three-dimensional space. Figure 1 shows a 3D model representing the LDR positions.

The LDRs have a voltage divider, and the microcontroller board reads its value. As light reaches the LDR, its resistance decreases. The design of the

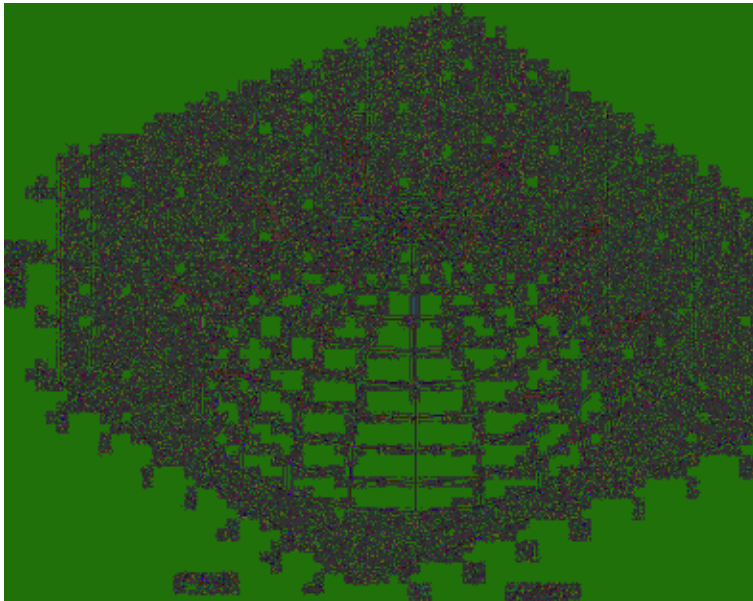


Figure 1.  
LDR surface 3D model, where the black arrows represent the position of the LDRs.

voltage divider was done in a way that its output voltage increases, so the more light reaches on the LDR, the higher the readings will be on the A/D converter.

However, the LDRs are sensitive not just to sunlight but also the environments reflected lights, and the A/D converter reads these lights with a small difference between them. In order to find which reading corresponds to the direct sunlight, a series of mathematical operations are performed, in a way that increases this difference.

When representing the LDRs in spherical coordinates  $\theta$ ,  $\phi$ ,  $r$ , we may change to the A/D converter read value. So, we can write the coordinates as  $L$ ,  $\theta$ ,  $\phi$ , where  $L$  is the LDR A/D reading on the corresponding  $\theta$  and  $\phi$  coordinates. Since the microcontroller A/D converter has a 12 bit resolution, its value range is seen on Eq. (1):

$$0 \leq L \leq 4095 \quad (1)$$

In order to find the most relevant readings, all of them are divided by the average and then squared. In this way, it is possible to obtain the most significant readings. These readings are represented by  $W$ ,  $\theta$ ,  $\phi$ , as seen on Eq. (2), where  $L_{avg}$  represents the average of the readings of all LDRs:

$$W = \frac{L}{L_{avg}} \quad (2)$$

The next step to obtain the position of the sun via the LDRs is to convert the spherical coordinates  $W$ ,  $\theta$ ,  $\phi$  to the Cartesian coordinate system  $x$ ,  $y$ ,  $z$  and then sum all elements. As a result, we obtain the coordinates of the position on the Styrofoam surface that represents a vector pointing towards the sunlight. The spherical coordinates to Cartesian equations can be seen on Eqs. (3)–(5):

$$x = W \sin \theta \cos \phi \quad (3)$$

$$y = W \sin \theta \sin \phi \quad (4)$$

$$z = W \cos \theta \quad (5)$$

Then, the result in spherical coordinates  $\theta_{final}$ ,  $\phi_{final}$ ,  $r_{final}$  is given by Eqs. (6)–(8), where  $x$ ,  $y$ , and  $z$  are the sum of the respective Cartesian coordinates of all LDRs:

$$r_{final} = \sqrt{x^2 + y^2 + z^2} \quad (6)$$

$$\theta_{final} = \cos^{-1} \frac{y}{x} \quad (7)$$

$$\phi_{final} = \sin^{-1} \frac{z}{\sqrt{x^2 + y^2 + z^2}} \quad (8)$$

Having the  $\theta_{final}$  and  $\phi_{final}$  coordinates, it is possible to adjust the position of the panel in such way it is perpendicular do the direct sunlight, using  $\theta_{final}$  to adjust the position of the robot and  $\phi_{final}$  to adjust the servomotor.

## 2.2 GPS approach

The use of the GPS device to obtain the position of the sun is based on a set of equations that return the coordinates of the sun in the horizontal coordinate system. These coordinates are the zenith angle, the altitude angle, and the azimuth angle, and all of them are seen **Figure 2**.

In this work, Eqs. (9)-(11) are the same from [9]:

$$z = \cos^{-1} \sin \delta \sin \phi + \cos \delta \cos \phi \cos H \quad (9)$$

$$90^\circ - z_n \quad (10)$$

$$A = \cos^{-1} \frac{\sin \delta \cos \phi - \sin z_n}{\cos \delta \cos \phi} \quad (11)$$

where  $z$ : incidence angle (or zenith angle); declination angle; altitude angle;  
 $\phi$ : local latitude;  $H$ : hour angle;  $A$ : Azimuth angle.

The declination angle is the angle between the equator and a line connecting the earth and the sun, and it varies according to the current date. The hour angle is the angle that depends on the current time, representing the position of the sun above the observer.

The GPS device used is shown **Figure 3**, and it provides the current time and location and, with these data, is possible to calculate the solar angles and correct the panel position accordingly.

It sends data on an interval of 1 second. The data received is a string that uses National Marine Electronics Association (NMEA) specification. The string contains coded phrases, and each phrase contains a specific set of information. Among the phrases, there is information containing the current location, time, and date. **Figure 4** shows an example of all phrases received.

The first phrase, being the one with the code \$GPRMC, contains all the information required to obtain the current position of the sun. Commas separate each part of the data. After the code, the first number is 134759.00, which represents the time 13h47min59s. The second number is 2319.68361 followed by the letter S, which

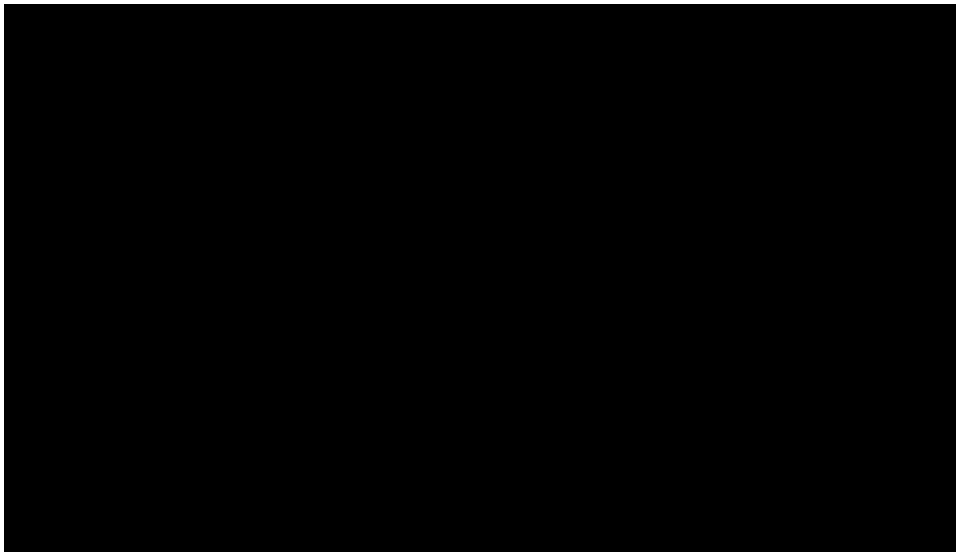


**Figure 2.**  
Azimuth and altitude angle of the sun (adapted from [6]).

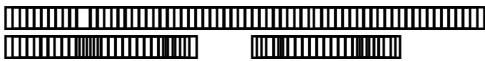


Figure 3.

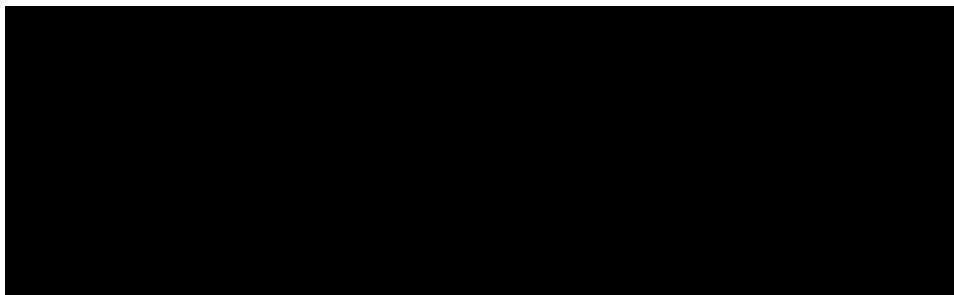


Figure 4.



represents south latitude  $23^{\circ}1,968,361$ . After that is the number representing the longitude followed by the letter W, which stands for west, so the longitude is  $51^{\circ}1215109$  West. The next piece of information, which is 0.019, is the current speed over the surface in knots, followed by the number 170518, which stands for the date, in this case meaning May 17th of 2018.

### 3. Implementation

A set of PWM signals drive the motors of the robot, and its speed is proportional to the duty cycle used. The duty cycle in turn is proportional to the difference between the direction of the robot and the direction of the sun. A picture of the robot is seen in Figure 5.

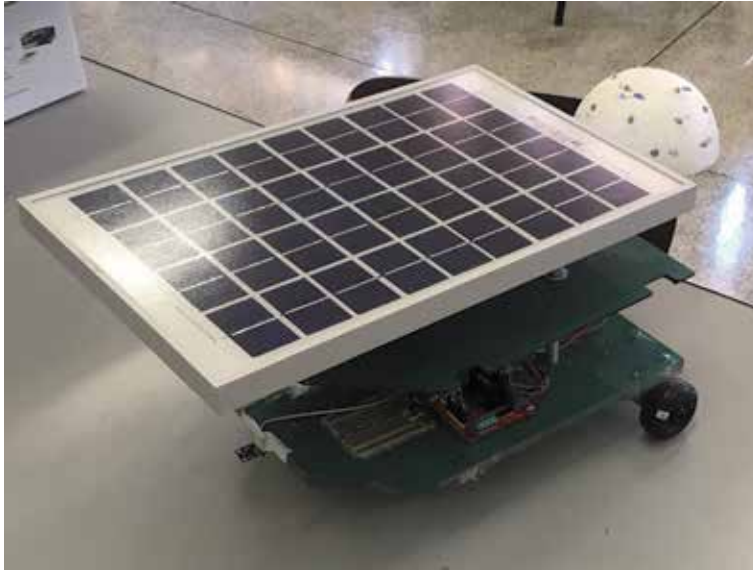


Figure 5.  
Picture of the mobile robot.

This difference is obtained calculating the Euclidian distance between the obtained position of the sun and the direction of either the front or the back of the robot (whichever is the nearest one) and minimizing it. As this difference is calculated using unit vectors, its range, as seen on Eq. (12), is never higher than 2:

$$0 \leq d \leq 2 \quad (12)$$

Sod is the maximum possible distance between the position of the robot and the position of the sun; therefore,  $d = 2$  implies a maximum use of the motors to correct the position of the robot, and  $d = 0$  means the robot is at the desired position.

However, as a control method,  $d = 0$  is not used as a parameter to determine if the desired position is achieved, for it is an ideal situation. Instead, a value close to 0 is used. So, for example, a possible condition to consider that the robot is in the correct position is to consider  $d < 0.01$ .

Sections 3.1 and 3.2 have a detailed description of each approach used to detect the direction of the sun, and Figure 6 contains a block diagram of the system.

### 3.1 LDR implementation

A half-sphere of Styrofoam was used to arrange the LDRs symmetrically, and the position of each LDR was chosen based on the manufacturing marks on its surface, having a total of 20 positions. All LDRs had a common terminal connected to a voltage source, and the other ends were connected to a multiplexer circuit. This multiplexer circuit is connected to the microcontroller, which selects the LDR and also reads its analogic value.

After the microcontroller calculates the position of the sun, it sends a signal to the motors of the mobile robot, to adjust its position in a way that its front or its back faces the sun and to the servomotor to adjust it to the proper inclination. The decision of if it is either the front or the back of the robot that should face the sun is based on which of these sides are closer to sunlight, in order to minimize the motion of the robot.

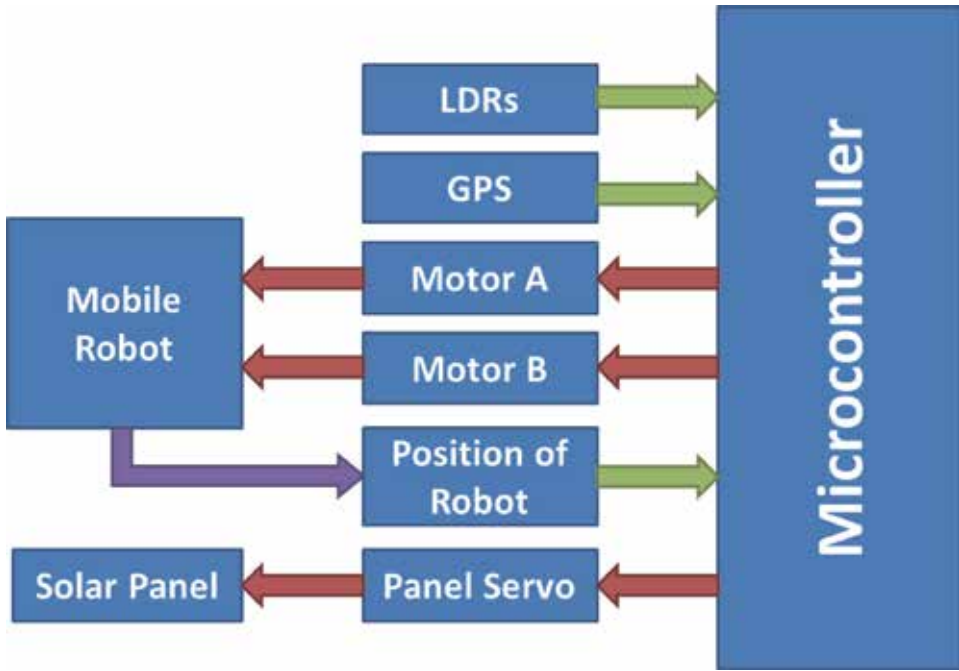
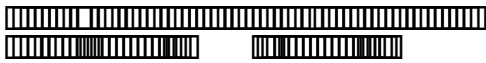


Figure 6.

The signal sent to the motors of the robot, as said in the beginning of Section 3, is a PWM signal, proportional to the Euclidian distance in the x-y plane of the position of the sun and the front, or back, of the robot, which is seen in Eq. (13):

$$d_{ldr} = \cos^2 \theta_{final} \sin^2 \theta_{final} y_{robot}^2 \quad (13)$$

The value of  $y_{robot}$  is either 1, if the sun is closer to the front of the robot, or -1, if the sun is closer to the back of the robot. As  $d_{ldr}$  gets closer to 0, it means the robot is getting closer to the direction of the sun.

### 3.2 GPS implementation

An electronic GPS device was used to obtain the required data to calculate the position of the sun, these data being latitude, longitude, day, month, year, hour, and minute. In addition, an electronic compass was used to obtain the angle the front of the robot formed with the north direction.

In order to keep the same reference as the LDR approach, the compass returns  $90^\circ$  when the front of the robot faces north and  $-90^\circ$  when its back faces north. The value of the zenith angle is used as a signal in the servomotor to adjust the inclination of the solar panel. To make the robot face the sun, the Euclidian distance between its front or its back, depending on which one is closer, and the azimuth of the sun must be minimized. Eq. (14) returns this distance, where  $\theta_n$  is the angle of the north direction and the robot:

$$d_{gps} = \cos^2 \theta_n \sin^2 \theta_n y_{robot}^2 \quad (14)$$

As in Section 3.1, the value of  $\theta_{\text{robot}}$  is either 1, if the sun is closer to the front of the robot, or -1, if the sun is closer to the back of the robot. As  $\theta_{\text{gross}}$  gets closer to 0, it means the direction of the robot is getting closer to the direction of the sun.

## 4. Results

### 4.1 LDR results

The preliminary tests on the LDR matrix were done in a darkroom with a flashlight. Figure 7 shows a picture of the position that was tested.

Then, with each LDR connected to the A/D converter, the data were collected and processed in order to obtain the light position on the surface. Table 1, written in the color red are the values read by the A/D converter, with the range mentioned on Eq. (1), for each LDR on its respective position. Figure 7, and NA (not applicable) represents the positions where there are no LDRs.

Then, the values from Table 1 are used as argument to Eq. (2), and as the next step, Eqs. (3)(8) are used.

Using the data of Table 1, the average is calculated, and the value, 1789.5 is obtained. So, all values in Table 1 below 1789.5 will become 0, and the remaining ones will be subtracted and then squared.

The sum of these values as vectors equals the resulting position,  $(\theta_{\text{final}}, \phi_{\text{final}})$ , which is seen as the blue arrow in Figure 8. The spherical coordinates obtained are  $(24.9525038, 55.2597, 44.2222)$ . However, in Figure 8, the coordinate was reduced in order to fit in the figure.

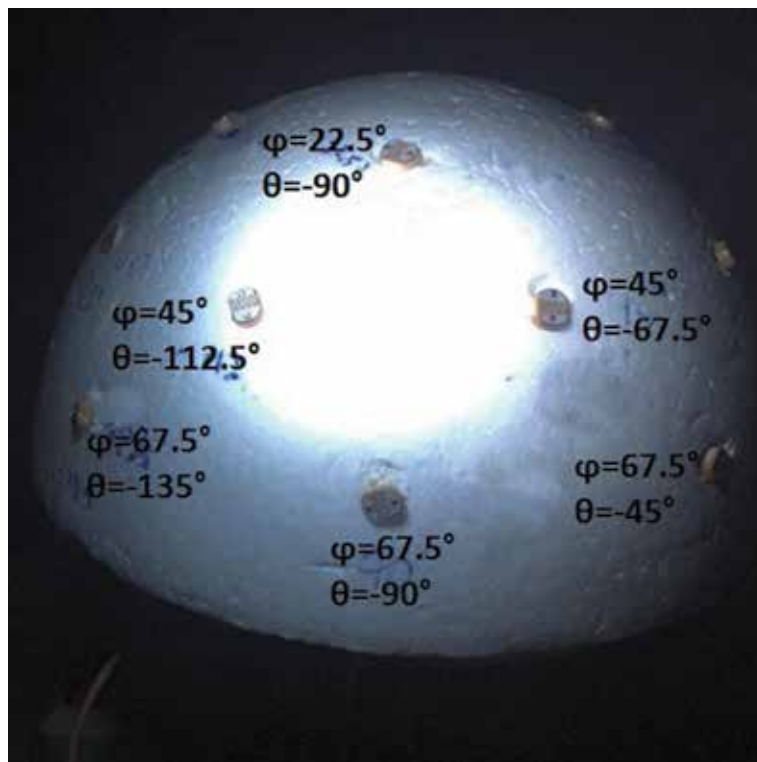
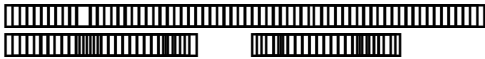


Figure 7.  
Photo of the first LDR sample with the coordinate of each LDR.





L ,			
LDR spherical coordinates	22:5	45	67:5
0°	2580	NA	840
225°	NA	481	NA
45°	NA	NA	429
67:5°	NA	361	NA
90°	914	NA	281
1125°	NA	292	NA
135°	NA	NA	154
1575°	NA	1673	NA
180°	2647	NA	1151
2025°	NA	3080	NA
225°	NA	NA	2478
247:5°	NA	3674	NA
270°	3616	NA	3433
2925°	NA	3668	NA
315°	NA	NA	2371
337:5°	NA	1667	NA

Table 1.

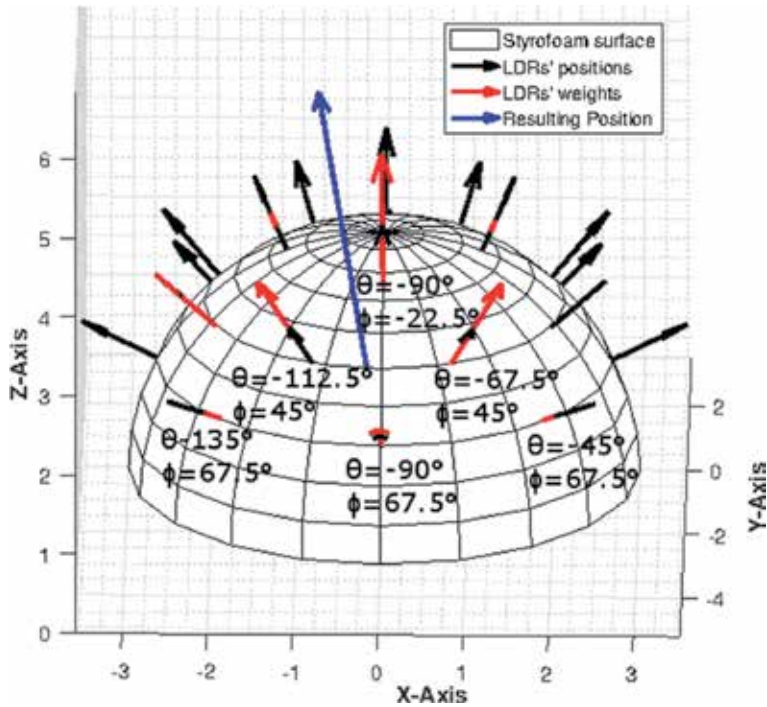


Figure 8.





Table 2 shows a set of 10 samples of Figure 7 on a 1 second interval, in which  $n = 1$  is the sample plotted in Figure 8. The table also includes the mean value of the samples and the standard deviation.

#### 4.2 GPS results

The GPS was tested under the following conditions:

Local: Londrina State University

Time: 13h48min

Sample time: 1 s

The GPS device received its fix data in the default interval of 1 second, and for each sample, an altitude angle and an azimuth angle were calculated. Table 3 shows the solar angle data and its mean values and standard deviations.

#### 4.3 Power results

Three test scenarios were executed. One is where the solar panel is fixed and the other two where the sun is tracked, one using LDR and the other using the GPS. The sampling period was 5 minutes.

In Figure 9 it is possible to observe the power generated by the panel on each scenario. The LDR and the GPS approaches have shown a very similar performance compared to each other, and both of them demonstrated to be much better than a fixed panel, having a gain of approximately 30%. The yellow line in the figure represents what would be the ideal maximum generated power by the panel,

Sample time (seconds)	coordinate [°]	coordinate [°]
1	38.555257	97.442222
2	38.422000	99.008884
3	38.570818	97.637040
4	38.551388	97.037137
5	38.575064	98.695924
6	38.503982	98.473986
7	38.545190	100.300662
8	38.470601	96.550539
9	38.586206	97.503065
10	38.445780	98.427292
Mean [°]	38.524916	
Std. deviation of [°]	0.068990	
Mean [°]	97.781321	
Std. deviation of [°]	0.855672	

Table 2.  
LDR samples over 10 s.

Sample time (seconds)	Altitude $[\circ]$	Azimuth A $[\circ]$
1	42.092760	28.719862
2	42.095466	28.704564
3	42.098172	28.689464
4	42.100877	28.674137
5	42.101605	28.714010
6	42.090841	28.697598
7	42.096462	28.700248
8	42.095976	28.684667
9	42.097934	28.675514
10	42.097912	28.675200
Mean $[\circ]$	42.096819	
std. deviation of $[\circ]$	0.003493	
Mean $\square[\circ]$	28.697007	
std. deviation of $\square[\circ]$	0.019659	

Table 3.  
GPS samples over 10 seconds.

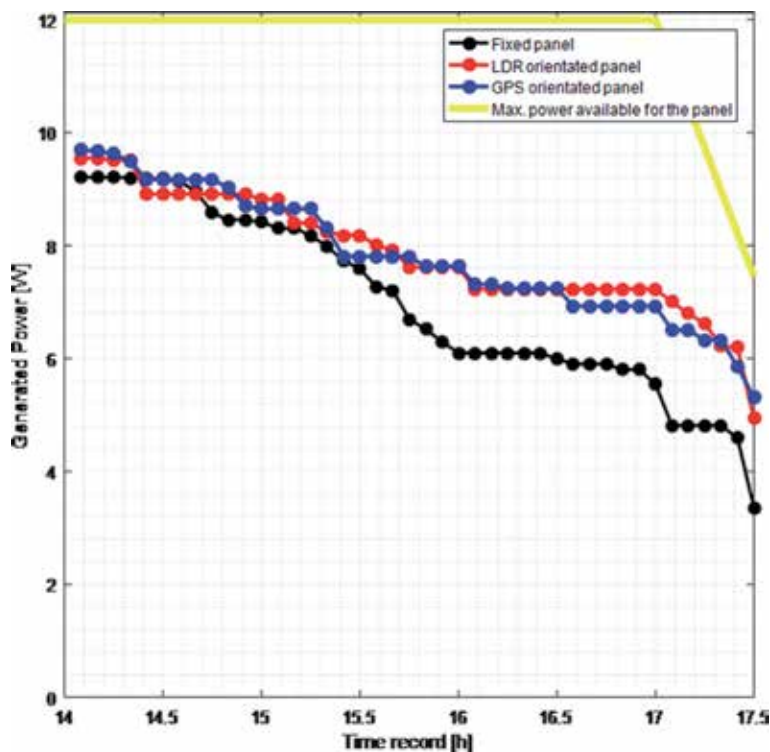


Figure 9.  
Power samples of the three tested scenarios.

considering the average solar irradiation nearby the site and the surface area of the panel. The LDR approach as the GPS has shown an efficiency of 80% compared to the ideal maximum power.

## 5. Conclusion

During the data collection, the LDR matrix has showed to be very sensitive to noise, so it presented a higher deviation. On the other hand, the GPS data had a much lower deviation. However, during the data collection, it took a certain amount of time to get a fix and obtain the current date, time, and location.

Besides the solar panel orientation, i.e., for applications in the mobile robotics, the GPS device provides navigation data that may be useful, which is an advantage. However, if the device takes too long to get a fix or loses the fix, the data will be null or delayed. So, in order for a mobile robot to obtain full-time orientation, both the GPS and LDR approaches may be used together.

For other applications, such as a panel on a fixed position, the latitude and longitude are fixed, so there is no need for a GPS device, just a real-time clock (RTC) device, which eliminates the GPS fix time issue and also has a lower cost compared to the LDR approach.


Having all things considered, the LDR is a low-cost method to track the position of the sun; however, it is more affected by noise. The sun-earth equations have shown problems only when depending of a GPS device to provide data; otherwise, it is the most precise approach.

## Author details

Dario Guilherme Toginho, Alex Archela and Leonimer Flávio de Melo\*  
State University of Londrina, Londrina, PR, Brazil

\*Address all correspondence to: [leonimer@uel.br](mailto:leonimer@uel.br)

## IntechOpen

© 2020 The Author(s). Licensee IntechOpen. Distributed under the terms of the Creative Commons Attribution - NonCommercial 4.0 License (<https://creativecommons.org/licenses/by-nc/4.0/>), which permits use, distribution and reproduction for non-commercial purposes, provided the original is properly cited. 



## References

- [1] Blakers A, Zin N, McIntosh KR, Fong K. High efficiency silicon solar cells. *Energy Procedia*. 2013;33:1-10
- [2] Fedor P, Perduková D. Use of fuzzy logic for design and control of nonlinear MIMO systems. In: Ramakrishnan S, editor. *Modern Fuzzy Control Systems and Its Applications*. London, UK: IntechOpen; 2017. DOI: 10.5772/68050
- [3] Mustafa FI, Al-Ammri AS, Ahmad FF. Direct and indirect sensing two-axis solar tracking system. In: 8th International Renewable Energy Congress (IREC). 2017. pp. 1-4
- [4] Mustafa FI, Shakir S, Mustafa FF, Naiyf AT. Simple design and implementation of solar tracking system two axis with four sensors for Baghdad city. In: 9th International Renewable Energy Congress (IREC). 2018. pp. 1-5
- [5] Ikedi C. Experimental study of current-voltage characteristics for fixed and solar tracking photovoltaics systems. In: Prabaharan N, Rosen MA, Campana PE, editors. *Recent Developments in Photovoltaic Materials and Devices*. London, UK: IntechOpen; 2019. DOI: 10.5772/intechopen.79710
- [6] da Rocha NMM, Passos JC. MPPT method based on temperature control of the photovoltaic cells. In: 12th IEEE International Conference on Industry Applications (INDUSCON). 2016. pp. 1-8
- [7] Kuhn VN, Gonzatti F, Franchi D, Miotto M, Camargo MN, Farret FA. Hybrid motor driver for solar tracking system. In: 12th IEEE International Conference on Industry Applications (INDUSCON). 2016. pp. 1-6
- [8] Chin CS. Model-based simulation of an intelligent microprocessor-based standalone solar tracking system. In: Katsikis VN, editor. *MATLAB A Fundamental Tool for Scientific Computing and Engineering Applications*. Vol. 3. London, UK: IntechOpen; 2012. DOI: 10.5772/46458
- [9] Fei Y, Lv H. Design of the solar-driven module on modular mobile robot. In: 19th International Conference on Mechatronics and Machine Vision in Practice (M2VIP). 2012. pp. 470-473
- [10] Milea L, Zafiu A, Oltu O, Dascalu M. Theory, algorithms and applications for solar panel MPP tracking. In: Manyala R, editor. *Solar Collectors and Panels, Theory and Applications*. London, UK: IntechOpen; 2010. DOI: 10.5772/10337
- [11] Zhan TS, Lin WM, Tsai MH, Wang GS. Design and implementation of the dual-axis solar tracking system. In: IEEE 37th Annual Computer Software and Applications Conference. 2013. pp. 276-277
- [12] Engin D, Engin M. Sensors and digital signal conditioning in mechatronic systems. In: Yildirim S, editor. *Design, Control and Applications of Mechatronic Systems in Engineering*. London, UK: IntechOpen; 2017. DOI: 10.5772/67986



---

## Section 2

# Lifetime and Reliability Issues

---



# Some Reliability Aspects of Photovoltaic Modules

Titu-Marius I. B jenescu

## Abstract

Solar cells and photovoltaic modules are energy conversion components that produce electricity when exposed to light. The originality of photovoltaic energy as we understand it here is to directly transform light into electricity. Thin-film silicon in particular is better at low and diffuse illuminations and decreases less than the crystalline when the temperature increases while reducing the amount of material and manufacturing costs. However, the quality of the material and the efficiency of the conversion limit their use on a large scale. If the light absorption of the ultra-thin layers of the active material could be improved, this would lead to low recombination currents, higher open-circuit voltages and higher conversion efficiency. PV systems often communicate with utilities, aggregators and other grid operators over the public Internet, so the power system attack surface has significantly expanded. Solar energy systems are equipped with a range of grid-support functions, which if controlled or programmed improperly present a risk of power system disturbances.

Keywords: climatic stress factors, useful life, PV module failure, LCoE, EVA, PID, LID, defects, MWT, field failures, failure analysis, influence of temperature, encapsulants, perspectives, conclusions

## 1. Introduction

Discovered in 1839 by Antoine Becquerel [1], the photovoltaic effect allows the transformation of light energy into electricity. This principle is based on semiconductor technology. It consists in using photons to release electrons and create a potential difference between the cells terminals that generate a direct electrical current. All photovoltaic devices have a p-n junction in a semiconductor through which PV voltage develops. Production costs have been reduced by about 20% [2] each time the production volume has doubled. The properties of copper oxide for rectifying alternating current were discovered for some 100 years.

Gravure printing electricity appeared in 1930 with copper oxide cells and then selenium. However, it was not until 1954, with the construction of the first silicon photovoltaic cells in the Bell Telephone company laboratories, that we saw the possibility of supplying energy. Very quickly they were used to power space vehicles in the 1960s with space satellite equipment. Then, from 1970, the first land uses the electrification of isolated sites. During the 1980s, terrestrial photovoltaic technology made steady progress with the installation of several power plants of a few megawatts and even became familiar to consumers through many low-power



products using it: watches, calculators, radio and weather beacons, solar pumps and refrigerators. In the early 1990s, when solar developers announced the price per kilowatt hour (kWh) of photovoltaic energy, everyone laughed: we were ten times above the price of electricity purchased from classical generators. Fifteen years later, the costs have been cut by two or three, and no one is laughing anymore. Philippe Malbranche, a specialist in solar technologies at the Atomic Energy Commission (AEC), made it clear: In the long run, solar energy will prevail. Not because of ideological choice or concern for the environment, but because it will be the most economically profitable.

When we look at the energy that comes directly from the sun per  $\text{m}^2$ , it is 1000 2000 times more, i.e. 1 2 MWh per square meter per year! About 70% of this energy can be recovered in the form of heat thanks to solar thermal energy: this represents a resource of almost 1 MWh/ $\text{m}^2$ /year. In the case of photovoltaics, with conversion efficiencies of 10 20%, 100 200 kWh/ $\text{m}^2$ /year can be recovered directly in electrical form.

When a photon interacts with an electron involved in chemical bonds between atoms, it moves it from its equilibrium level (occupied level of the valence band) to a higher excited level of energy (unoccupied level of the conduction band). The electron then returns to equilibrium at its initial level by re-emitting the absorbed energy, which can be in the form of heat, light and chemical energy as in the case of photosynthesis or electrical energy if it can be recovered. In the latter case, we are talking about photovoltaic energy. In the case of a p-n junction of a semiconductor, an electron hole pair is created under the action of a photon, the hole being the equivalent of a positive charge. Under the action of the electric field this created at the n-p interface, there is separation of charges and creation of a photocurrent.

At the beginning of studies on the chemistry of plasma-assisted deposition, the growth of deposition was atom by atom. One of the major discoveries was to increase the growth rate of the deposit by generating small clusters in the vapor phase before depositing them on the surface. In this case, silicon nanocrystals are obtained within an amorphous matrix. This technology is currently in full expansion and corresponds to significant yield increase prospects. Although the deposition of each layer requires the control of delicate chemical problems, we now know how to produce and market this type of product on a large scale.

### 1.1 New thin-film dies: the cadmium telluride dies

The interest in this technology and this explains its success is that the deposition processes are extremely fast (from a few seconds to a few minutes), which makes it possible to achieve high production rates and thus reduces production costs (less than one dollar per watt). The arrival of this technology marked a real breakthrough in the competitiveness of photovoltaic.

The copper indium diselenide die (CIS die) is expected to develop significantly as cells based on the same thin-film system achieve yields of more than 20% in the laboratory. Industrial production modules have yields of up to 13%, but this nascent production (1.7% of the market) is in full development. These cells use polycrystalline materials, filled with defects, and grain joints, materials that photovoltaic specialists would not have paid the slightest interest a few years ago. However, through the miracle of understanding the chemistry of these materials and their very complex interfaces, it works and even works very well!

The modulation of thin-film technologies is not based on the serialization of wafers glued next to each other, as is the case in conventional silicon technologies. In the case of thin-film modules, all this is done directly on the panel by insulating thin strips, oft using lasers, which are then connected in series with each other.



The structure of a PV module.

This is called the “monolithic” connection. The serial connection allows increasing the voltage delivered by the module by adding the elementary voltages produced by each cell (here by each band). This specificity in the production technique of thin-film cells allow a great flexibility in the models of cells produced and a great adaptability to the needs according to the field of application.

The first amorphous silicon wafers were made in 1980 by Wolf [3] by simulating the ideal parameters for record efficiencies. Reducing the thickness of the layer, the voltage of the open circuit is increased by saturation of the current, as a result of the reduction of the geometric factor. The first publications concerning the manufacture of amorphous silicon cells (a-Si) appeared late, in 1960 [4, 5]. These entities still consist of silicon but only to a thickness of about 1  $\mu\text{m}$ . The first amorphous silicon solar cell was made by Carlson in 1976 [6], and the first products appeared on the market in 1981. The type of system used influences the cost of the system, the stand-alone systems with batteries and auxiliary power generators which are more expensive than grid-connected systems. The interconnected and encapsulated solar cells form a photovoltaic module (Figure 1). Solar products have a great promise for a low-carbon future but remain expensive relative to other technologies.

The components of a photovoltaic power system are various types of photovoltaic/solar cells interconnected and encapsulated to form a photovoltaic module<sup>1</sup> (Figure 1).

<sup>1</sup> Photovoltaic modules are typically rated between 50 W and 300 W with specialized products for building-integrated PV systems at even larger sizes. Quality PV modules are typically guaranteed for up to 25 years by manufacturers.

Solar PV has a great promise for a low-carbon future but remain expensive relative to other technologies.

The ugliest problem with the solar cells is decreasing the cell efficiency with the panel temperature increase. The circuit control techniques include things like (1) using a smaller portion of the cells, when the load demand is low; (2) the wear leveling; (3) short-circuit, overload and other types of protections, current limiting, etc. The solar panels are subjected to the following environmental effects: (a) wind stresses and (b) cyclic thermal stresses from day to night and from summer to winter. These are two main observed defects caused by the repetitive environmental effects. Newer techniques involving varying levels of electroluminescence and photoluminescence, better panel coating technologies preventing debris accumulation on the surfaces of panels in the field, and of course, the technological approaches as ways of mitigating cost and risk currently exist in the industry.

Three IEC standards are used: IEC 61215 part 2 through part 4 (for mono- and multicrystalline silicon modules), IEC 61646 (for thin-film modules) and IEC 62108 (for concentrator modules). However, these standards can be viewed as general guidelines. In reality, the life of the PV modules mainly depends on intensity, distribution (UV content) and total dosage of sun radiation energy, ambient temperature, humidity, maximum operational voltage, wind speed and direction of the site. As these conditions vary widely over different sites, it may not be possible to define one standard or test to decide their lifespan. Further, the operation life depends on other conditions like salt and mist conditions and the presence of gases like  $\text{NH}_3$ ,  $\text{SO}_2$ , etc. Separate IEC standards are available to address these conditions. Therefore, it is very important to know the site conditions. The components that can fail and be repaired are module failure, string failure, DC combiner failure, inverter failure, transformer failure, AC disconnect failure and tracker failure.

Solar PV power plants are composed of thousands of solar modules. It is a known fact that 2% of them will fail after year 10 of operation, causing losses as high as 27% of total income.

Reduced cost of capital has resulted in the out years having real value in discounted cash flow analysis. The advantages and limitations of PV solar modules for energy generation are reviewed with their reliability limits. The high reliabilities associated with PV modules are indirectly reflected in the output power warranties usually provided in this industry (40-year module lifetimes may not sound as exciting as new photovoltaic materials, but it's essential to make solar power economic). Reliability evaluation based on degradation models is commonly applied in highly reliable products as a cost-effective and confident way of evaluating their reliability. About 80% of the current production uses wafer-based crystalline silicon technology [4, 7].

The development of photovoltaic materials comprised of non-toxic, abundant elements is an important step toward increasing the economic viability of solar energy to meet growing global energy needs.

The performance of a solar cell is a sensitive function of the microstructure of the component materials. Recombination of photo-excited carriers at defects is one of the main contributors to low efficiency. The focus of this contribution is on PV modules with crystalline silicon (c-Si) cells, which represent the dominant technology with over 90% of the market share and of cumulative installations. It is expected that a broad variety of technologies will continue to characterize the PV technology portfolio, depending on the specific requirements and economics of various applications [8].

Among the renewables, the conversion of sunlight into electricity by photovoltaic (PV) devices is a reliable choice to cope with the growing energy consumption.



Can a module durability of 30 years be guaranteed by combining components found to have no change in physical properties after 5000 h of pressure cooking testing or high-temperature/high-humidity testing? It seems this approach has been investigated, but there is currently deeply rooted resistance to it; it is difficult to confirm the effect that the gases and oxides generated from encapsulant components have on a variety of other components and difficult to estimate how vapor permeability changes over time when non-uniform tensile and other forces are applied by module creation. It is also impossible to determine the interactions caused by adhesion between components. As a wide variety of components are developed, the development of new reliability test methods (service life verification methods) should inevitably follow in the future [9].

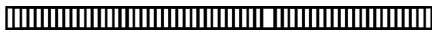
The introduction of a new technology must be competitive with the technologies that it is replacing. It must be cost-effective and ensure an appropriate return on investment (ROI) for investors. The return on investment for governments will take the form of job creation and positive environmental impacts. Each new technology must be capable of generating such a high quantity of revenue that the production costs are reduced to a minimum (economies of scale). In an effort to introduce the use of renewable energy sources, governments worldwide have created incentives to encourage the development of renewable technologies in order to improve our environment. These encouragements help to ensure that the desired volumes are achieved at the early stages of market introduction, so that economies of scale drive the prices to the point of being competitive without the need for other motivations.

PV modules are often considered to be the most reliable component of a photovoltaic system. The alleged reliability has led to the long warranty period for modules up to 25 years. Their real lifespan is unknown; some can last much longer, probably 40 years with very little degradation of their performances. However, since the solar sector is relatively young, it is difficult to have figures in the long term; their conditions and lifespan depend on a wide variety of factors related to their location: a panel installed in Germany will not face the same problems as another used in the Sahara or on the top of a mountain. The panels have a guarantee of a maximum yield loss of 0.7% per year, i.e. after 25 years a maximum loss of about 15%.

When assessing the reliability of a PV system, it is important to consider not only the PV module but the system as a whole. An installed PV system can only provide the expected service if all its components function properly and the complete PV system is properly serviced, from the solar cell to the high-voltage connection.

While it is difficult to measure the performance of a single module in a PV system due to the lack of feedback on the different degradation modes of PV modules, errors that lead to module degradation are generally not taken into account. It is important to remember that, from an economic point of view, consumers are increasingly interested in the reliability and lifetime of their photovoltaic systems. The lifetime and reliability of a PV system largely depends on the energy efficiency of the modules and their different degradation modes. Therefore, research must more and more focus on the degradation of photovoltaic modules.

The panels are materials intended for use under blazing sunlight, in the open air, and therefore subject to the constraints of weather, climate and many other factors. Damage to panels in operation is numerous and can affect different parts of the panels. UV exposure alters the polymers used to encapsulate the photovoltaic cells and modifies the mechanical characteristics of these polymers. Moisture can



penetrate the panel and degrade welds, cables and connections. Freezing can cause mechanical stress, while in the desert, sand can erode materials. In very rare cases, the panels can overheat and ignite [10].

While the reliability, quality and lifetime prediction are well established for most products, a complete understanding of these disciplines for PV modules is not yet possible because the desired lifetime is several decades and a first-hand assessment of lifetime predictions is not possible.

However, even today, the risks associated with module in-service performance over long periods of time are not completely clear. High-quality, publicly available field data on the long-term operational performance of PV systems are limited. In most cases, the production of field data takes many years and the technology has changed. That is why independent and high-quality laboratory data have been established in recent years to assess the long-term quality and reliability of photovoltaic modules.

PV systems are rightly regarded as low-maintenance and less susceptible to faults. These positive experiences must not be influenced by difficulties and reliability problems with additional features that may compromise the initial characteristics. For example, electronics on the module might be more susceptible to overvoltages, and this increases the risk of failures.

Comprehensive monitoring, evaluation, inspection and measurement methods detect possible defects and failures at an early stage, which can lead to performance deficits and reliability problems.

Since 2012, PV modules have been included in the EU WEEE Directive [11]. Collection and recycling of discarded end-of-life PV modules are mandatory to an extent of 80%.

## 2. Climatic stress factors

Solar irradiation, UV irradiation, humidity, wind, snow, rain, hail, high/low temperatures, temperature changes, salt, sand, dust and gases ( $\text{NH}_3$ , etc.). The module aging and the decrease in performance with time are complex processes that involve the interaction of several factors, namely, (a) reliability in PV, (b) service use weather conditions, (c) module materials (cell technology, encapsulant material, etc.) and design, (d) module mounting system and (e) module manufacturing process and quality control practices. Discoloration of the polymeric encapsulant is the most frequent degradation mode in hot climates. One degradation mode can be caused by a combination of various environmental stresses.

According to international report [12], at least 2% of the solar photovoltaic (PV) modules in operating solar plants will fail after 10 years of operation. As the modules are series-connected to other healthy modules in strings, they can lead to monetary losses as high as 27% of total income depending on location, type of solar plant and remuneration fee.

## 3. HALT and HASS

Just like pulling on a chain until the weakest link breaks, HALT methods apply a wide range of relevant stresses, both individually and in combination, at increasing levels in order to expose the least capable element in the system. A highly accelerated life test (HALT) is a process that requires specific adaptation when it is applied to almost any system and assembly. A highly accelerated stress screening (HASS) is an ongoing application of combinations of stresses, defined from stress limits found

empirically during HALT to detect any latent defects or reduction in the design's strength introduced during mass manufacturing.

Any stress that exposes design weaknesses that would show up in the normal environments is suitable even if these stresses do not occur in the normal environments to which the product will be exposed. This is due to crossover effect. High reliability can be attained with careful testing that targets possible design problems, based on the physics of the failure modes, HALT testing and field data.

The highly accelerated stress test (HAST) is a process that applies increasing levels of stress (beyond the environment for which it is intended), for a short period of time, to highlight design and process weaknesses. It consists of a search for the real limits of the product based on its ability to resist environmental constraints such as random vibrations and cold and hot temperatures. This type of test is first of all focused on the very quick identification of defects. Then, corrective actions are implemented to quickly increase the product's robustness. As a result, the product is able to withstand much greater stresses than those it will experience during the normal life cycle. This method is used from the design phase to highlight design problems, also during the production phase to detect process errors. It is essential (i) to reduce product development time, (ii) to increase product reliability and (iii) to reduce after-sales service and other catastrophic youth defects in cost and brand image. It is no longer enough to measure the reliability of a product and perform a simple function test before distribution. It becomes necessary to build reliability from the upstream study around the product. Tests such as HALT and HASS allow this.

Dedicated combined environmental resources and a test time of about a week, combined with product monitoring during the tests, are the key to the success of a fast and efficient method. HALT allows you to do in a week what other environmental tests do in several months. HASS takes place during the production phase of the products. A profile is applied for 4 h (called burn-in) during which it undergoes thermal variations, random vibrations and electrical stresses. This profile allows to transform existing weaknesses on the product into measurable defects. In this way, potentially defective products are not distributed, and after-sales costs are avoided. This test takes place during the production phase of the products.

#### 4. Useful life

The useful life corresponds to the majority of the system's lifetime. During this period, the failure rate may be:

- Increasing for mechanical elements due to wear, fatigue and corrosion.
- Constant for electronic components because there are no aging phenomena.
- Decreasing in the case of software with error correction, to improve reliability.

The age period corresponds to the failures defining the end of use of the product regardless of the type of technology. The default rate in this period is growing rapidly. During this period, products that had not been deficient during the useful period generally become deficient over a very short period.

The lifetime of PV modules is a function of a few key major field stresses such as temperature, humidity, UV light and system voltage. The accelerating factor is the relation between the time spent in the field test (or in use) and the time spent in the accelerated test. The purpose of these tests is to shorten the duration of the tests

under simulated test conditions that are much stricter than actual field operating conditions, without changing the actual failure mechanisms in the field. In the AT programs, the stress tests of PV modules are performed at higher levels than the field/use stress levels along with pre- and post-characterization of materials and modules from reliability, durability and safety perspectives.

## 5. Levelized cost of electricity (LCoE)

The LCoE is a present value assessment of the total system costs over its lifetime and the system returns. Financial factors (the inflation or the cost of capital) are also taken into account and discounted depending on the LCoE formula in use

$$\text{LCoE} \left[ \frac{\text{€}}{\text{Wh}} \right] = \frac{\text{lifecycle cost}}{\text{lifetime energy yield}} \quad (1)$$

To reduce LCoE, current research focuses on a few well-defined topics:

Decreasing cell-to-module loss to increase module power.

Simulation and optimization of outdoor module performance for increased energy output.

Developing new module designs and fabrication processes for cost reduction.

Understanding degradation mechanisms with the aim to improve module reliability and durability. PV module reliability is dependent on the quality and integrity of the process used to manufacture the module. Even small variations in material quality or manufacturing processes can impact the reliability of a component.

## 6. Degradation and failure

Multiple factors affect the reliability and long-term performance of PV modules. The quality and characteristics of the used materials, the interaction of the components, the manufacturing process and the local climate at the operating site play a significant role. The main degradation modes are known and their causes have been identified in most cases. To identify the main modes of degradation, accelerated aging is used with climate chambers, in situ monitoring and the variation of test parameters. The nanoindentation was used as a suitable destructive method to investigate the changes in hardness occurred during dampheat (DH) aging of components in the PV modules with a high spatial resolution [13]. Certification tests are designed to ensure a nominal level of safety and design quality, and not to indicate whether or not a product will last for its warranted lifetime; these tests are designed to ensure safety and identify infant mortality issues due to basic manufacturing quality.

The root causes of different module failures are (i) snail trails and pearl chains, (ii) cell cracks, (iii) solder joint, (iv) breakages, (v) light-induced degradation (LID), (vi) potential induced degradation (PID), (vii) hot spots and (viii) delamination. Dominant failure pathway (for modules manufactured in the early 2000s) [14]: (1) cell interconnects become more resistive, apparently due either to corrosion or fatigue of the interconnect ribbons or solder connections; (2) interconnects resistively heat, which increases the severity of temperature cycling and leads to even higher resistive heating (3) interconnect overheating or breakage leads to backsheet blackening,

power loss, or other failure events. The primary underlying causes of module failures in the field were due to cell/interconnect breakage and corrosion.

In addition to failure rate, power degradation is a critical module behavior; a power degradation of a few percent has a direct effect on production over a module's lifetime, and such a small percent drop would not justify a claim under most module warranties. Subtle variations between cells, such as cell thickness, can have very large impacts to mechanical stability and reliability.

## 7. Predominant degradation modes

Corrosion, discoloration delamination and breakage of PV module encapsulant are the main modes of product degradation. Temperature and humidity are factors of PV module degradation in almost all identified degradation modes. One key factor of reducing the costs of photovoltaic systems is to increase the reliability and the service lifetime of the PV modules. Models can help to overcome the long-term experiment obstacle in order to study PV module degradation under real conditions. To increase the reliability and the service lifetime of the PV modules, it is necessary to reduce the costs of PV systems.

In addition to degradation analysis, the stress tests available today are very effective at screening for PV module defects that cause severe degradation or safety issues such as bad solder joints or a poorly adhered junction box.

## 8. Environmental factors influence the degradation

Even bird droppings can significantly reduce the output of a photovoltaic module. However, many causes of faults are not visible to the naked eye. In such cases, special devices such as a thermal imaging camera are required for localization.

With a thermal imaging camera, the following defaults in the modules can be detected: (a) production failures, (b) damage such as cracks, (c) faulty power connections and connections, (d) contamination and shading, (e) defective cables and (f) inverter damage.

## 9. PID and LID

PID and LID are two different kinds of induced degradation of PV modules. In the first case, potential induced degradation (PID) is conducted by high voltages and the other light-induced degradation (LID) conducted by sunlight (real or simulated).

PID is the "new disease" of the PV module; highlighted in 2010, it begins to affect more and more photovoltaic modules. The first symptom of this phenomenon is a rapid and unexplained degradation of power. This decrease in module efficiency, which can reach more than 20% in a few months, is neither due to conventional module aging nor to improper module installation. Individual modules in PV systems are often connected in series to increase the system voltage. The potential difference of the chain thus formed can sometimes reach a few hundred volts [15]. In order to protect people from electric shock, all metal structures of the modules are often grounded. Thus, leakage currents can occur due to a lack of insulation between the structure and the active layers (PV cells) [16]. This phenomenon can lead to polarization that can degrade the electrical characteristics of photovoltaic cells. This phenomenon known as potential induced degradation (PID) is characterized by the progressive degradation of the performance of crystalline



silicon-based photovoltaic modules due to the presence of an induced electric current at the very heart of the module [17, 18]. Hacke showed that PID was more common in humid climates than in hot and dry environments [19]. Schütze et al. go in the same direction by showing that leakage currents increase with humidity [15]. In his study, a ramp voltage of 600 V at sunrise and 0 V at sunset is applied between the metal structure and the contact of a module composed of 60 cells. His experience has shown that leakage current increases with humidity. The various studies have shown that the main factors favoring PID are the voltage of the system in which the module is used, humidity and operating temperature. PID is triggered by a combination of high temperature and relative humidity. Furthermore, some degradation mechanisms are interdependent. The PID process that occurs more often in p-type cells is a PID of the shunting type, sometimes denoted by PID-s. Other types of PID in p-type cells are the dissolution of the antireflective coating and the corrosion of the cell fingers [20]. Quality control during the module manufacturing process is essential to ensure a good performance in the long run.

ID usually occurs when modules are in strings operating at high voltages (near 1000 V<sub>P</sub>, but not only), combined with very warm and humid weather. Dust and glass degradation (releasing sodium ions) may catalyze the PID phenomenon. Potential induced degradation (PID) is an effect that affects some PV modules with crystalline Si cells; the degradation of performance that can occur after a few years can arrive to 30% or more.

Light-induced degradation (LID) has been identified to be a critical issue for the long-term stability of solar cells and modules from boron-doped silicon substrates. Besides the well-known LID of excess charge carrier lifetime within Czochralski-grown silicon substrates induced by the activation of the boron-oxygen complex, significant performance degradation has been observed also for certain multicrystalline silicon (mc-Si) solar cells and modules [21]. This degradation is significantly more pronounced at elevated temperatures and, therefore, referred to as LeTID for “light and elevated temperature-induced degradation.” If not controlled, LeTID can induce a decrease of conversion efficiency by more than 10%, particularly for solar cells with dielectrically passivated surfaces. LeTID needs therefore to be suppressed by adapted cell processing.

For the younger installations (less than 10 years of operation), the most observed degradation modes are hot spots and internal circuitry discoloration (both related to electric interconnections), encapsulant discoloration, broken cells and PID (Figure 2).

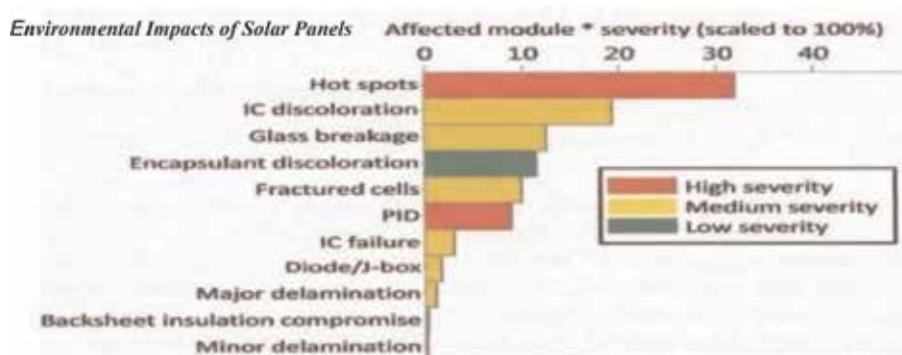
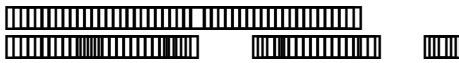


Figure 2.

Pareto chart of the most significant degradation modes for systems installed in the last 10 years. PID is ranked as a high-severity degradation mode. Interconnection failures, which include hot spots and internal circuitry (IC) discoloration, also play a large role in degradation. Image adapted from [22, 23], with kind permission.



The LID for crystalline silicon modules varies between 0.5 and 3%; some modules have a loss of up to 5%. Manufacturers using n-type silicon cells have no loss of LID. Manufacturers take this into account by considering a power loss of 3% during the first year of the module warranty [24].

## 10. Failures in the electric interconnections

Interconnection failures are generally caused by thermo-mechanical fatigue. Because of the different coefficients of thermal expansion of the materials in the module sandwich (e.g. cells, encapsulant, glass, back sheet), thermal variations result in a displacement of solar cells in the module. The same effect can occur when the module is exposed to mechanical stresses, e.g. due to wind or snow loads.

The reliability of ribbons has gained increasing attention in the last few years. In [23] how the module performance is affected when one or more ribbons are broken was investigated. It was quantified, by experimental measurements, the actual impact on the electric performance when one or more ribbons connecting adjacent cells are disconnected. In [23] a simplified electrical model in LT-Spice that is able to reproduce experimentally measured IV characteristics and the variation in the module's electrical parameters induced by the breakage of the cell interconnect ribbons were proposed.

## 11. Defects

A defect is everything in a PV module that is not as it is expected to be. A large number of defects are known in PV c-Si modules. Some of these can be identified by visual inspection [25, 26]:

- Broken glass by volley or mechanical accidents
- Delamination (busbars, EVA foil)
- Broken or deformed frames
- Brownish color caused by hot spots
- Charred electrical connection box
- Defects in connectors
- Environmentally altered surfaces
- etc.

## 12. Rate of defective panels

The rate of defective panels leaving the assembly lines—evaluated thanks to returns and complaints from customers—is well below 0.1%. Highly demanding quality standards have been defined by the IEC, an international body that sets design and quality standards.

The youth period refers to early failures due to design problems (incorrect sizing of a component, etc.) or production (deriving from a process of manufacturing). The default rate is decreasing in this period. In the case of modules, youthful failures can be eliminated before delivery to the customer by practicing debugging. Burn-in consists of turning on the components to be delivered under conditions that may reveal failure modes. This practice is expensive and the failure rate at delivery is equal to that at the beginning of the useful period. Many manufacturers do not perform this burn-in on their products for reasons of cost. In this case, a warranty period is put in place during which the manufacturer undertakes to change or repair the defective product. For example, for photovoltaic modules, manufacturers guarantee them for an average of 5 years for mechanical failures (unrelated to the power delivered by the modules). In reliability studies, defects that appear during this warranty period are not taken into account and are mainly concerned with the useful life of the product.

### 13. Failures

Typically failures of products are divided into the following three categories: infant failures, midlife failures and wear-out failures. During initial exposure to light, crystalline silicon modules generally undergo a permanent reduction in output power emissions. This phenomenon is called light-induced degradation or LID. On average, the LID for crystalline silicon ranges from 0.5 to 3% due to traces of oxygen included in the molten silicon during Czochralski process. Manufacturers take into account a 3% power loss during the first year of the module warranty. Be aware of LID degradation [27]. Crystalline p-type boron-doped silicon solar cells generally exhibit a degradation of conversion efficiency during the first hours of exposure to the sunlight. Understanding light-induced degradation of c-Si solar cells is associated with the formation of the well-known boron-oxygen complex which acts as a harmful defect and reduces the minority carrier diffusion length accordingly. LID is therefore related to both, boron and oxygen concentrations.

For thin-film PV modules, there are far fewer experiences accumulated in the past years than for crystalline Si PV modules.

Failure modes are directly related to module material and; hence, they continuously evolve with the material adjustments made by module manufacturers.

Infant-mortality failures occur in the beginning of the working life of a PV module. Flawed PV modules fail quickly and dramatically impact the costs of the module manufacturer and the installer because they are responsible for these failures.

Failures occurring in the midlife of PV modules are described in a study of DeGraff [28]. Figure 3 shows the analysis and statistics of specific field failure distribution. The predominant PV module failures are delamination, cell part isolation due to cell cracks, and discoloring of the laminate.

The so-called ribbon kink (between the cells and the joint between the cell interconnect ribbon and the string interconnect) is prone for fatigue breakage. The possible causes are poor soldering connections. A too intense deformation during the fabrication of the ribbon kink between the cells mechanically weakens the cell interconnect ribbon. A narrow distance between the cells promotes cell interconnect ribbon breakage. Physical stress during PV module transportation, thermal cycle and/or hot spots by partial cell shading during long-term PV system operation forces mechanical weak ribbon kinks to break.

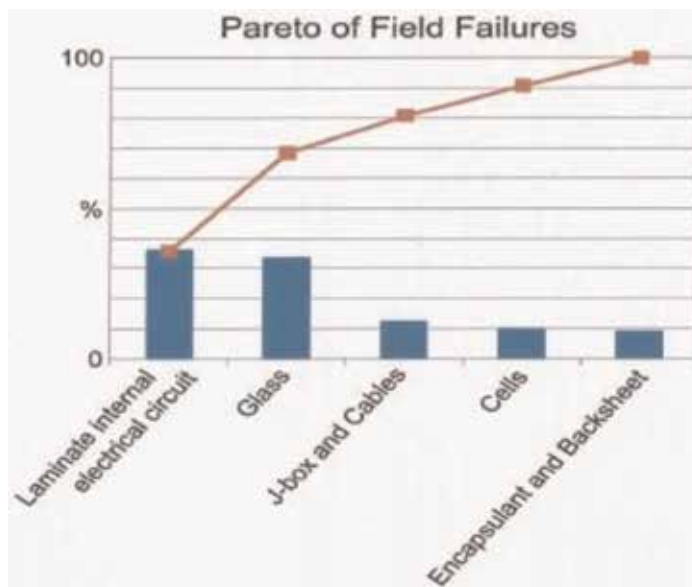


Figure 3.  
 Analysis and statistics of specific field failures (with kind permission of SunPower Corp.)

### 13.1 External causes

Some failures are typically difficult to define as a PV module failure or as a failure of the contractor, of the installer or the system designer or even for other reasons. The specific field failures are their analysis and statistics (Figure 3).

### 13.2 Clamping

A relatively often seen failure in the field is glass breakage of frameless PV modules caused by the clamps. Major problems caused by glass breakage are electrical safety issues, because the insulation of the modules is no longer guaranteed, in particular in wet conditions, and because glass breakage causes hot spots, which lead to overheating of the module.

### 13.3 Transport and installation

Even in well-designed transport containers, the cells of PV modules may crack during "normal" transport. The cause of cell breakage is much more difficult to decide. Only an electroluminescence image or a lock-in thermography image can reveal the damage.

### 13.4 Quick connector failure

Quick connector failure in the most cases is not considered a PV module failure.

### 13.5 Lightning

A defective bypass diode caused by a lightning strike is caused by an external source, for which the module is not designed.

### 13.6 Defect

Much wider than a failure, the defect does not result in a loss of power or safety of a PV module but specifies a part of a PV module that is different from a perfect PV module.

## 14. Field failures

Field failures of PV equipment can stem from materials, fundamental product design flaws or failures in quality control during manufacturing. Failure modes in the field which occurred during operation are (a) yellowing/browning of encapsulants and back sheets with and without power loss, (b) delamination of encapsulant and back sheet, (c) bubble formation, (d) oxidation of busbars, (e) discoloration of busbars, (f) corrosion of connections, (g) cracking of back sheet, (h) hot spots, (i) cell breakage and (j) microcracks.

Testing and certification are important to assure a certain quality level, taking into account that more than 1/3 of new module types still fail during testing for certification in the laboratories.

Check the module for damage due to transportation before the installation. Do not use or install damaged modules. Damaged modules may cause fire or electric shock, resulting in property damage, fire and or death.

LEDs are gaining an increased market share in applications requiring light in the UV spectrum [29]. This trend is driven by big technological advancements and various advantages of LEDs compared to the conventional UV light sources. These advantages include a higher efficiency, a longer lifetime, more constant radiance and less heat generation [30].

It was imperative to evaluate the option of using UV LEDs in PV module and component degradation. The UV LEDs have proven their long lifetime and slow degradation at room T and RH. However, also polymeric materials only degrade slowly in those conditions. This emphasizes the need to apply UV light and other stress factors at the same time in accelerated aging and degradation testing [31].

## 15. The most common failures of PV modules

Four major materials are assembled to realize a PV module: glass, metals, polymers and solar cells/active semiconductor thin-film layer.

Aging and failure mechanisms seen over the past several decades have been documented over a wide range of power plant locations and material sets (figure 4).

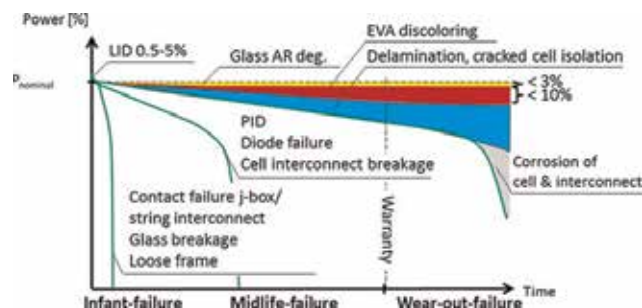


Figure 4.

Three typical failure scenarios for wafer-based crystalline photovoltaic modules are shown. Definition of the used abbreviations: LID, light-induced degradation; PID, potential induced degradation; EVA, ethylene-vinyl acetate; jbox, junction box [32]. With kind permission of IEA.

indicates leading PV module aging and failure mechanisms that occur as infant mortalities, midlife failures and wear out. Laminates containing EVA foils with a systematic variation of the additive formulation, i.e. the crosslinking agents, ultraviolet (UV) absorber, hindered amine light stabilizers and antioxidants, were subjected to UV aging. Failures are the following: EVA discoloration; cell cracks; snail marks; loss of adhesion of the back sheet; interconnection tapes of the cell and disconnected wires; junction box failure; frame failure; burn marks; potential induced degradation; defective bypass diodes; failure of thin-film modules, such as microarcs at hot spots of bonded connectors; shunts and front glass failure; and rear contact degradation [32].

## 16. Ethylene-vinyl acetate (EVA)

One of the most overt degradation mechanisms for PV modules is the discoloration of the ethylene-vinyl acetate (EVA) or other encapsulation materials (considered as an esthetic issue). EVA is usually formulated with additives, including UV and thermal stabilizers. But if the choice of additives and/or their concentrations are inadequate, the EVA may discolor.

Delamination may be more likely at the interface between EVA and the solar cell, because the interfacial strength may initially be more limited there than at the EVA/glass interface. On the other hand, UV degradation and subsequent embrittlement may limit the long-term adhesion of interfaces exposed to the sun.

It is quite common to see symmetric patterns and sometimes multiple rings based on the effects of limited chemical diffusion, both into and out of EVA and the existence of multiple chemical pathways that produce similar chromophore species.

It was possible to show a link between changes in mechanical properties with both the transient temperature and the degree of long-time thermal aging [33].

The overall EVA degradation is higher in the Indonesian equatorial zone, in the African semi-arid zone and in the Chinese cold desert (Figure 5).

Results from environmental degradation simulations highlighted the effect of climatic zones on degradation, with higher degradation in hotter, warmer and more irradiated zones. The overall EVA degradation is higher in the Indonesian equatorial zone, in the African semi-arid zone and in the Chinese cold desert [34]. With kind permission of the authors.

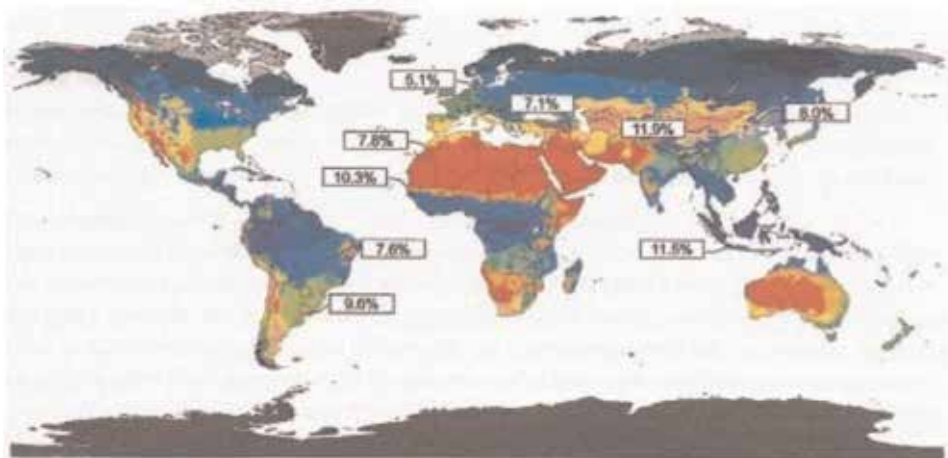


Figure 5.  
 Köpper's map and overall EVA degradation, calculated after a 20-year exposure in different climatic zones.

Glass can be a source of module reliability problems if not properly fabricated. Glass reliability issues can include brittle failure due to mechanical and thermal stresses, surface weathering, lamination adhesion, transparent conductive oxide (TCO) adhesion, moisture ingress and antireflective coating durability.

## 17. Failure analysis

The search for physical-failure root causes is aimed at breaking through any technology barrier in each stage of chip development, package development, manufacturing process and field application, offering the real key to eradicate the error. Testing provides us with information on the electrical performance; FA can discover the detractors for the poor performance [15].

Failure modes in the field which occurred during operation are analyzed [31]: microcracks, cracking of back sheet, corrosion of connections, hot spots, cell breakage, delamination of encapsulant and back sheet, oxidation of busbars, yellowing/browning of encapsulants and back sheets with and without power loss, bubble formation and discoloration of busbars.

Most of the failure modes observed are polymer defects such as delamination, yellowing (there are no obvious results that show a direct relationship to power losses in the event of yellowing) and browning, bubbling and cracking of polymers used for encapsulants and back sheets. Oxidation and discoloration of busbars and corrosion of connectors are also easily detected without special measuring equipment; they lead to increased resistance in series. Microcracks, cell failure and hot spots have a greater impact on performance [31]. The detection of these defects requires IR cameras.

Modules under test both in the field and during qualification testing have exhibited several types of failure resulting from moisture intrusion. Poorly designed cell assemblies can damage or break the cells.

Failures observed during the analysis are the following: (i) moisture intrusion, (ii) differential thermal expansion, (iii) plus UV exposure, (iv) wind loading, (v) off-track charring and (vi) hot spot. The types of failures resulting from moisture intrusion are (1) cell strings shorting to ground; (2) terminals shorting to ground; (3) high ground fault currents, preventing inverter from coming on; (4) modules filling with water; (5) corrosion; and (6) degradation of optics.

## 18. New techniques for failure analysis

Dark lock-in thermography (DLIT) has recently emerged as a new powerful technique for failure analysis of PV modules; it provides information on the thermal behavior across the whole module at high spatial resolution, besides complementing and overcoming some of the limitations of electroluminescence (EL) and conventional passive infrared (IR) cameras. Its basic principle consists in stimulating the module by applying a periodic current signal, while a highly sensitive IR camera detects and measures the surface temperature stimulated by the current signal.

Scanning acoustic microscopy<sup>2</sup> (SAM) has proven to be a powerful technique for the investigation of failures and defects in solar cells and modules [35]. This technique is needed to advance the assessment of module quality and, thereby, improve

<sup>2</sup> SAM is a non-invasive and non-destructive technique that can be used to manage the internal features of a specimen, in particular its interfaces. SAM is a superior tool to detect delamination even of submicron thicknesses (down to 100 nm).

their long-term performance. The PV modules were placed flat into a water tank and scanned.

PV modules (20 × 20 cm<sup>2</sup>) were prepared by laminating a layer of polymer-based backsheet foil (BS) and two layers of ethylene-vinyl acetate (EVA) sandwiching a monocrystalline silicon cell and a transparent glass cover.

The very fine resolution achieved with SAM allowed a clear visualization of the location and shape of the air pockets detected on the rear side of the module. These air pockets seem to form only on the silver pads next to a ribbon, which may indicate that the EVA did not adhere completely to the silver pads, thus giving rise to air gaps. In acoustic micrographs, air pockets and delaminated areas are easily detected as very bright features because air-filled interfaces reflect almost all incoming sound.

The depth profile analysis indicated that SAM can be applied to detect thickness variations within the BS and encapsulant layers. SAM has proven to be a very sensitive technique to detect interfacial faults, such as cracks on the solar cell, bubbles and air pockets at different interfaces. A correlation between SAM and DLIT images with regard to the encapsulation homogeneity and adhesion defects could be verified, suggesting both techniques are complementary to study defects of this nature. Therefore, SAM is a reliable and complementary technique to DLIT and EL in investigating PV modules [10].

## 19. Influence of temperature

Temperature is extremely significant to the PV module degradation process, especially hot spots, encapsulant bleaching, delamination failure on interconnections, corrosion, discoloration and bubbles on the panel surface.

Crystalline silicon PV cells/module degradation exposed under temperature and heat effect has been investigated. This revealed:

- Delamination of encapsulant and back sheet.

- Bubble formation, oxidation of busbars, yellowing/browning of encapsulants and back sheets with and without power loss.

- Discoloration of busbars.

- Corrosion of connections.

- Cracking of back sheet.

- Hot spots, cell breakage and microcracks are the dominant modes of degradation.

Temperature is responsible for most of the chemical reactions and extremely significant to the PV module degradation process, especially hot spots, encapsulant bleaching and delamination failure on interconnections, corrosion, discoloration and bubbles on the panel surface.

The leakage current increases rapidly with increasing number of hot spots. The effect of discoloration causes loss of transmittance of the encapsulant EVA and reduces the photocurrent density ( $J_{sc}$ ) (owing to a decrease of absorption and therefore the power loss. Discoloration does not affect the fill factor (FF) and ( $V_{oc}$ ) more, but the corrosion causes a decrease of the PV module maximal power ( $P_{max}$ )).



Accelerated Stress Test	Failure mode	International regulation
Thermal cycling	Broken interconnections Cell cracks Solder bond failures Module open-circuit Potential for arcing Junction box adhesion	IEC 61215
Dampheat	Corrosion Delamination Encapsulant loss of adhesion & elasticity Junction box adhesion Inadequate edge deletion	
Humidity freeze	Delamination Junction box adhesion Inadequate edge deletion	
UV exposure	Delamination Encapsulant loss of adhesion & elasticity Encapsulant & backsheet discoloration Ground fault due to backsheet degradation	
Static Mechanical Load	Structural failures Broken glass Broken interconnect ribbons Broken cells Solder bond failures	
Dynamic Mechanical Load	Broken glass Broken interconnect ribbons Broken cells Solder bond failures	
PID test	Potential-induced degradation	IEC 62804 [59]

Table 1.  
Summary of the main accelerated tests for c-Si PV modules (Adapted from [37]).

	Qualification	Comparative	Lifetime
Purpose	Minimum design requirement	Comparison of products	Lifetime estimation
Quantification	Pass/fail	Relative	Absolute
Climate	Not differentiated	Differentiated	Differentiated

Table 2.  
Three types of accelerated tests employed in the PV industry.

when the delamination of the PV module reduces the thermal conductivity locally and hence increases the temperature of the cell [36] (Tables 1 and 2).

## 20. Accelerated tests

The International Photovoltaic Quality Assurance Task Force (IPVQAT) gathers the efforts of many research groups worldwide in order to improve the understanding of the reliability of PV modules. One goal is to propose a climate-specific test protocol.

## 21. Qualification tests

The qualification tests have been essential to identify materials that lead to early failures in the field and to achieve a high reliability for PV modules. However, they present some limitations if one wants to interpret them as reliability-predictive tests. Presently, PV modules are only going through qualification tests (such as performed according to the IEC 61215 for crystalline silicon-based modules) which

provide limited information as (i) they do not provide information on the maximum lifetime that can be expected and (ii) they do not consider climate specificities [39].

Testing and certification of a PV module focuses on verifying that the fundamental design requirements have been fulfilled. Reliability testing increases confidence in production quality and usually takes less time and costs less than durability tests [40].

The purpose of the qualification tests is to screen new designs and new production runs for susceptibility to known failure mechanisms: (1) The tests do not establish field lifetimes; (2) cell assemblies and complete modules are tested separately.

## 22. Photometric testers

Measurements with photometric testers give additional hints on defect PV modules (defect bypass diodes, broken or delaminated connectors and wires). These inspections of modules often can be done while these modules are still installed. However, analysis with photometric testers addresses the modules as a whole and cannot localize the defect within the module; defects may be localized by thermographic cameras.

All critical areas that are detectable via the IR camera at long wavelength could as well be detected with the near-infrared (NIR) camera. However, NIR images are more suitable for the defect analysis since they have higher local resolution [41].

Typically the NIR images show an affine distortion. This has to be corrected carefully to an orthoimage. Furthermore NIR image is brighter at the center than in the outer regions. This must be numerically compensated.

## 23. Combining up to three stress factors targeting specific mechanisms

The necessity for combining multiple stress factors into fewer tests has been recognized for some time, as demonstrated by efforts made by various other groups [42–45]. While important results have been produced, these efforts are typically limited to combining up to three stress factors targeting specific mechanisms. In this work, a combined-accelerated stress testing (C-AST) capability has been developed which combines multiple stress factors from the natural environment including light, humidity, temperature, rain, mechanical loads and voltage stress. The test has been developed with the philosophy that it is agnostic to a priori known failure mechanisms such that mechanisms in new module designs or materials may be identified before deployment. C-AST is applied here to mini-module specimens to allow for possible adverse material interactions.

The test includes six 4-cell p-PERC mini-modules with three back sheets based on polyvinylidene fluoride, polyamide and polyvinyl fluoride, as well as two types of polyethylene-co-vinyl-acetate (EVA), one UV blocking and one UV transparent. The experiment demonstrated C-AST's ability to identify backsheet cracking and other failure mechanisms such as UV-induced degradation, solder bond breakage, minor corrosion and cell cracking.

## 24. Encapsulants

Encapsulation materials are of critical importance for long-term reliability and safety of PV modules. Only months in the field may lead to drastic power output

degradation, for example, due to potential induced degradation (PID), and also in the longer run adhesion and discoloration issues (hot spot) can reduce power output or even may lead to critical electrical safety issues. These findings are not sufficiently covered by IEC 61215 and other standard testing. Additional and different types of tests are required for an in-depth understanding of the encapsulation materials impact on PV module performance [46]. PID can be critical for many of the solar parks built in the early phase of PV deployment (2002); however, it can still occur in modern modules when lower encapsulants are used in PV manufacturing, a choice often driven by the need for cheap solar electricity.

## 25. Key performance indicators

Typical key performance indicators (KPIs) used in solar industry for assessment of the performance of solar modules and balance-of-system (BOS) components were investigated in [47]. From the point of view of an investor in PV systems, it is important to have a comprehensive insight into the reliability of solar modules. Since reliability and longevity of such components are crucial for the long-term financial success of the project, corresponding KPIs are desired. To this end solar industry has traditionally provided KPIs for both solar modules and inverters on the base of relating the number of failed (claimed) product to the number of installed (or sold) product. The denominator of these KPIs may be referred to as either related to the same period as the numerator or to a cumulated number of installations. The study [48, 49] has shown that currently used KPIs are not sufficient when comparing the ability of solar manufacturers to produce reliable solar modules or inverters.

Presently, PV module manufacturers typically guarantee 80% of the nominal power for 25 years. If we assume a linear power degradation rate, this corresponds to an annual degradation rate  $D$  of 0.8%/year.

To recover the losses, a continuous repowering would be necessary, substituting the modules that fail with new ones. Failures in modules lead to hot spots that can be detected by visible (VIS), IR thermography and electroluminescence (EL) images. This inspection, mainly manual, is rapidly reducing costs by the increasing penetration of drones, which will very probably become soon the state of the art [50–53].

## 26. Metal-wrap-through (MWT) concept

The metal-wrap-through (MWT) concept, which was developed in 1998 by Kerschaver et al. [54], represents an alternative approach for reducing shading while at the same time ensuring reliable measurability and purely rear-side contacting. MWT solar cells differ from conventional solar cells in that the front-side contact finger is not routed to busbars, but to the rear side via metallized vias. This makes it possible to connect the cells on the rear side only, but the cell structure otherwise corresponds to that of conventional solar cells.

Critical points such as the recombination in the area of the vias, the influence of the rear n-contacts to the series resistor as well as the arrangement of the rear contacts for a reliable and low-loss external circuit are to be dealt with in simulations and experiments. The selection of suitable passivation layer systems as well as the reliable insulation of the vias and the rear side n-contacts against the p-base is also the central aspects regarding the minimization of leakage currents. Another

important factor for reliable module integration is the behavior of the cells when negative voltage is applied externally.

This operating state can occur during partial shading of photovoltaic modules and can lead to local overheating within the cell if the current flux is not controlled. Investigations into the backward behavior of the developed solar cells are, therefore, of great importance for the long-term stability of the solar cells and the modules produced from them.

The reliable connection of the front contact grid with the rear contact surface through vias is a central task in the development of MWT solar cells.

The efficiency of solar cells available in practice is reduced by a multitude of further loss mechanisms [55] and depends both on the quality of the materials used and on the available technologies. Predictions of the practical reachable maximum are, therefore, highly error-prone.

High reliability: service life between 10 and 20 years, depending on location installation.

## 27. Perspectives

The continuous evolution in cell technologies and the implementation of new encapsulation materials will lead to the appearance of new degradation modes, which might require years before being detected in the field. The case of the so-called light and elevated temperature-induced degradation (LeTID) effect that was observed in PERC cells only in 2015 is an example. Also new applications of PV such as building-integrated photovoltaics (BIPV) lead modules to operate in new conditions (resulting, e.g. in higher module temperature excursions) and employ new materials, which may result in a different evolution of the typical degradation modes as well as in the appearance of new degradation modes.

With regard to new cell technologies, we expect that in passivated emitter and rear cells (PERC), where the only differences with respect to standard p-type cells lay in the rear surface, the mechanism of PID is in general the same as for the standard p-type cells. It is expected therefore that the study of PID mitigation strategies [23] is applicable to PERC cells as well. The mechanism of PID in silicon heterojunction (SHJ) cells is instead very different in that it does not consist of cell hunting, but corrosion of the transparent conductive oxide (TCO) layer (similar to thin-film modules) requires a different study.

## 28. Conclusions

The reliability of PV power plants and modules has been and will continue to be—an issue for investors, owners and utilities.

A global network is required to improve the quality and reliability of PV systems and components by collecting, analyzing and disseminating information on their technical and financial performance.

PV will utilize new materials, manufacturing methods, module and systems designs in order to lower costs and hopefully increase or maintain reliability.

New module materials and constructions and new system concepts are necessary for increased reliability and lifetime [56].

## Author details

Titu-Marius I. Băjenescu<sup>1,2</sup>

1 Military Technical Academy of Romania, Bucharest, Romania

2 Technical University of Republic of Moldova, Chişinău, Moldova

\*Address all correspondence to: [tmbajenescu@gmail.com](mailto:tmbajenescu@gmail.com)

## IntechOpen

© 2020 The Author(s). Licensee IntechOpen. Distributed under the terms of the Creative Commons Attribution - NonCommercial 4.0 License (<https://creativecommons.org/licenses/by-nc/4.0/>), which permits use, distribution and reproduction for non-commercial purposes, provided the original is properly cited.



## References

- [1] Chapin DM et al. A new silicon p-n junction photocell for converting solar radiation into electrical power. *Journal of Applied Physics*. 1954; 25: 676
- [2] Becquerel AE. Memoire sur les effets electriques produits sous l'influence des rayons solaires. *Comptes Rendus de l'Académie des Sciences*. 1839; 9: 561-567
- [3] Goetzberger A et al. Solar cells: Past, present and future. *Solar Energy Materials & Solar Cells*. 2002; 74: 11. Available from: [http://193.140.122.139/solar/resources/e-books\\_and\\_papers/web-editions%20-%20goetzberger%20-%20Solar%20cells,%20past,%20present,%20future.pdf](http://193.140.122.139/solar/resources/e-books_and_papers/web-editions%20-%20goetzberger%20-%20Solar%20cells,%20past,%20present,%20future.pdf)
- [4] Wolf M. High efficiency silicon solar cells. In: *Proceedings of the 14th IEEE Photovoltaic Specialists Conference*; San Diego; 1980. p. 674
- [5] Chittick RC et al. The preparation and properties of amorphous silicon. *Journal of the Electrochemical Society*. 1969; 116: 77
- [6] Spear WE, LeComber PG. Investigation of the localised state distribution in amorphous Si films. *Journal of Non-Crystalline Solids*. 1972; 8: 727
- [7] Carlson D, Wronski C. Amorphous silicon solar cell. *Applied Physics Letters*. 1972; 20: 671
- [8] Essakiappan S et al. Current status and future trends in solar technology A comparative study of Texas and California. Technical Report: TR-2010-ECE689-Fall Group No. 1; December 10, 2010
- [9] Kurtz S. Reliability and Durability of PV Modules. 2017. DOI: 10.1002/9781118927496.ch44
- [10] European Commission. Directive 2012/19/EU of the European Parliament and of the Council on Waste Electrical and Electronic Equipment (WEEE); July 4, 2012
- [11] Köntges M et al. Review of failures of photovoltaic modules. Report IEA-PVPS, T13:01; 2014
- [12] Gray KA, Paschkewitz JJ. Next Generation HALT and HASS, Robust Design of Electronics and Systems. John Wiley & Sons, Ltd; 2016
- [13] Mansour DE, Swientek F, Kaaya I, Philipp D, Bauermann LP. Nanoindentation analysis of PV module polymeric components after accelerated aging. In: *Proceedings of the 35th EU PVSEC 2018*; September 24-28; Brussels; 2018. pp. 1333-1336
- [14] Owen-Bellini M, Hacke P, Spataru S, Miller DC, Kempe M. Combined-accelerated stress testing for advanced reliability assessment of photovoltaic modules. In: *Proceedings of the 35th EU PVSEC 2018*; September 24-28; Brussels; 2018. pp. 1101-1105
- [15] Schütze M, Junghänel M, Friedrichs O, Wichtendahl R, Scherff M, Müller J, et al. Investigations of potential induced degradation of silicon photovoltaic modules. In: *26th European Photovoltaic Solar Energy Conference*; Hamburg, Germany; September 5-9, 2011
- [16] Schütze M et al. Laboratory study of potential induced degradation of silicon photovoltaic modules. In: *37th IEEE PVSC*; 2011
- [17] Pingel S et al. Potential induced degradation of solar cells and panels. In: *35th IEEE PVSC*; 2010
- [18] Berghold J et al. Potential induced degradation of solar cells and panels. In: *25th EUPVSEC*; 2010. pp. 3753-3759

- [19] Hacke et al. System voltage potential-induced degradation mechanisms in PV modules and methods for test. In: 37th IEEE PVSC; 2011
- [20] IRENA and IEA-PVPS. 2016
- [21] DeGraaff D, Lacerda R, Campeau Z. Degradation mechanisms in Si module technologies observed in the field; their analysis and statistics. Presentation at PV Module Reliability Workshop 2011. NREL, Denver, Golden, USA; 2011. Available from: [http://www1.eere.energy.gov/solar/pdfs/pvmrw2011\\_01\\_ple\\_n\\_degraaff.pdf](http://www1.eere.energy.gov/solar/pdfs/pvmrw2011_01_ple_n_degraaff.pdf)
- [22] Yole Developpement. UV LEDs Technology, Manufacturing and Application Trends Report. 2018
- [23] Muramoto Y, Kimura M, Nouda S. Development and future of ultraviolet light-emitting diodes: UV-LED will replace the UV lamp. *Semiconductor Science and Technology*. 2018;9(8): 0848004
- [24] Mitterhofer S, Jankovec M, Topi M. Using UV LEDs for PV module aging and degradation study. In: Proceedings of the 35th EU PVSEC 2018; September 24-28; Brussels; 2018. pp. 1323-1327
- [25] Ferrara C, Philipp D. Why do PV modules fail? *Energy Procedia*. 2012;5: 379-387
- [26] IEA. Review of failures of photovoltaic modules. Report IEA-PVPS T13-01:2014; 2014
- [27] Badiie A, Ashcroft IA, Wildman RD. The thermo-mechanical degradation of ethylene vinyl acetate used as a solar panel adhesive and encapsulant. *International Journal of Adhesion and Adhesives*. 2016;8: 212-218
- [28] Gagliardi M, Paggi M. Long-term EVA degradation simulation: Climatic zones comparison and possible revision of accelerated tests. *Solar Energy*. 2018; 159:882-897
- [29] Conference 35th EUPVSEC Key Performance Indicators and PV Module Reliability Problem; September 2018
- [30] Mesquita LV, Mansour DE, Philipp D, Bauermann LP. Scanning acoustic microscopy as a non-destructive method for the investigation of PV module components. In: Proceedings of the 35th EU PVSEC 2018; September 24-28; Brussels; 2018. pp. 1318-1322
- [31] Hounkpatin GF, Kounouhéwa BB, Agbomahéna M, Madogni VI. Degradation of crystalline silicon photovoltaic cells/modules under heat and temperature effect. *Physical Science International Journal*. 2018;19(1):1-12
- [32] Virtuani A, Annigoni E, Martins A, Niquille X, Gnocchi L. PV Modules: Reliability and Performance Prediction. Available from: <https://pvlab.epfl.ch/page-131402-en.html>
- [33] Breitenstein O et al. Lock-in Thermography-Basics and Use for Evaluating Electronic Devices and Materials. Springer; 2010
- [34] Koehl M, Hoffmann S, Weiss K-A. Combined stress factor testing of PV modules. In: Proceedings of 29th European Photovoltaic Solar Energy Conference and Exhibition; 2014
- [35] Masuda et al. Sequential and Combined Acceleration Tests for Crystalline Si Photovoltaic Modules. 2016
- [36] Gambogi W. Sequential stress testing to predict photovoltaic module durability. In: 7th World Conference on Photovoltaic Energy Conversion; 2018
- [37] Tamizhmani G. Long-term sequential testing (LST) of PV modules.

In: Photovoltaic Module Reliability Workshop; 2012

[38] Pingel S, Janke S, Stannowski B, Fechner S, Podlowski L. Advanced testing of PV module encapsulants. In: Proceedings of the 35th EU PVSEC 2018; September 2428; Brussels; 2018. pp. 1346-1351

[39] Kleiss G. Key performance indicators and PV module reliability. In: Proceedings of the 35th EU PVSEC 2018; September 2428; Brussels; 2018. pp. 1355-1359

[40] dos Reis Benatto GA et al. Luminescence imaging strategies for drone-based PV array inspection. In: Proceedings of the 33rd EUPVSEC; Amsterdam; 2017. pp. 2016-2020

[41] Koch S et al. Outdoor electroluminescence imaging of crystalline photovoltaic modules: Comparative study between manual ground-level inspections and drone-based aerial surveys. In: Proceedings of the 32nd EUPVSEC; Munich; 2016. pp. 1736-1740

[42] Lanz M et al. Drone-based assessment of cleaning effects on PV installations. In: Proceedings of the 32nd EUPVSEC; Munich; 2016. pp. 1960-1963

[43] Kerschaver EV, Einhaus R, Szlufcik J, Nijs J, Mertens R. A novel silicon solar cell structure with both external polarity contacts on the back surface. In: Proceedings of the 2nd World Conference on Photovoltaic Energy Conversion (Vienna); 1998. pp. 1479-1482

[44] Swanson R. Approaching the 29% limit efficiency of silicon solar cells. In: Proceedings of the 31th IEEE Photovoltaic Specialists Conference (PVSC); Orlando, FL, USA. Piscataway: IEEE; 2005. pp. 889-894. DOI: 10.1109/PVSC.2005.1488274

[45] Jordan DC, Kurtz SR. Photovoltaic degradation rates: An analytical review. Progress in Photovoltaics: Research and Applications. 2012; 1: 12-29. DOI: 10.1002/pip.1182

[46] T.-M. I. B. jenesco, Advances and trends in photovoltaics, Electrotehnic , Electronic , Automatica vol. 61(2013), nr. 1, p. 7-13

[47] T.-M. I. B. jenesco, Present and future of photovoltaics, Electrotehnic , Electronic , Automatica vol. 63(2015), nr. 1, p. 31-38

[48] B jenesco T-MI. La photonique verte. Electrotehnic , Electronic , Automatic . 2017;65(1):7-12

[49] B jenesco TI. Problèmes de la Fiabilité des Composants Électroniques Actifs Actuels. Paris & Arm, Suisse: Masson; 1980. ISBN: 22225699607

[50] B jenesco T-MI. Achievements and trends in photovoltaics. Electrotehnic , Electronic , Automatic . 2017;65(4): 123-127

[51] B jenesco T-MI. State of the art of photovoltaics. Meridian Ingineresc. 2016;4:13-23

[52] B jenesco T-MI, Bâzu M. Reliability of Electronic Components: A Practical Electronic Systems Manufacturing. Berlin and New York: Springer; 1999. ISBN: 354065722-3

[53] Reduced cost of capital has resulted in the out years having real value in discounted cash flow analysis

[54] Jordan DC, Silverman TJ, Wohlgemuth JH, Kurtz SR, Vansant KT. Photovoltaic failure and degradation modes. Progress in Photovoltaics: Research and Applications. 2012; 5: 318-326

[55] Annigoni E. Reliability of photovoltaic modules: From indoor



testing to long-term performance  
prediction [PhD thesis]. EPFL; 2018

[56] IEA. Trends 2017 in photovoltaic  
applications—Survey report of selected  
IEA countries between 1992 and 2016.  
Technical Report IEA-PVPST 13-09:  
2017. IEA International Energy Agency;  
2017

>

>

>

›  
›  
›  
›

›

›

›

›

›

›

›

›

›

.....

.....

>

>

>

>

>

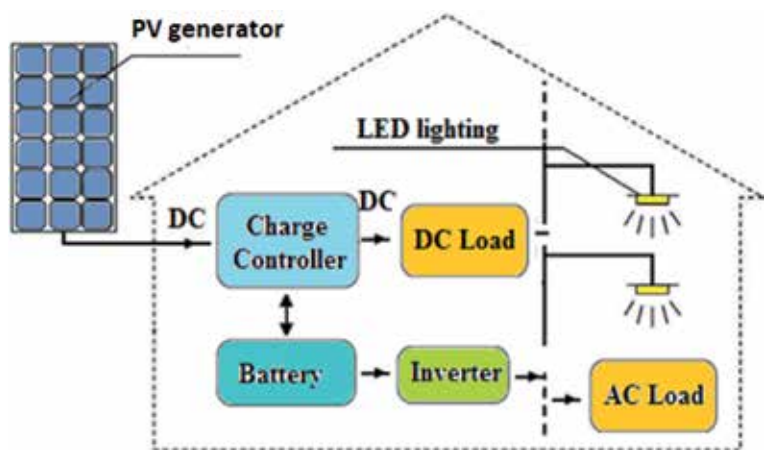
i

>

i

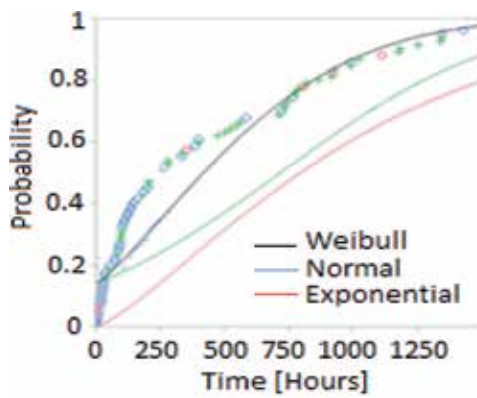
>

>

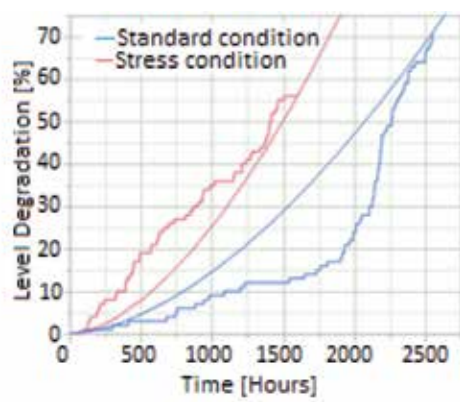




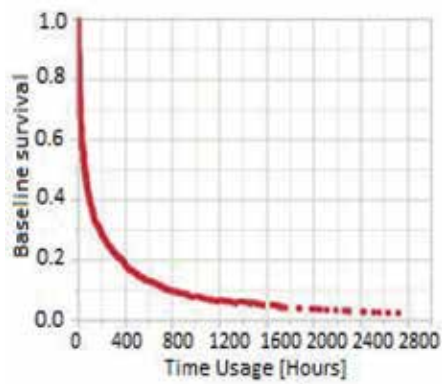
>



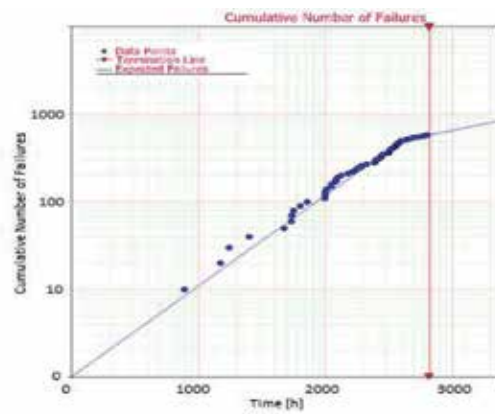
a)



b)



a)



b)

>

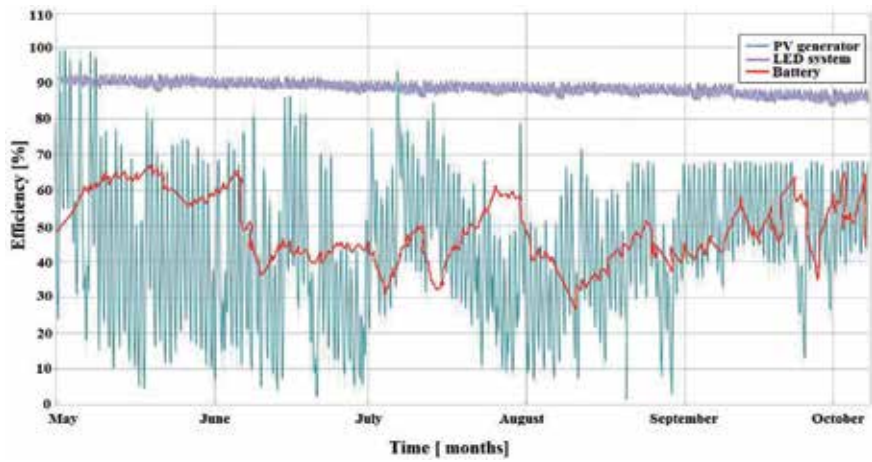
>

>

>

>

>>



.....

•

•

-

€

•

, - €

-

€

.....f.....

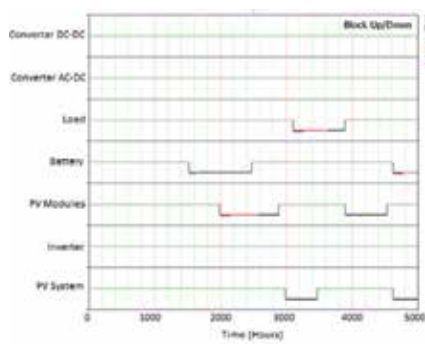
-

€

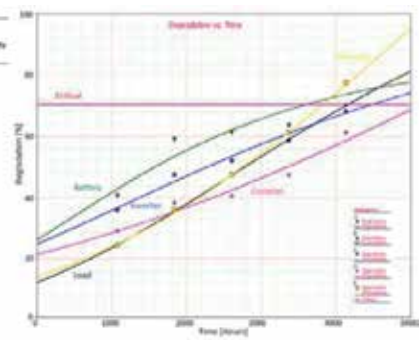
.....

...

.....



a)



b)

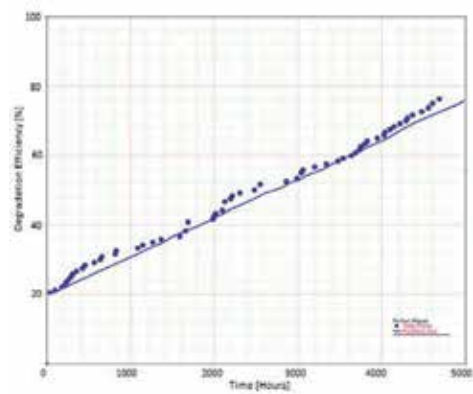
•

•

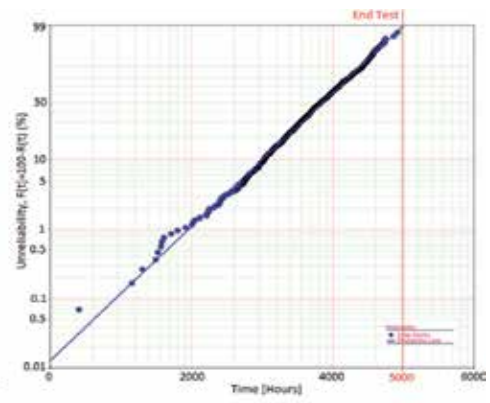
•

•





a)



b)

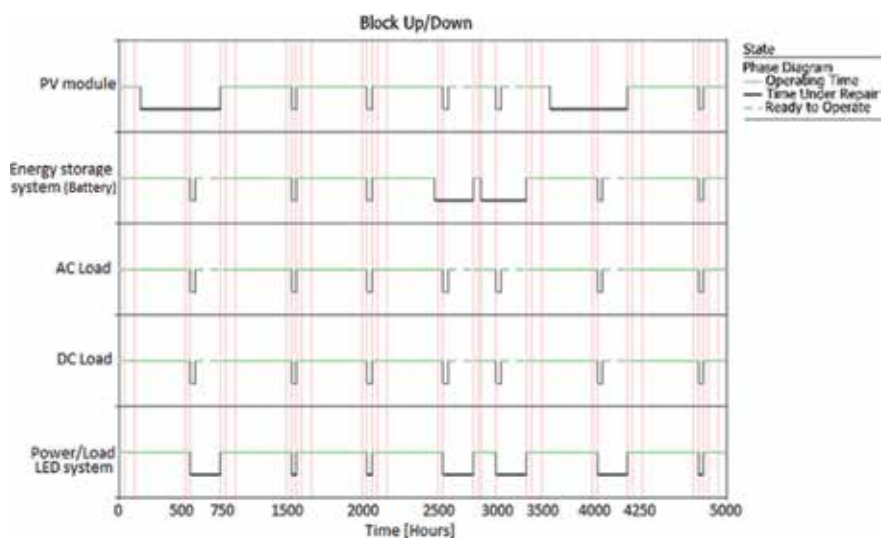
•

>

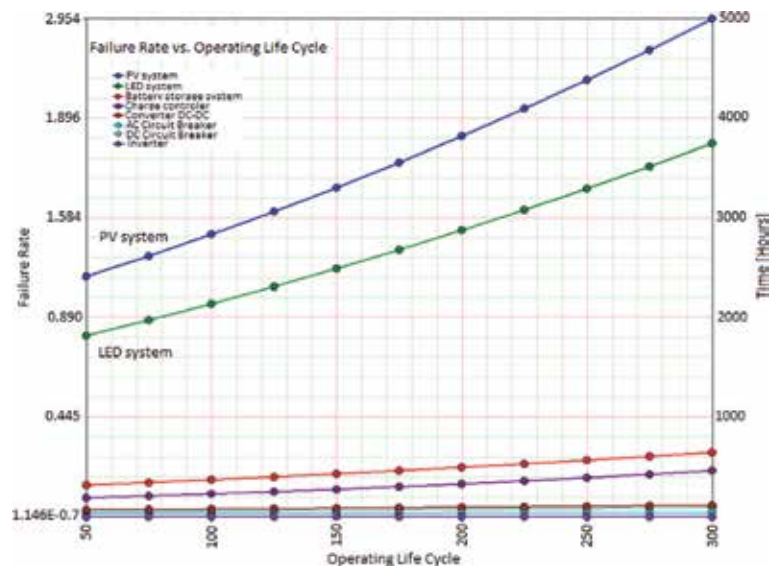
>

>

>



•





$f_{\text{„}}$      $\dots \text{€} \uparrow$      $f$      $\dots$   
 $\dots \text{€} \downarrow$      $\wedge$      $- \text{‰}$      $\text{€} \text{‰}$      $\text{€} \text{Š}$   
 $- \text{Š}$      $\text{€} \text{‰}$      $\text{€} \text{Š}$   
 $\uparrow$      $\dots$      $\dots \text{€}$

IntechOpen

---

$\dots$      $\dots$      $\dots$      $\dots$   
 $\dots \text{€}$      $\text{€}$      $\dots$      $\dots$   
 $\dots$      $\dots$      $\dots$      $\dots$

. . . . .  
 .  
 - € ,f „ ...†††  
 ... ^ . . . %<sub>00</sub> Š  
 . . . - .  
 . . . „  
 . . . . .  
 .( . . . € Œ „  
 Ž•‘ ^ . ’- „ ...†  
 “ ” . . . ^  
 . ‘ . . . Œ -  
 . < ... ‘ . %<sub>00</sub> Ž  
 — . . . ~ „ †† —™~—š  
 - •‘%<sub>00</sub> . - . .  
 . )- .  
 . . . . %<sub>00</sub>  
 Œ— . ‘ . . .  
 %<sub>00</sub> „ ††™  
 ™ . , , Œ , ž ” ~  
 . . .  
 Œ . . . .  
 . . . . .  
 . . . . .  
 . ...† „ •Ÿ†  
 œ %<sub>00</sub> ‘  
 . . . .  
 . . . .  
 • - „ ...††-  
 Ÿ“~š†  
 Ÿ %<sub>00</sub> . . .  
 .  
 . . . .  
 .  
 - „ ...††“ †...~“††  
 š € . . . Œ ž .  
 ” € ” •œ  
 .( . . . .  
 ~ . . . .  
 . . .  
 . . . .  
 . . . . < ŸŸŸŸ“ .  
 . •%<sub>00</sub> .

%<sub>00</sub> • - ••„ ŸŸŸ“† „  
 ...††  
 † - ” ‘ .  
 . .  
 ~ . . . . .  
 . . . . .  
 . . . . .  
 . ...† ...„ •Ÿ“~ Ÿ†  
 † - - . .  
 . .  
 i —  
 ž . . . . .  
 ...† ...„ . . “-ŸœŸ-  
 ... ž•† ™™™œ...† ...œ“-ŸœŸ-  
 . - . . . .  
 . Œ . ž  
 - . . . . ...††  
 ... € - ^ . —  
 £ . ‘( . .  
 ~ α  
 .( . . . .““ .  
 - . %<sub>00</sub> . „ ††œ  
 “ ž € .  
 . .  
 ¥ . . .  
 . ††š„ •-†™™...  
 - ” | -  
 — . .  
 †š†„ •š™~š™†  
 ™ . . . .  
 § . α . .  
 . . . .  
 . . . .  
 - „ ...†††  
 œ . £ € ” . ‘  
 , •§ - - . !  
 . . . . .  
 . . . . .  
 . . . . .  
 - . %<sub>00</sub> . „ ...††š  
 Ÿ %<sub>00</sub> ‘ - .  
 - — - . ^ —  
 ¥ .  
 .

•••••  
- € , -  
f  
• „ ...†€„•  
• ‡ - ^••• %<sub>00</sub>  
- Š , ( - (

( ‡

••œ Ž( 'œ •(• - •(  
, ••• -

“ €  
f “ Š

• ' "( (•••  
- Š -  
- f Š  
-

•••(• Ž( Ž'•

•  
• — •...~€...~

...•™ Š œ š- (

- “  
•  
š- š ~

„• “ Š™••  
Š “ -

• -  
f Š • Š  
- • ••€†...

†• ' "•f Š , -  
Š € €

†

—• ^•( ) - ••• -

,  
• Š (•• f —

~• ' Š •••  
Š -

-  
- ( ,  
( - •

•~€~†

•• ,œž- œ•( f €  
- Š

Š -  
• „

• ‡ - ^•š €  
- Š

” , f “  
• ( ”f š%„'€† €.....†— ...  
•~€•...

...•, ‡ ”•'  
- • (

• - - - •  
f “ Š “  
• Ÿ “ “  
- ‡ ...

...•j ^•( ) ‡• ^•  
ø- ••š €  
Š • ,

...• - - ' ( - š( •(  
) Š •( ' -•' œ

Š š' Š  
-œœœ £ -  
“ œ ” ɹ

- ~ “  
~%~•€...€... €—... †€†¥ ...

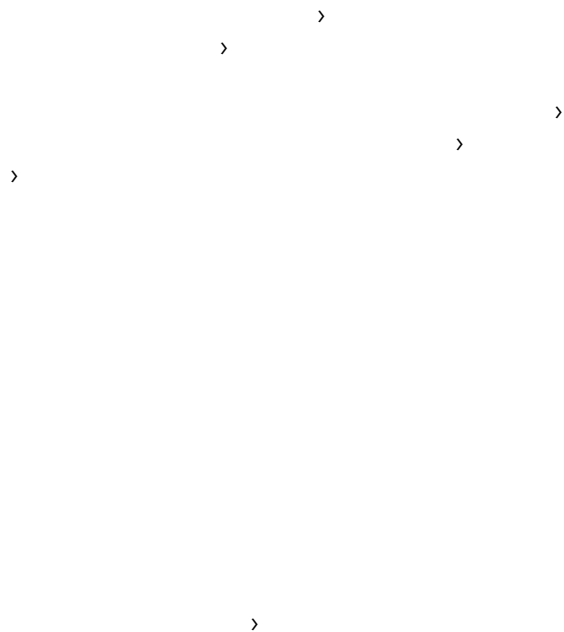
.....• • Š  
%œ%œ“““ %œ %œ  
“ • ‘ Š  
~•

...„• ( ( ” † )  
f Š - Š -  
“ Š Š -

š , “

f ( f ~

›  
› › ›





>

>

>

i

>

>

---

---

---

---

•

•

•••

•

•



• • • • •  
• • • • •  
• • • • • € •  
• • • • •  
• • • • •  
f f " " " " †† " ^%\_ ,%\_ "%\_  
S,, Œ  
•  
• Ž •  
• %\_ \_

[illegible]

›  
›

›

›

›

›

›

›

›

i

i

›

›

€ ›

i

£

i

i

/

›

›

›

¥

f

§²

' " ›

§

f ".... † †... €...  
 † ^ € ... †% „ Š • œ „...  
 Ž... €... †% € €  
 € •• f „ ••  
 f ... „ € f € € ... '... †  
 „ € ... „ „... † • € † f  
 • € † € „ f † „ f  
 f € € € € † ... † f  
 „ „ ... € ... € „  
 € ... • € „  
 “ % f ' „ „ •• ... „ ••  
 € œ „ † „ ... „  
 € „ € „... „  
 † €... † •• – „  
 „ — € † € „ „ „... † •••  
 ~TM € € € € ... •• “ „  
 „ € ' € -š € •• ›  
 „ † † • ... •-... „ „  
 •, f „ €... € € f „ Š•  
 œ „ „ „ „ € • ••  
 œ ... „ œ ' „ ... • € „ ^ €  
 f „ € „ „ ž „... • € „  
 Ÿ % € „ f € € œ  
 ^ † € ... € œ †  
 † € ... š •• € „ „ f” „  
 € • „ € „... „ ~ „ œ † †  
 „ € „ € „ € „... f ...  
 „ € € f ... † € „  
 „  
 iœ• „... † f € €  
 -š •• iœ• % f † „ € iœ „  
 ... € •• œ €  
 ... € „ € ... „ •  
 ^ f „ † „ €... f  
 ... „ — „ „ •• iœ• †  
 „ € † „... „ „ € „  
 ... •• f † „... % f € „ € f  
 ... „ † „ „ € „ „ €” ...  
 € € iœ „ % „ € † ...  
 ••  
 œ „ „ „... € „  
 € † € € € ... € ... €  
 € „ € † „... „ € ... „  
 „ „ € € ... „ „ • f †  
 € ... † € † ... „ f € •  
 „ ž f œ € ... €  
 € ^ € † ... € • f †  
 „ € „ „ † „ ... „ • % €  
 ... € f ... €

$f, „...†..... •^€$ 
 $f, „...†...† •†€$

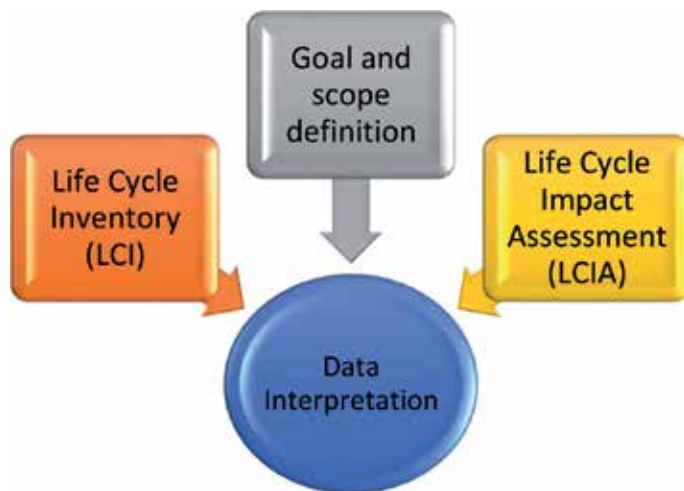
$\%$ 
 $\check{S}$

$\check{S} \text{ } \text{œ} \bullet$

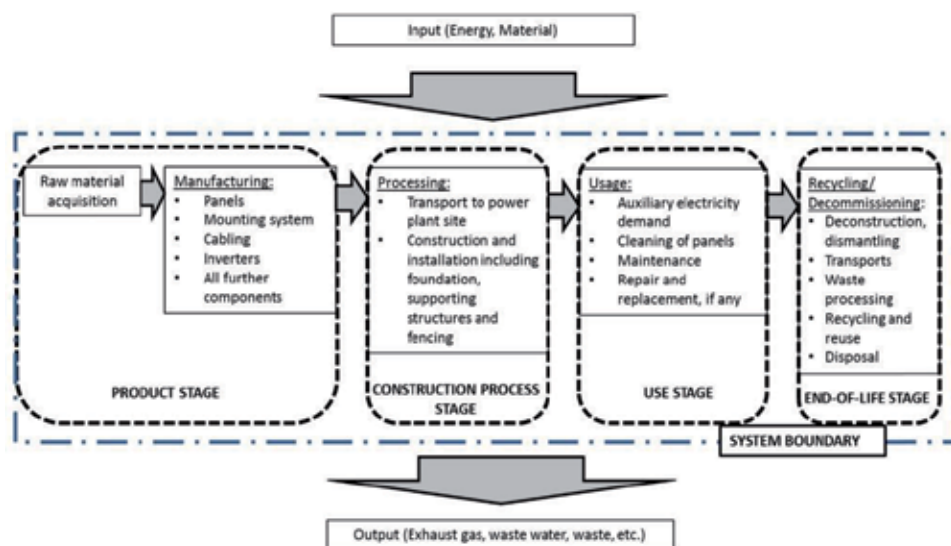
$\check{Z}$ 
 $\check{S}$

$\check{S}$

$\text{TM}\check{S}$ 
 $\text{TM}\check{S}$ 
 $\bullet \text{ } \text{œ}$



• • • • •



> >

> >

>

›

›

›

›

›

›

›

›

i

i

¢

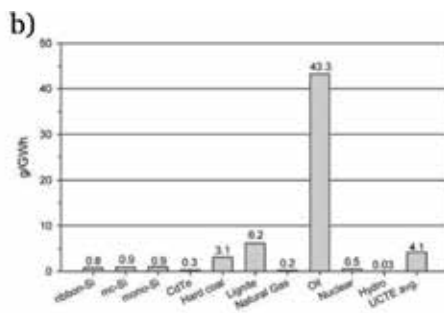
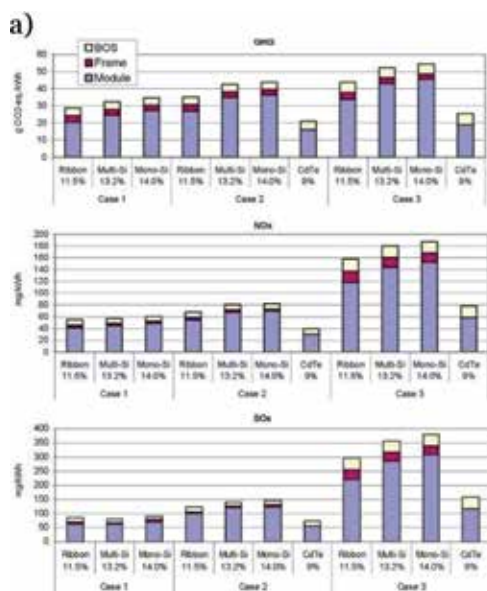
i

£

›

›

• • •••



• • •••

•

> >

>

>

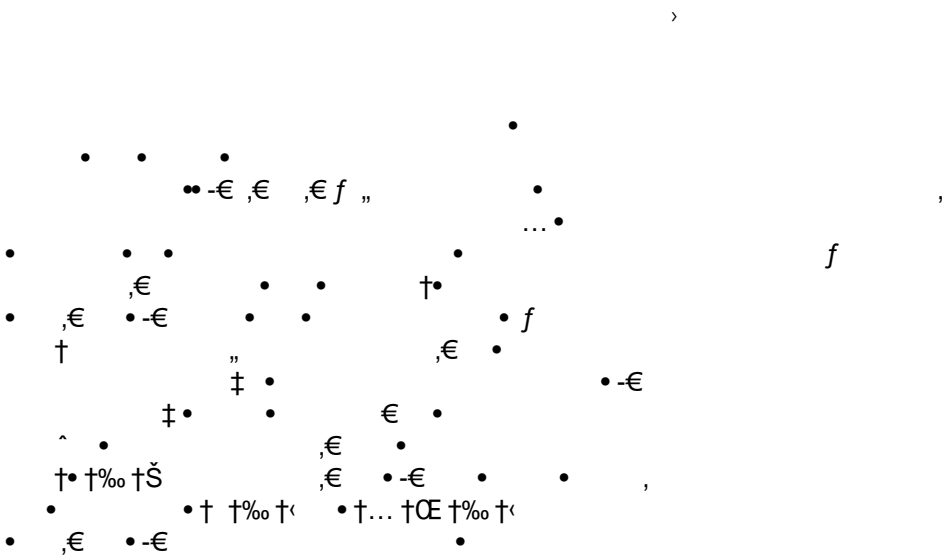
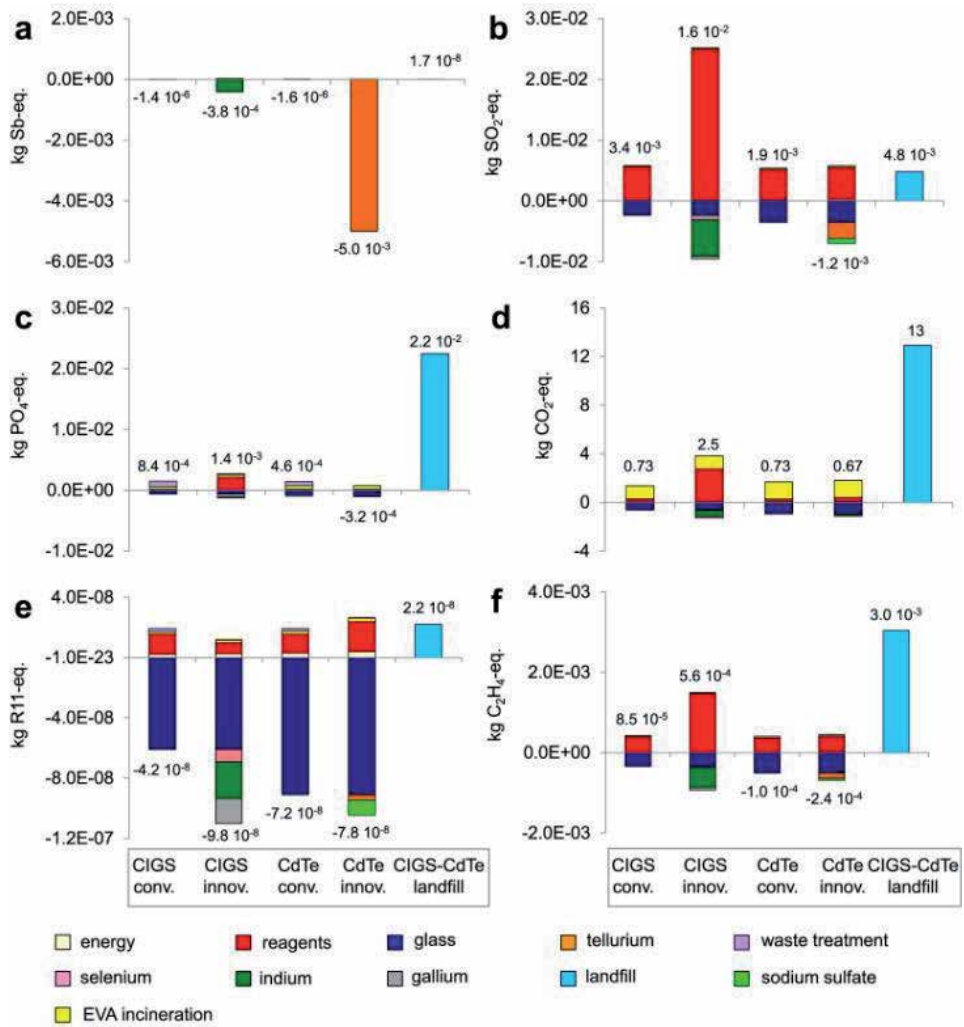
>

> >

>

>

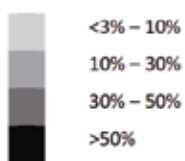


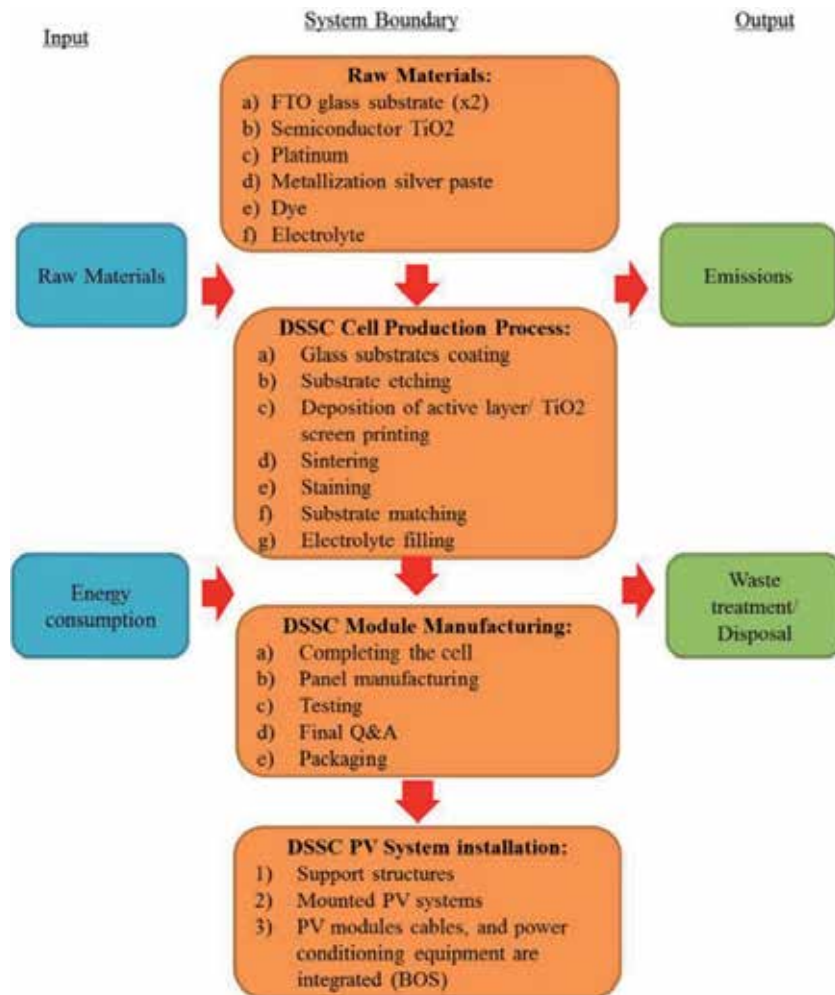


Metal	Cancer potential			Non-cancer potential			Ecotoxicity potential		
	c-Si	a-Si	CIGS	c-Si	a-Si	CIGS	c-Si	a-Si	CIGS
Ag									
As									
Ba									
Be									
Cd									
Co									
Cr									
Cu									
Hg									
Mo									
Ni									
Pb									
Sb									
Se									
Sn									
Tl									
V									
Zn									

1	3	5
2	4	6

1. Urban Air
2. Rural Air
3. Fresh Water
4. Sea Water
5. Natural Soil
6. Agricultural Soil





...

[illegible]

● ● ●● ●●

&gt; &gt;

&gt;

> >

&gt;

&gt;

&gt;

&gt;

&gt;

i

&gt; &gt; &gt;

&gt;

¢

&gt;

&gt;

£

/

/

¢

/

&gt;

¥

&gt;

/

&gt;

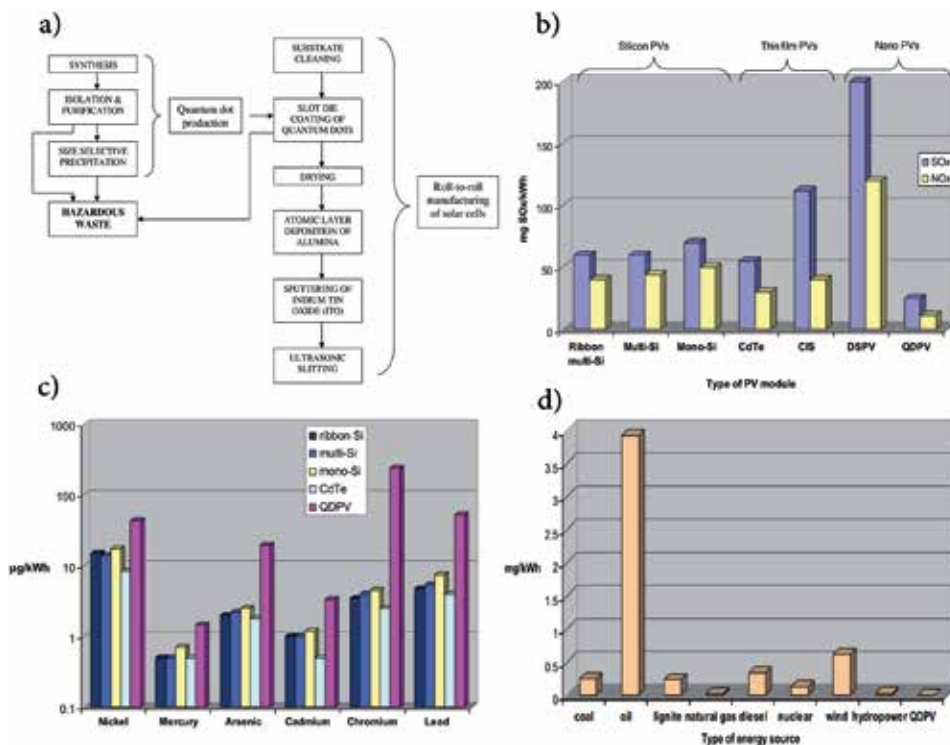
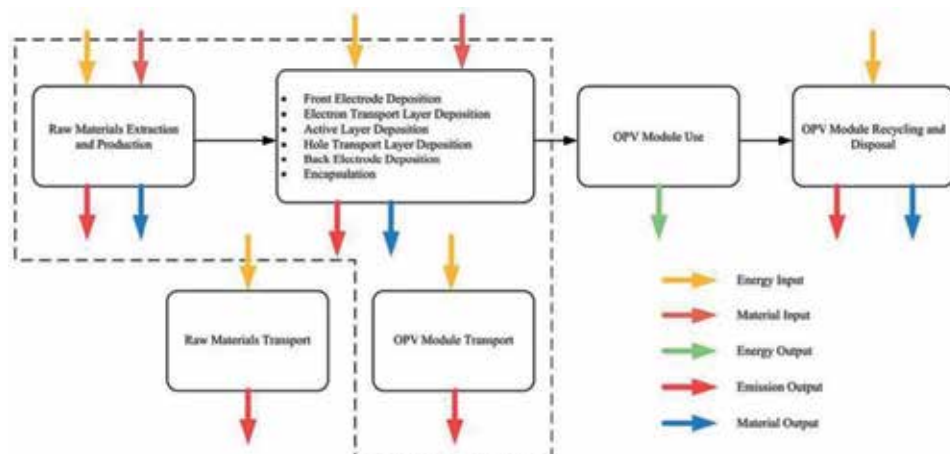
&gt;

&gt;

&gt;

&gt;





a)

Nucleation Sites

mp-TiO<sub>2</sub>

Pre-activation

mp-TiO<sub>2</sub><sup>\*</sup>

Deposition of supersaturated PbI<sub>2</sub> in DMF

PbI<sub>2</sub> Nucleus

PbI<sub>2</sub>.DMF@mp-TiO<sub>2</sub>

Slow Evaporation

PbI<sub>2</sub>(sol)@mp-TiO<sub>2</sub>

Dipping in MAI solution

MAPbBr<sub>3</sub> Nucleus

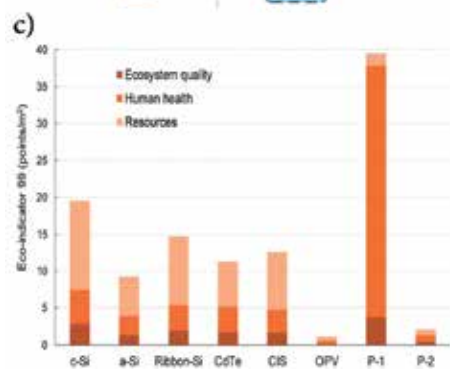
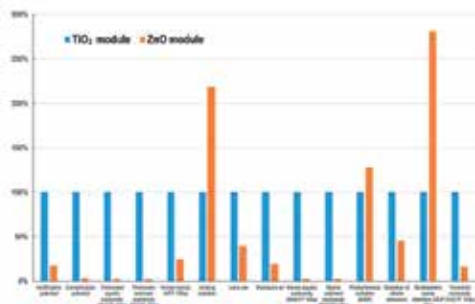
MAPbBr<sub>3</sub>.DMF@mp-TiO<sub>2</sub>

Crystal Growth

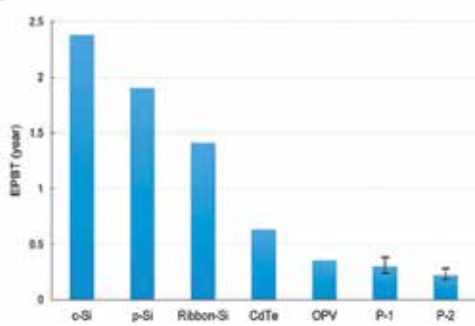
MAPbBr<sub>3</sub>@mp-TiO<sub>2</sub>



**b)**



d)





›

›

›

›

i ›

i

›

›

› ›

i

› ›

¢ ¢ £¢ › /

• • • • •

•

- € , f „ ... € ... † - ‡ € f ^

f • • • • • ‰ • • • • Š • • • • •

† • ‹ ‰ ‰ ‰ ‹ • ‹ Š Ž • ‘ •

^ - • • - ‹ •

” “ ‡ ”

IntechOpen

• † - † - • ‰ Š • ‹ — •

• ... • ~ — ‰ “TMTM TM

TM TM™\_TMŠ



"

§

>

>

«

ü

α

f

§

i

>

>

i

¢

'

α

>

£

§

>

/

¥

/

¥/

,

>

f

§

α

§

§

"

§

i

f

<

i

>

α

>

'

/

§

§

£

α

>

i

i

,

>

>

[illegible]

$\rightarrow \alpha \bullet \in \rangle$   
 $\check{S}(\langle \in \check{Z} \phi^{(1)} \rangle \neq$   
 $\check{S}$   
 $\dots$   
 $\text{„ } f - f \dots$   
 $\bullet f \dots \dots, f \dots$   
 $\dots \dots \dagger \dots \check{S} \dots$   
 $\bullet \check{S}(\langle \in \check{Z} \phi^{(1)} \neq \bullet \in , '$   
 $f^{''''} \dagger \dots \dagger \check{Z} - \check{Y} \rangle \langle \in \langle$   
 $\check{S} \check{S} \dots \dots \dagger \dots \sim$   
 $\dots \text{„ } \dagger \dagger$   
 $\bullet, f \dots \dots$   
 $\bullet \dots, ff \dots \dots$   
 $\check{S}(\langle \in \check{Z} \phi^{(1)} \neq \check{S} \rangle - \check{Y},$   
 $\langle \langle \phi \rangle \text{“} \text{“} \rangle \check{S}$   
 $\check{S} \rangle - \check{S} - \dagger \dagger \dots$   
 $\bullet \alpha \dots \bullet \check{S}(\check{S} \in \check{Z}) \text{“} \text{“}$   
 $\phi \bullet \in , ' f^{''''} \bullet -$   
 $\text{“} \bullet \text{“} f \bullet \check{S}(\check{S}$   
 $\check{S} \in \sim - \dagger \dots \bullet - f$   
 $f \dots \dots, \dagger \in$   
 $f \dots \dots \bullet \dots$   
 $\bullet, - \dots f \bullet \bullet \in \dots$   
 $\bullet \dots - \dots \bullet \dots$   
 $\check{S}(\langle \in \check{Z} \rangle \check{S} \bullet \in , '$   
 $f^{''''} \dagger \dots \dagger \check{Z} - \check{Y} \rangle \in \check{S} \rangle \langle$   
 $\check{S} \text{“} \dagger \dots \bullet \dots -$   
 $\alpha \dagger \dots \text{“} a - \dots \text{“} \bullet$   
 $\bullet \bullet f \dots \bullet, \in$   
 $\in \dots \bullet \bullet f \bullet \dagger \bullet$   
 $\check{S}(\neq \in \check{Z} \text{“} \text{“} \check{S} \check{S} \check{S} \text{“}$   
 $\check{S} \phi - \langle \bullet \bullet \alpha \dagger \in - \bullet \bullet$   
 $\text{“} \alpha \bullet \text{“} \text{“} \dagger \bullet f \dots$   
 $\in \bullet \dagger \bullet \bullet \bullet$   
 $\bullet \bullet \check{S}(\neq \in \check{Z} \text{“} \rangle \check{S} \rangle \in - \check{Y},$   
 $\langle \check{S} \text{“} \langle \langle \text{“} \text{“}$   
 $\check{S} \neq \text{“} \bullet \bullet \bullet f \dots -$   
 $\alpha \bullet \bullet \dots - \bullet$   
 $- \dagger \bullet \bullet, \dagger \bullet \bullet \bullet$   
 $\dagger f - \dots \dagger \dots$   
 $\check{S} \bullet \check{S}(\langle \in \check{Z} \text{“} \rangle \check{S} \langle$   
 $\rangle \text{“} \langle \bullet \bullet \in , ' f^{''''} \text{“} \text{“}$   
 $\bullet \bullet \bullet \text{“} \bullet \text{“} \text{“} f \text{“}$   
 $\langle \check{S} \neq \check{S} \in \langle \check{S} \phi \langle$   
 $\check{S} \in - \bullet \check{Y} \bullet \bullet \bullet$   
 $\text{“} - \bullet \ddot{u} \text{“} \bullet \bullet f$

€ ( ^...^ •...Š ‡ OE  
 ( „„ f „ž  
 „ (¢ f  
 ž ž fž ( ž  
 • • • • • š  
 „ „„„„  
 • • • •  
 ^ • • • § „ • š

^ ^ . .  
 † . .  
 α ”  
 -€-f†-†^- Š• • †• †◀◀  
 ŒŒŒŒ < < <  
 ( €†-†—— € Ž€†~ TM%\_Š••  
 Ž £ œœœ ~α “ š  
 “ ^ .  
 . . .  
 ^ . . ¥ Œ  
 | .  
 α  
 § • • -€Žf „€...†—€^—,  
 šj† € €Ž€(-%\_—€, —€Ž —€—Ž  
 ‡ • • › £ ” •  
 • • ‘ • • ¥  
 Œ ^ i~ i  
 Œ • ^ ¥ Š ” Š  
 • Š  
 -€%\_f †%\_, ^%\_Ž€  
 —€ • • • • Š  
 ” • • • • Š• ^ ¥  
 •  
 ¥ Œ  
 †•  
 •  
 • • •  
 • Š ” Š  
 -€%\_f †—^-%\_-  
 — • • • • Š •  
 • • ” • •  
 ¥ ¥ ¥  
 | ¥ |  
 | •  
 • • Œ  
 • ^ ¥  
 • Š ” Š  
 -€%\_f †‡,-€-  
 — • • •  
 ” • • •  
 ¥ ¥ |  
 | •  
 | Œ  
 • ^ ¥  
 α • •  
 -€-f „Ž...†-Ž,

□ □

›

§  
§ §  
/

›

¢ ' £ £ "

¥

›

£

›

›

i

¢

£

¢ £

¢ «

/

¥

¥

*f*

£

< £ £  
£

fi

¥

› i '

§ § /

£ £

"

"

§

• • • • •  
• • • • •  
- • • • • €  
  
, f „...€ † ^...% ^š† † „†  
„ † % š† œ % ž, ‘  
• € ‘€ „... % ... € •  
„ % „ € • - % % €  
„ ... % % €  
% % —  
• • • • •  
~~~~ % €  
%  
„ • - • • • TM-š ...  
  
, f ^...% šœ† ‘ † œ ‘  
œ... % ... € • % „ € ž  
† % € % € %  
~ ‘€ % € „... % ...  
€ % „ † % ~  
% € „... % —% † ~  
• - • • •  
~~~~ % € %  
„ • - • • • TM-š ...  
  
, f ø % Ÿ š† • • i ‘ %  
% % %  
“... % ... € œš†  
~ “... % ...  
... ^... % ‘ % † €... %  
• • • • •  
~~~~ % € %  
„ • • • -  
  
, f „ % € † ž £ £ †  
š £ † † “ † ‘ „ † i  
£ † ‘ † •  
€ † † œ † š  
... % % - %  
— % • •  
~~~~  
% € %  
„ • • • • • € € ¥ € ¥  
  
, f • † ž £ £ †  
† † „ † ‘ % †  
š † ‘ — † ‘ š % •  
% % € ... € €  
...  
€ % •... ‘ š  
• -  
- • • - •

• - • • - • •  
• • • - € • €  
  
, f £ £ ž † † † ‘ % † š  
‘ š • %  
€ % -  
„ % © % ... % ...  
~ % € €  
‘ „...’ • • • • -  
š-© • • • • -  
  
, f ž ... % † — % † † ... €  
a % € € † ž ‘ © %  
  
% „ € ...  
% • ... % •  
% % © % %  
‘ % % † % † — % €  
i • % † š — † ‘ © ‘ †  
© † © — • ‘...  
„  
€ ... % • • • -  
  
, f „ % ^† a % — † i ... † † † †  
‘ % š† • % † ‘ † % ... •  
€ € „ % „ € %  
% „  
‘ „...’  
• • • • š-© • •  
•  
  
, f i ... œ † œ % † † œ † † † † a %  
— † † ‘ % † † † † — % % €  
~  
~ • ... €  
~ % „ % — % %  
€ % € † ... % †  
• — • • š-© • •  
€ • •  
  
, f „ € † † † a % € € †  
£ £ ž † œ % š† „ † ‘ š  
% † © -  
... % ... %  
„  
€ ‘ „...’  
• • • - • • • • •  
  
, f š % † š % „ † ž ... † ‘  
† i •  
% % % € % % %  
— % ® — % % %  
„ % • • • • •



Available from: <http://xlink.rsc.org/?DOI=C EE E>

[ ] Celik I, Song Z, Cimaroli AJ, Yan Y, Heben MJ, Apul D. Life cycle assessment (LCA) of perovskite PV cells projected from lab to fab. *Solar Energy Materials & Solar Cells*. ; : - . Available from: <https://www.sciencedirect.com/science/article/pii/S> ?via Dithub

[ ] Krebs FC, Espinosa N, Hösel M, Søndergaard RR, Jørgensen M. th Anniversary article: Rise to power—OPV-based solar parks. *Advanced Materials*. ; ( ): - . DOI: . /adma.

[ ] Yoo YG, Park J, Umh HN, Lee SY, Bae S, Kim YH, et al. Evaluating the environmental impact of the lead species in perovskite solar cells via environmental-fate modeling. *Journal of Industrial and Engineering Chemistry*. ; : - . Available from: <https://www.sciencedirect.com/science/article/pii/S X X>

---

Section

# Ecological Concerns

---



€, f, „ ...

>

€, ...

€ ...

€ ‡...

†

‡

^ ^ ^

• • • • • • • • • •  
• • • • • • • • • •  
• • • • • • • • • •  
• • • • • • • • • •  
• • • • • • • • • •  
• • • • • • • • • •  
• • • • • • • • • •  
• • • • • • • • • •  
• • • • • • • • • •  
• • • • • • • • • •

• • • • • • • • • •  
• • • • • • • • • •  
• • • • • • • • • •  
• • • • • • • • • •  
• • • • • • • • • •  
• • • • • • • • • •  
• • • • • • • • • •  
• • • • • • • • • •  
• • • • • • • • • •  
• • • • • • • • • •

„ €

„ ... •

„ •

„ •

„ -

„ €

„ • †

„

„ ‡ • •

-€ • • • • •

-€ • • • • •

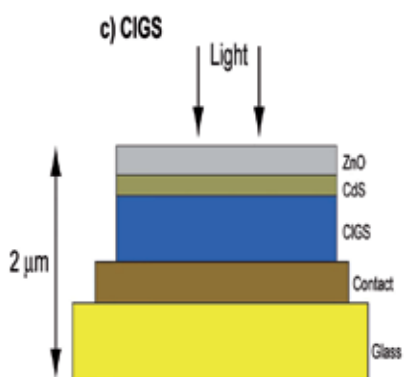
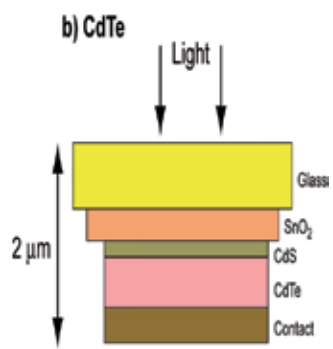
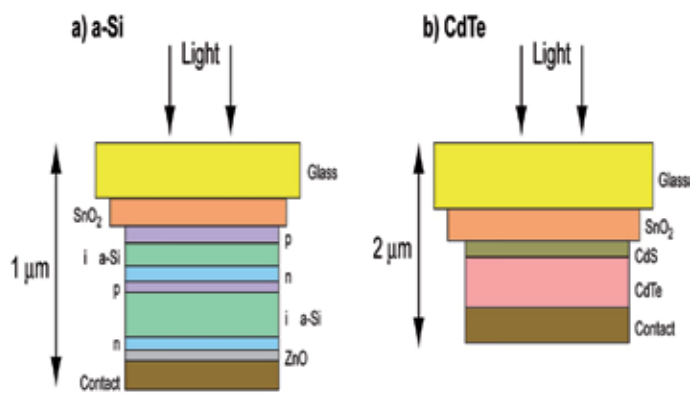
€ - • • • • • • • • • •

€ ‡ • • • • • • • • • •

€ ^ • • • • • • • • • •

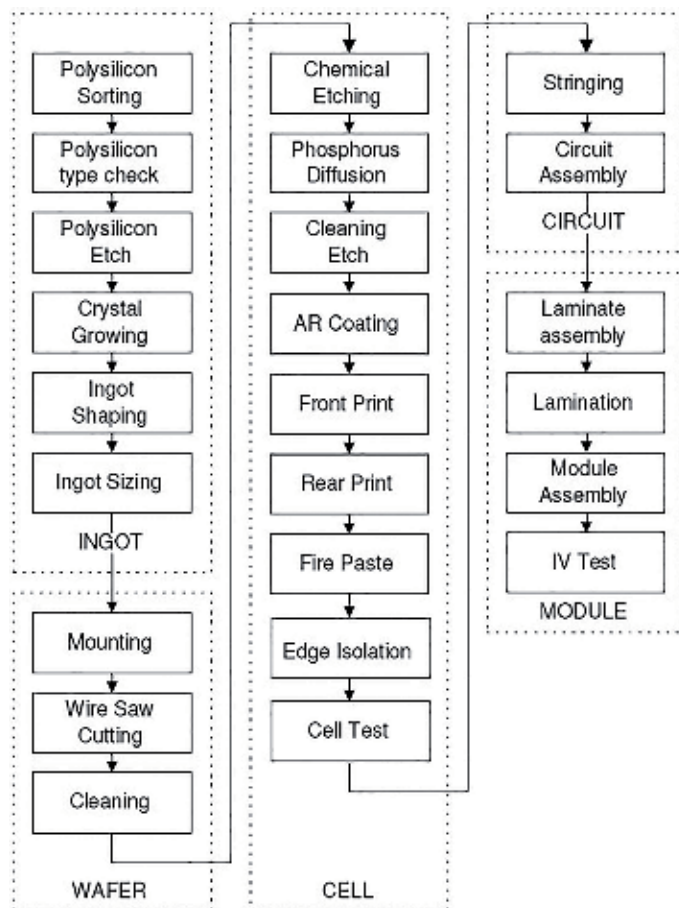
€ - • • • • • • • • • •

€ - • • • • • • • • • •

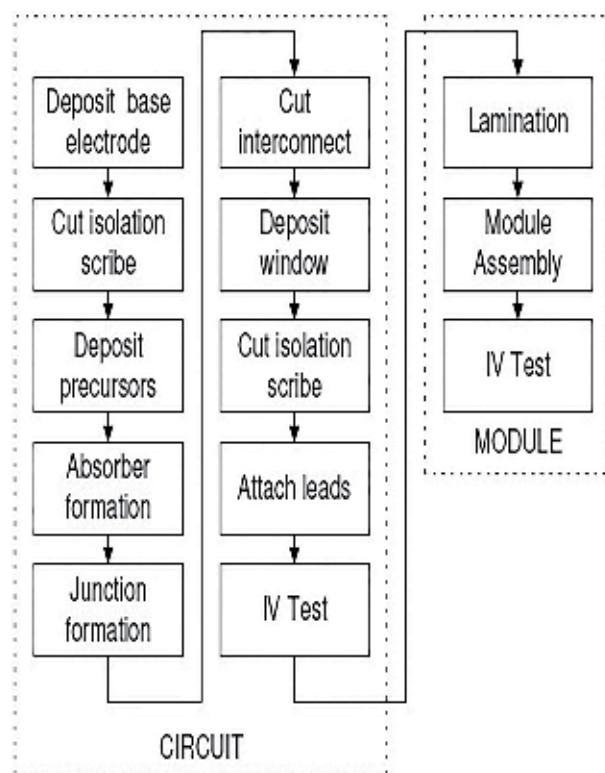


	•œ" — € •	•,, — € •	~	~š~	— €	ž	—,,
TM	•• ( — €,,	—... — €,,	• f š	—•š	—•€	—œ,	
	•. " — € •	—... — € •	•	—",š	•	"€	—ž,
	•- € — €,,	—žœ — € •	•	—...š•	•€,		
	—€ • — € (	€			•,š		
%	—€ • — € (	... -			%	••,	
%	žž — € ...	•• - — € ž	%	•	•,š%	•	•,,
	—€ — € •	€			) œ	••,	

••

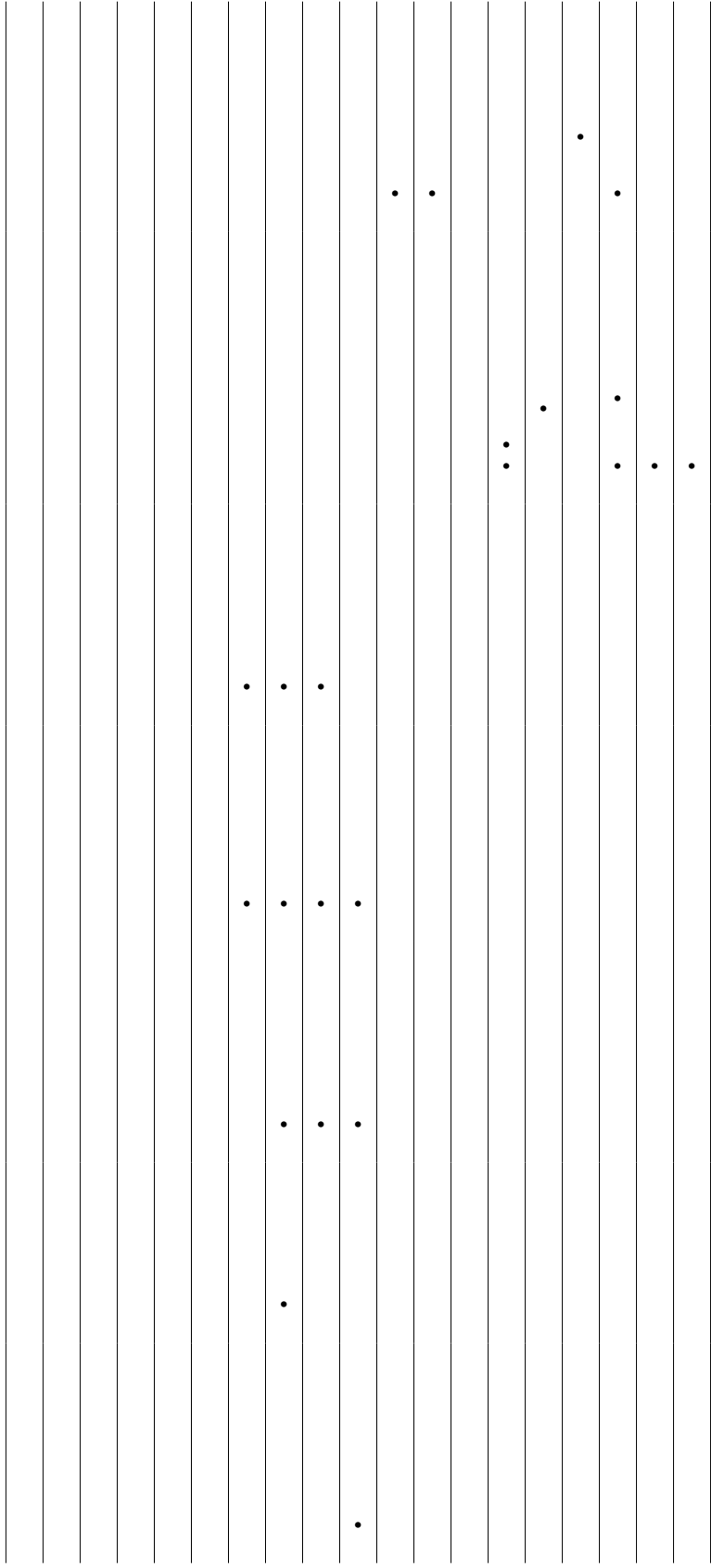






>

>



•

••

•

••• - € • ••• , - €  $f_{\bullet} \dots \dagger$

•••

€  $f_{\dagger} \dots$  ^ • €

• , , • , - •

•  $f_{\dagger} \dots \%$

•

‰	Š ‰	•
‰	Š ‰ •œŽ	‘ ^
•	• ••	• ^
	•• €	
œ	•	
œ	•	•
œ “		•
œ “		•
‘	• Š ‰	•
	• €•••	
‘	•	•
‘	•	“
‘	•••	‘ •
‘	••• • €•••	• “
•	••• •Š•	”
•	Š ‰	“
•		
	• Š “	
	•	‘ • “
	•	• ^
•	••• •••	•
•	•	•
		“
•	•	

	•••••	•••••	
•	'•	"	'
•		•	"
•		•	"
•		•	"
•	•€	•	"
•		•	

	••		
•	•	•••• - €	••
,		••	
•		$f_{\mathfrak{N}^{\cdots}}$	
	€	•†••	
	• ‡ <sup>^^</sup>	$f^{\% \% \% \ldots} \in \% \check{\mathfrak{S}}\langle$	
$\% \mathfrak{O} \ddagger \langle$		€	œ ‡ ‹
	• <sup>•</sup> ^ <sup>•</sup> „ ‹		
	^ ^ Š ‹	$f^{\% \% \% \ldots}$	
•	••		
	•		
	†		
ž			
••	•		
€		$f_{\mathfrak{N}^{\cdots}}$	
	•		
		$f_{\mathfrak{N}^{\cdots}}$ ,	
	••	•	
	••	†	
	€		

[illegible]

•  
-  
  
... † ‡ ^ % f ,  
• • ^  
• Š  
‘  
Ž  
... • ^  
‘  
... ’ ^ %  
”  
^  
Ž  
Ž

f  
’ ” f  
”  
œ  
”  
%  
... ^ %  
%

The diagram consists of the following elements:

- Top Left:** A plus sign with a vertical line through it, enclosed in double quotes.
- Top Center:** A double quote.
- Top Right:** A double quote.
- Middle Left:** A plus sign with a vertical line through it, preceded by a dot.
- Middle Center:** A plus sign with a vertical line through it, preceded by three dots.
- Middle Right:** A plus sign with a vertical line through it, preceded by a double quote.
- Bottom Left:** A plus sign with a vertical line through it, preceded by a double quote.
- Bottom Center:** A plus sign with a vertical line through it, preceded by a double quote.
- Bottom Right:** A plus sign with a vertical line through it, preceded by a double quote.
- Other Symbols:** A tilde, a percent sign, a less-than sign, a greater-than sign, a double less-than sign, a double greater-than sign, a double colon, a single colon, a double dash, a single dash, a double underline, a single underline, a double overline, a single overline, a double tilde, a single tilde, a double percent sign, a single percent sign, a double less-than-or-equal sign, a single less-than-or-equal sign, a double greater-than-or-equal sign, a single greater-than-or-equal sign, a double not, a single not, a double infinity, a single infinity, a double square, a single square, a double circle, a single circle, a double triangle, a single triangle, a double diamond, a single diamond, a double asterisk, a single asterisk, a double hash, a single hash, a double dollar sign, a single dollar sign, a double at sign, a single at sign, a double percent sign, a single percent sign, a double less-than sign, a single less-than sign, a double greater-than sign, a single greater-than sign, a double plus sign, a single plus sign, a double minus sign, a single minus sign, a double multiply sign, a single multiply sign, a double divide sign, a single divide sign, a double modulo sign, a single modulo sign, a double power sign, a single power sign, a double root sign, a single root sign, a double integral sign, a single integral sign, a double differential sign, a single differential sign, a double partial sign, a single partial sign, a double summation sign, a single summation sign, a double product sign, a single product sign, a double limit sign, a single limit sign, a double subset sign, a single subset sign, a double superset sign, a single superset sign, a double intersection sign, a single intersection sign, a double union sign, a single union sign, a double difference sign, a single difference sign, a double symmetric difference sign, a single symmetric difference sign, a double complement sign, a single complement sign, a double absolute value sign, a single absolute value sign, a double floor sign, a single floor sign, a double ceiling sign, a single ceiling sign, a double square root sign, a single square root sign, a double cube root sign, a single cube root sign, a double nth root sign, a single nth root sign, a double factorial sign, a single factorial sign, a double double factorial sign, a single double factorial sign, a double triple factorial sign, a single triple factorial sign, a double subfactorial sign, a single subfactorial sign, a double superfactorial sign, a single superfactorial sign, a double hyperfactorial sign, a single hyperfactorial sign, a double double factorial sign, a single double factorial sign, a double triple factorial sign, a single triple factorial sign, a double subfactorial sign, a single subfactorial sign, a double superfactorial sign, a single superfactorial sign, a double hyperfactorial sign, a single hyperfactorial sign.

›

›

›

›

›

›

† ‡ ‹ ŒŽ‘ ’ ‹ ‡ † ‘ “

—

Š -” • - † f “ ‹ ŒŽ ‘ ‹ ‡ †  
‘ “ ‡ † f ~  
Š TM - •











>  
 €      €      ,  
 ††††      f      „      >      ...  
              ^      ‰

>

€

,

>

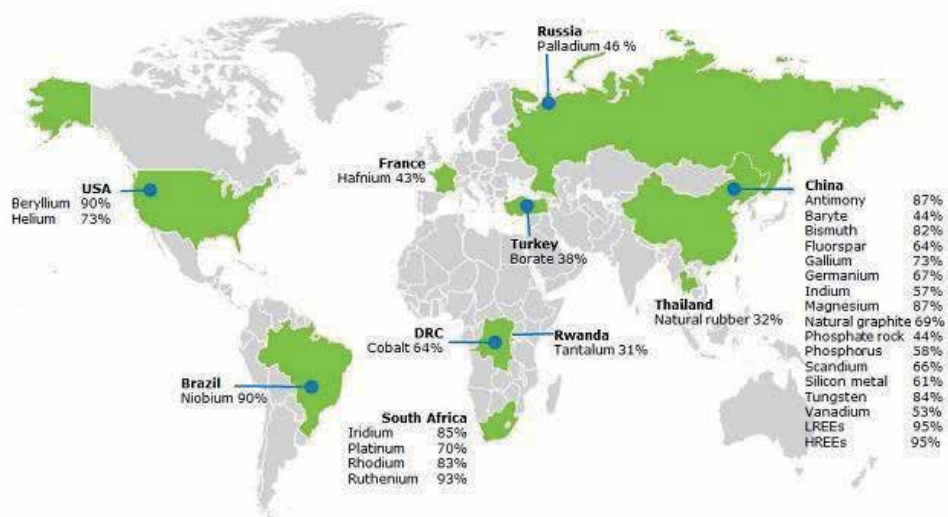
$f$

$f$

" ..††<sup>^</sup> $f$

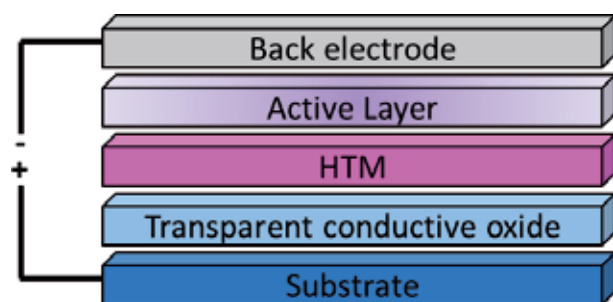
%00

..Š <†



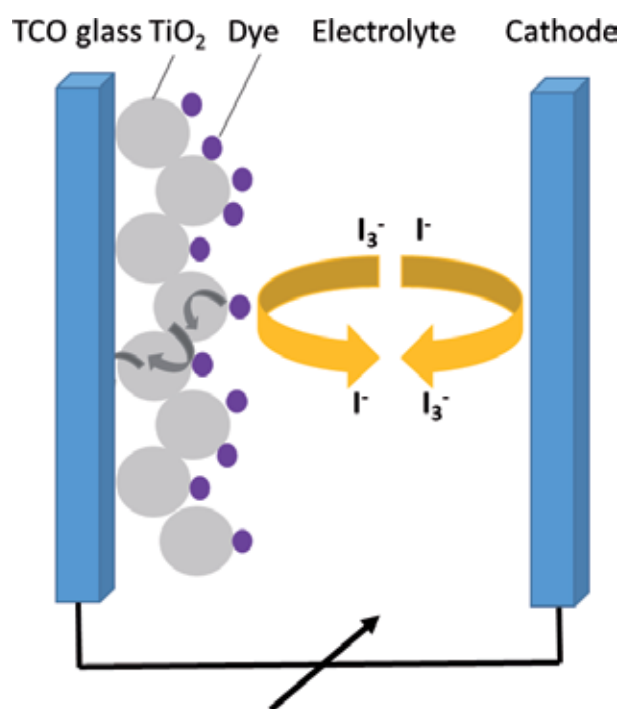








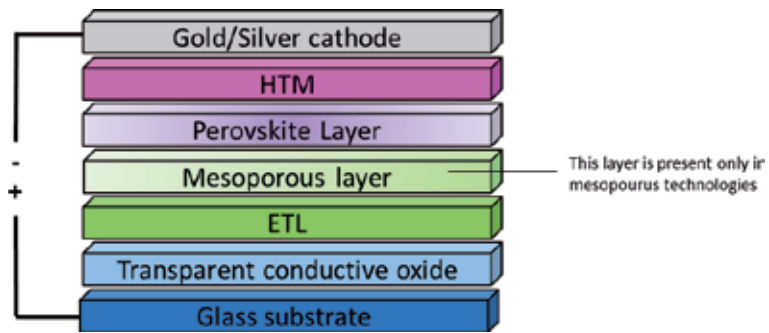






































>

€

**IntechOpen**

